Assessing the efficacy of salt marshes in mitigating wave run-up and overtopping on a dike.

A large-scale experiment under extreme storm conditions.

P.G.Vouziouris

December 2024
Delft University of Technology

TU Delft

Assessing the efficacy of salt marshes in mitigating wave run-up and overtopping on a dike

A large-scale experiment under extreme storm conditions

by

P. G. Vouziouris

in partial fulfillment of the requirements for the Master of Science degree at the Delft University of Technology,
to be defended publicly on **Thursday, 12th of December, 2024, at 16:30**.

Student number:	5619211	
Faculty:	Faculty of Civil Engineering, TU Delft	
Thesis committee:	Dr. Ir. Alessandro Antonini,	TU Delft, supervisor
	Dr. Ir. Bas Hofland,	TU Delft
	Dr. Marion Tissier,	TU Delft
	Ir. Dimitris Dermentzoglou,	TU Delft
	Ir. Jos R. M. Muller,	University of Twente
	Dr. Bas Borsje,	University of Twente

An electronic version of this thesis is available at http://repository.tudelft.nl/.

Cover image: Salt marshes located in Peazermelanen, Friesland. Photography by P.G. Vouziouris.

TU Delft

LIVING DIKES

Abstract

Sea dikes have long been one of the main coastal defense infrastructures in the Netherlands, protecting against flooding and storm surges. As climate change intensifies severe phenomena and sea level rises, dikes must be heightened to protect the coast efficiently against future threats. Meanwhile, nature-based solutions are emerging as viable alternatives. One of these solutions is the use of salt marshes as coastal protection in front of dikes instead of heightening the dike, which could potentially lead to a more cost-effective solution. A salt marsh vegetated foreshore not only dampens the incoming waves but also adapts to the advancing waters of the sea level rise by trapping sediment.

This study's main objective is to assess the efficacy of salt marshes in mitigating wave run-up and overtopping on a real-scale sea dike with a vegetated foreshore.

To carry out these large-scale experiments were carried out at the Deltares Delta Flume. Experiments were carried out for low (0.75 m), medium (1.5m) and high (2.5m) water depths above the foreshore, designed to simulate the extreme storm scenarios experienced by the Friesland dikes in the northern Netherlands. In addition to these conditions, the tests were performed for three different qualities of vegetation, good damaged, and mowed vegetation. First, the experiments ran for a fully vegetated foreshore, then after several runs the vegetation was assumed damaged as an important part of the biomass had eroded. Finally, the vegetation is mowed to leave a bare foreshore which is the baseline scenario.

The acquired run-up results are compared with empirical equations from literature. In addition, the results were compared with those of similar research on salt marshes. Finally, the other important objective of this study is to quantify the reduction in wave loads according to vegetation conditions by introducing certain damping ratio parameters.

To measure the important parameters for the completion of this study, three wave gauges offshore and three wave gauges close to the toe of the dike were used for the measurement of the wave characteristics. For the wave run-up a camera was placed above the dike slope to capture the run-up events over time, and at the same time a LIDAR laser scanner recorded the same slope to collect data on run-up and overtopping.

From the wave analysis, the spectral parameters offshore and at the toe of the dike were calculated. From this, it was possible to have a first estimate of the wave attenuation by comparing the incident significant wave height at these two locations. The results reveal a 14 to 30 % decrease in wave height for low conditions. For medium and high storm conditions the attenuation was decreased to a range between 5 to 15% and 4 to 19% respectively.

The video process run-up measurements were in good agreement with the literature with RMSE = 0.18 - 0.19 m. An additional method was used to validate the results of the run-up. The detection of the run-up was completed visually, by tracking the waves that exceed the markers on the slope, for part of three experiments to compare their signal with the signal derived from the video process. The bias between the signals ranged from 0.017 to 0.022 m, indicating a strong agreement between the methods. One of the most important findings from this study is that the reduction in run-up is not directly attributed to the presence of vegetation itself, but rather to the role played by the significant wave height at the toe of the dike. The run-up was reduced between 2 and 16% for low storm conditions and a reduction between 4 and 24% for medium storm conditions, with an average value of 10.3%. At the same time, the reduction of run-up from damaged vegetation to fully vegetated foreshore is up to 9% with an average of 7.7%. The laser scanner was also used to measured the wave run-up. The signal obtained from the laser is compared with the signal of the visual detection method and reveals a bias between 0.032 and 0.037 m. The run-up 2% results were also compared with the same results from the video camera, revealing a 0.14 m (7%) deviation which may be due to the accuracy of the laser.

The laser scanner also obtained the overtopping results using the virtual overtopping method. From this method, the virtual volume and the virtual overtopping discharge can be calculated and then compared with the equations from the literature. The comparison reveals a strong agreement between the calculated and predicted values, which proves that the equations predict accurately the overtopping discharges for the case of a living dike. For low storm conditions, a decrease of 2 to 50 % of the maximum virtual overtopping volumes is possible, while for medium conditions a maximum volume decrease of 5 to 54% according to the crest height. For the highest storm conditions, this volume decrease is calculated to be between 20 to 28%.

Preface

This report represents the completion of my Master of Science degree in Hydraulic Engineering at TU Delft, presenting the findings and outcomes of my graduation thesis as the final milestone of this academic journey. This study was conducted as part of the "Living Dikes" project, a collaborative effort involving numerous universities and organizations. The experiments central to this research were carried out at the Delta Flume, a large-scale testing facility operated by Deltares in Delft.

Prior to this study, I had the privilege of working as a student assistant for TU Delft, contributing to the preparation of experiments in the Delta Flume. Furthermore, I was fortunate to collaborate as a researcher alongside an outstanding team of professionals to support the successful execution of the experiments conducted in the flume.

The successful completion of this thesis would not have been possible without the invaluable guidance and support of my thesis committee. First, I would like to express my deepest gratitude to the chairman of my thesis committee, Alessandro Antonini, for his constant belief in my potential and his helpful support in guiding me to success throughout this past year. I would also like to extend my heartfelt thanks to Bas Hofland and Marion Tissier for their enthusiasm and the invaluable support they provided, which were crucial in completing this research. At this point, I wish to express my heartfelt gratitude to my daily supervisor, Dimitris Dermentzoglou, who was always available to offer guidance and support, both academically and personally. His constant help, from my early days as a student assistant to the completion of this study, has been essential. I would also like to thank Jos Muller for the emotional and academic support he provided throughout this journey, as well as Bas Borsje for his guidance and insightful contributions during the progress meetings. Last but not least, I want to thank Eleni Mousteri for always being by my side and believing in me, as well as my friends and family for their unwavering support throughout this journey.

P.G. Vouziouris
Delft, December 2024

Contents

1 Introduction

1.1. Background

In response to the escalating global challenge of rising sea levels and the increase in extreme weather phenomena (Calvin et al., 2023) engineering structures and nature-friendly solutions have been implemented over the past decades to protect vulnerable coastal environments worldwide (Van den Hoven et al., 2022). The most widely used infrastructure on the Dutch coasts is sea dikes. These structures have been used throughout history to protect the lower land from flooding, as they can protect from storms that may disrupt human activities. Dutch dikes have also been created to withstand extreme phenomena (Van Loon-Steensma, 2015).

Rising sea levels are diminishing the effectiveness of dikes in protecting inland areas, necessitating their enlargement in the near future. Such a solution would not only be costly, but also would also take space from natural landscapes and leads to unappealing coastal environments (Van den Hoven et al., 2022).

Meanwhile, the cost-effective and adaptive attributes of coastal vegetation, such as salt marshes, emerge as an alternative solution, which can adapt to rising sea levels by using sedimentation trapping mechanisms (Duarte et al., 2013; Koch et al., 2016; Spalding et al., 2014). In addition, these ecosystems play a crucial role in reducing the energy of incoming waves (Astorga-Moar & Baldock, 2023; Manousakas et al., 2022). As a result, salt marshes are being examined to acquire insights that can contribute to a deeper understanding of their coastal protection capabilities. This knowledge will then be used in collaboration with more hard solutions to produce optimal results (Baker et al., 2022).

Salt marshes are intertidal vegetated areas that is submerged in salty water sporadically. Recently, salt marshes have declined in size as a result of human interventions like increase in agriculture, population, and construction around the coastal environment (Esselink et al., 2017). In the Netherlands, salt marshes naturally exist in the Wadden Sea and in mainland regions where they are classified as semi-natural but create ideal environmental conditions to support a large diversity of species (Van Loon-Steensma, 2015). Salt marshes in the Wadden Sea make up about 20% of salt marshes in Europe (Esselink et al., 2017).

For the design of dikes, it is crucial to be able to estimate the expected run-up and overtopping volumes as overtopping may lead to dike failure. Salt marshes with their wave-dissipating abilities have the potential to reduce run-up and overtopping when placed in front of dikes (Baker et al., 2022; Marin-Diaz et al., 2023). From this perspective, it is essential to understand the effect a salt marsh has on these two variables. The aim of this study is to understand how salt marshes impact wave attenuation, as well as their role in reducing wave run-up and overtopping on a dike during extreme severe storm conditions (Van Wesenbeeck et al., 2022).

1.2. Problem statement

In recent years, studies have explored how salt marsh vegetation reduces wave energy, often using flume experiments with scaled setups and artificial or natural vegetation. Some studies also evaluated dike run-up (Keimer et al., 2021) and overtopping (Baker et al., 2022), but the wave load predictions frequently deviated from established equations. These discrepancies, possibly due to scaling effects, cast doubt on the equations' reliability for full-scale dikes with salt marshes on the foreshore.

In the cases where a combination of a video camera and laser scanner was used to measure the wave run-up on a dike, the differences in precision of the two methods are compared. The use of a video camera requires a computer vision algorithm for the data processing and is based on the visual differences between

frames. The placement is relatively easy but the accuracy depends on the video resolution. On the other hand, the use of a laser scanner requires only a preprocessing procedure and the accuracy depends on the calibration and the movement of the device. In past studies of large-scale experiments in wave flumes with high wave conditions, the results from the laser scanner led to more accurate results of wave run-up (Cete, 2019; Hofland et al., 2015). The same equipment combination has not been used for extreme storm conditions.

Furthermore, the effectiveness of salt marshes in reducing wave energy and wave loads on a dike across different conditions of vegetation has not yet been fully studied. Previous studies have focused on differences in the thickness and length of the vegetation but did not account for the effects of deterioration of vegetation. The mechanical properties of vegetation vary throughout the year and can be damaged following a severe storm. Under this context, it is not fully understood how the different states of vegetation could influence loads on a dike. For this reason, quantifying the wave load reduction on a dike based on vegetation conditions holds significant value.

Lastly, previous studies with salt marshes were performed under a variety of storm conditions (e.g. H_s = 0.15 - 0.9) (Ma et al., 2023; Maza et al., 2015; Möller et al., 2014), but there is a lack of studies focusing on salt marshes under extreme storm conditions. Such scenarios, which could lead to high loads and significant biomass loss, are increasingly likely due to the impacts of climate change and thus need to be examined to ensure that dikes can withstand them.

1.3. Research questions

Based on the scope of this report, the following research questions and sub-questions are addressed:

- How do salt marshes affect the run-up on a dike?
  - How well can wave run-up be predicted with existing empirical formulas?
  - What is the difference in accuracy between measuring wave run-up using a video camera and a laser scanner?
- How do salt marshes affect overtopping on a dike?
  - How well can wave overtopping be predicted with existing empirical formulas?

1.4. General approach and scope

The aim of this thesis is to quantify and understand the effect of a salt marsh on wave run-up and overtopping under various wave conditions and different vegetation states. To this end, large scale experiments were conducted at the Deltares Deltaflume using a real salt marsh and an artificial dike. Finally, the measured run-up values on the dike are compared with the expected values calculated using empirical equations from the literature. These equations, sourced from EurOtop (2018) and Van Gent et al. (1999), are also compared against each other.

In addition, this study will assess the effect of salt marsh vegetation on different storm intensities on the overtopping of a dike. The study will primarily concentrate on computing the cumulative overtopping volumes. After obtaining the desired results, there will be a comparison with values produced using the equations found in the literature. Finally, there will be an attempt to quantify the decrease of the overtopping volumes according to the vegetation conditions.

1.5. Thesis outline

This study is organized into the following chapters. In chapter 2, a review of the literature and the topics relevant to this report is analyzed. chapter 3 describes the model setup, equipment, and methods used to process the data from the experimental runs. The findings of this study are detailed in chapter 4. chapter 5 explores key results and additional related topics and gives recommendations for future research. Finally, chapter 6 presents the conclusions of this thesis.

2

Literature survey

2.1. Literature review

Conducting a comprehensive review of the existing literature is essential to identifying gaps in the research on a specific topic. For this review, several studies have been investigated regarding field measurements and experiments in wave flumes with artificial or natural vegetation around salt marshes.

In Vuik et al. (2016) the effectiveness of salt marshes in reducing wave energy and wave loads on dikes has been investigated by contacting field measurements and using numerical wave modeling. After data collection and processing, the EurOtop (2018) equations have also been used to compare the results. From this study, several important results can be acquired. First, the relative importance of vegetation depends on the ratio between wave height and water depth. Another result was that energy dissipation is higher for shallower foreshores, but the relative importance of vegetation increases for larger depths, where energy is gradually dissipating. The study also demonstrates that the vegetated foreshores reduced the wave loads on the dike but not as significantly as they reduced the wave characteristics on them (reduction of 25-50%). This study was carried out under moderate wave conditions, while the importance of vegetation in energy dissipation and reduction of wave loads on a dike remains unknown in the case of extreme storms. Furthermore, this study does not produce results that show the significance of the quality of vegetation and its quantified reduction in wave energy and wave loads.

Another recent study on flume experiments with artificial vegetation aimed to investigate the effectiveness of marsh vegetation in dissipating wave energy and reducing wave overtopping discharges for four different scenarios of vegetation densities (Baker et al., 2022). For the experiments, the Spartina Alteniflora salt marsh species was modeled using idealized surrogate vegetation fixed to plywood. This study gives insight into the change of mechanisms for an increase in vegetation density and height. The larger and thicker the vegetation, the larger the rate of attenuation, the reduction of overtopping, and the damage on the dike. More specifically, the significant wave height H_{m0} for low, mid, and high densities was reduced by 28, 40, and 46 % respectively compared to the results of no vegetation. Even though energetic storm conditions were simulated in this scaled experiment, a flume experiment using real scale dimensions and extreme wave conditions over a foreshore with salt marsh vegetation has still not been conducted to assess the wave loads on a dike. Moreover, this experiment does not assess the effect of real vegetation on waves and their complex responses according to their conditions.

In Keimer et al. (2021) the study aimed to to investigate the potential reduction of vegetation on wave run-up by using rigid PVC rods as vegetation. The most important results of this study were that for the wave run-up, a reduction of up to 16.5 % with increasing vegetation height was calculated, while the mean wave run-up reduction was 9.6 %. In this study, the quantification of run-up decrease for different conditions of the salt marsh vegetation has not been investigated. Furthermore, extreme storm conditions and the calculation of wave overtopping quantities are also missing.

Another important research was completed from Möller et al. (2014), where the aim was to explore the dissipation of waves over a vegetated marsh canopy under storm conditions. The research was carried out on a real-scale experiment using real vegetation of the Elymus Athericus, Puccinellia Maritima, and Atriplex Prostrata species in end-of-summer profile conditions. Some other important aspects of the experiment were that the flume had no dike section and that the experiments were carried out under different storm

conditions (including energetic storm conditions). This knowledge gap is important, as the effectiveness of salt marshes in mitigating wave loads on a real scale dike has not been investigated for severe to extreme storms. In general, the results showed a decrease in wave height of up to 17.9% for low conditions, 14.7% for mid conditions, and 16.9% for the highest wave conditions.

To fulfill the requirements of the literature review, several additional studies were analyzed to provide useful insights and address knowledge gaps. These studies consist of research conducted on salt marsh vegetation, but also research made on different vegetation as valuable information for the current experiment can be derived from them Table 2.1. In this table several parameters are mentioned for the characteristics of the research, these are: the height of vegetation h_v, the depth of the water above the salt marsh d_m, the significant wave height H_s, the peak period of the waves T_p and the steepness of the waves S_{op}.

Table 2.1: Additional studies and their information for: type of vegetation, aim of research, characteristics and results

Publication	Type of research	Vegetation	Aim of research	Characteristics		Results
Paul and Amos (2011)	Field measurements	Seagrass	Spatial and seasonal variation in wave attenuation	h_v = 6-22 cm d_m = 0-2.5 m d_m/h_v =11.36		15-20% wave attenuation (according to the month)
Maza et al. (2015)	Flume experiment	Salt marsh	Influence of different flow and vegetation parameters on the wave attenuation provided by salt marshes	h_v=0.47&0.28 m d_m = 0.4-1.0 m d_m/h_v=0.85-3.52	H_s = 0.12-0.2 m T_p=1.2-2.2 s	High correlation between wave damping coefficients and water depth
Augustin et al. (2009)	Flume experiment	Artificial Salt marsh	Laboratory and numerical studies of wave damping by emergent and near-emergent vegetation	h_v = 0.3 m d_m = 0.4 m d_m/h_v = 1.33	H_s = 8 cm T_p = 1.5-2 s	20.3-41.2 % wave attenuation
Ma et al. (2023)	Flume experiment	Artificial Salt marsh	The objective of this study is to quantify the wave attenuation by vegetation with flattened flexible stems	h_v=0.1 m d_m=0.58-1.13 m d_m/h_v=5.8-11.3	H_s=0.05-0.15 m T_p=1.2-3 s	Less attenuation by flattened but the characteristics showed a similar pattern with standing vegetation
Koftis et al. (2013)	Flume experiment	Meadow	This study aims to assess the degree of wave attenuation over the meadow	h_v=55 cm d_m=1.10-1.70 m d_m/h_v = 2-3.1	H_s=0.28-0.40 m T_p = 2-4 s	Maximum wave attenuation up to 35%
Manousakas et al. (2022)	Flume experiment	Seagrass	This study examines the effectiveness of seagrass vegetation for wave runup reduction	H_s=0.12 m T_p=1-4 s S_{op}=0.096-0.024		Run-up reduction up to 30 %

2.2. Wave Attenuation

Salt marshes play a vital role in wave attenuation by effectively reducing wave energy (Rupprecht et al., 2017). This is happening due to the reduction of the current velocity and the increase of the turbulence through the canopy of the salt marsh vegetation (Duarte et al., 2013; Koch et al., 2016). This energy dissipation holds significant importance as it mitigates the risk of coastal erosion (Baker et al., 2022; Li et al., 2023). Previous research, based on both experimental studies and field observations, points to the fact that wave attenuation is a result of various physical attributes of the vegetation, including stem density and stiffness (Zhao et al., 2023). Furthermore, hydrodynamic factors such as water depth (h), wave period (T), and wave height (H) are known to play a vital role in influencing this mechanism (Augustin et al., 2009; Rupprecht et al., 2017).

Past research efforts have concentrated on a combination of field measurements (Marin-Diaz et al., 2023; Vuik et al., 2016) and laboratory experiments. In some cases, these experiments replicated salt marshes using synthetic materials (Baker et al., 2022; Zhao et al., 2023), others utilized actual salt marsh vegetation samples within wave flumes (Möller et al., 2014; Rupprecht et al., 2017) and in some cases they used flattened vegetation (Ma et al., 2023). Some of these studies assume mild wave conditions while others escalate to energetic phenomena (Baker et al., 2022; Möller et al., 2014).

Comparison with the results of dissipation with mowed vegetation showed a decrease of 60% to the reduction in wave height (Möller et al., 2014). For wide marshes under mild conditions, the attenuation may reach even 80% (Möller & Spencer, 2002). In other cases with a 40m wide marsh, the dissipation of energy for more energetic conditions reached 16.9% for regular and irregular waves (Möller et al., 2014).

2.3. Wave Run-up

The effect of vegetation in wave run-up on a dike has already been studied for the case of salt marshes (Keimer et al., 2021), but also for other cases such as seagrass (Manousakas et al., 2022).

In the field of coastal engineering, wave run-up is described as a collection of distinct maximum values in water level elevation which is measured vertically on the foreshore with respect to the still water level (SWL) (Stockdon et al., 2006). Moreover, run-up refers to the combination of wave set-up and swash uprush, which must be included in the overall water level caused by tides and wind. Understanding wave run-up is vital for evaluating the safety of sea dikes or other coastal structures (Franklin & Torres-Freyermuth, 2022).

To calculate the run-up on a dike EurOtop (2018) suggests using the parameter $R_{u2\%}$. This parameter is the wave run-up that is exceeded by the 2% of all the incoming waves (Van der Meer, 1998). The visualization of this parameter can be located in Figure 2.1.

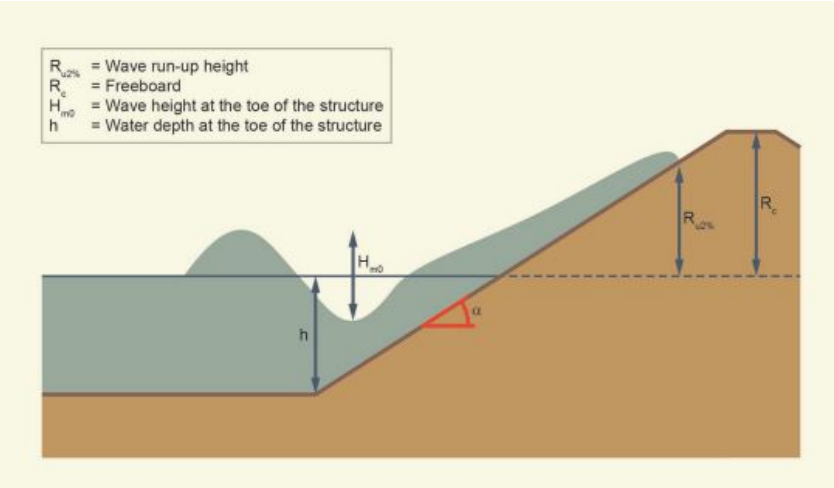

Figure 2.1: Visualization of the run-up height $R_{u2\%}$ on a impermeable slope EurOtop (2018)

The general equation for the 2% run-up height is given as EurOtop (2018):

$$\frac{R_{u2\%}}{H_{m0}} = 1.65 \cdot \gamma_b \cdot \gamma_f \cdot \gamma_\beta \cdot \xi_{m-1,0} \tag{2.1}$$

In Equation 2.1 the ratio $R_{u2\%}/H_{m0}$ signifies the relative run-up, with H_{m0} being the spectral significant wave height at the toe of the structure (Van der Meer, 1998).

The breaker parameter $\xi_{m-1,0}$, also called the Iribarren parameter, has once again a correlation with the significant wave height H_{m0}, the deep water spectral period $T_{m-1,0}$ and the angle of the slope of the dike α as follows (Stockdon et al., 2006):

$$\xi_{m-1,0} = \frac{tan\alpha}{\sqrt{\frac{H_{m0}}{L_{m-1,0}}}} \tag{2.2}$$

The deep water wave length L_0 in this case is equal to:

$$L_{m-1,0} = \frac{gT_{m-1,0}^2}{2\pi} \tag{2.3}$$

In Equation 2.1, certain influencing factors can be observed:

$\gamma_b[-]$ is the berm influence factor. The berm on a dike can be proved useful in reducing the wave run-up and overtopping. In this case, this dike is not equipped with a dike berm and so the berm influence factor $\gamma_b = 1$. The second influence factor is the one for the slope roughness $\gamma_f[-]$. According to the roughness of the dike, it is possible to have different dissipation of energy. In case the slope of the dike is assumed to be smooth the factor becomes $\gamma_f = 1$. The next factor $\gamma_\beta[-]$ is about the oblique wave attack. The angle at which the waves arrive at the dike may result in different run-up values. In this case, the experiments will be conducted in a flume, meaning that the oblique wave attack angle will be straight ahead (0°). This leads the influence factor to be $\gamma_\beta = 1$

$T_{m-1,0}$ is the spectral wave period and is used for the calculation of the run-up, for a variety of unusual wave spectra (e.g. JONSWAP). To calculate this spectral parameter Equation 2.4 is used.

$$T_{m-1,0} = \frac{m_{-1}}{m_0} \tag{2.4}$$

where m_{-1} , m_0 the spectral moments calculated from the n^{th}-order spectral moment:

$$m_n = \int_0^\infty f^n E(f) df, n \in \mathbb{Z} \tag{2.5}$$

If the spectrum is uniform (single peaked) the spectral period can be calculated using the peak period as EurOtop (2018):

$$T_p = 1.1 T_{m-1,0} \tag{2.6}$$

The maximum value of the run-up is given by EurOtop (2018) in Equation 2.6.

$$\frac{R_{u2\%}}{H_{m0}} = 1.0 \cdot \gamma_b \cdot \gamma_f \,(4 - \frac{1.5}{\sqrt{\gamma_b \cdot \xi_{m-1,0}}}) \tag{2.7}$$

The relation of the breaker parameter $\xi_{m-1,0}$ with the wave run-up is linear regarding breaking waves or waves with a small breaker parameter ($\xi_{m-1,0} < 1.8$). In contrast, for non-breaking waves or larger breaker parameters, the increase is milder and reaches a stable value (EurOtop, 2018).

In cases where vegetation protection is installed in front of a structure, the effectiveness of the vegetation in reducing the wave run-up on the slope can be investigated using the damping ratio ζ. This parameter equals (Manousakas et al., 2022):

$$\zeta = \frac{R_v}{R_0} \tag{2.8}$$

where R_v is the wave run-up height with vegetation and R_0 without vegetation.

Another pair of state-of-the-art equations that are used to estimate the run-up on a dike are those of Van Gent et al. (1999), which read:

$$\frac{R_{u2\%}}{H_{m0}} = \begin{cases} c_0 \cdot \xi_{m-1,0} & \text{for } \xi_{m-1,0} \le \frac{1}{2}\frac{c_1}{c_0} \\ c_1 - \frac{c_2}{\xi_{m-1,0}} & \text{for } \xi_{m-1,0} > \frac{1}{2}\frac{c_1}{c_0} \end{cases} \quad , \quad c_2 = 0.25\frac{c_1^2}{c_0} \tag{2.9}$$

For these equations, the most suitable period used is the spectral period $T_{m-1,0}$ taking also into consideration the significant wave height H_{m0} at the toe of the dike. The coefficients can get two different values from two different methods. The first method uses the results derived from a computational model, with values of $c_o = 1.45$ and $c_1 = 3.8$. The second method is the use of the fitted values of the coefficients which match the results of very thin layers of run-up, to represent higher run-up values on a dike (Van Gent et al., 1999). The values used for the second method where $c_o = 1.55$ and $c_1 = 5$. These lead Equation 2.9 to Equation 2.10 and Equation 2.11.

$$\frac{R_{u2\%}}{H_s} = \begin{cases} 1.45 \cdot \xi_{m-1,0} & \text{for } \xi_{m-1,0} \le 1.31 \\ 3.8 - 2.49/\xi_{m-1,0} & \text{for } \xi_{m-1,0} > 1.31 \end{cases} \quad , Eq.1 \tag{2.10}$$

$$\frac{R_{u2\%}}{H_s} = \begin{cases} 1.35 \cdot \xi_{m-1,0} & \text{for } \xi_{m-1,0} \le 1.61 \\ 4.7 - 4.09/\xi_{m-1,0} & \text{for } \xi_{m-1,0} > 1.61 \end{cases} \quad , Eq.2 \tag{2.11}$$

2.4. Overtopping

Wave overtopping refers to the time-averaged quantity of water that flows over a hydraulic structure with a crest height above still water level (SWL). It is measured as the mean discharge per linear meter of width, q ($m^3/s/m$ or $l/s/m$) (Allsop et al., 2007). The occurrence of wave overtopping is crucial in designing durable structures, especially for features like dikes, as it is associated with breaches and failures, impacting their long-term safety and integrity. This mechanism is influenced by various factors, primarily related to the wave conditions and the structure's geometry (Koosheh et al., 2021).

Wave overtopping discharge occurs when waves run up the slope of a hydraulic structure. If the level of wave run-up surpasses the crest height, water spills over the top of the flood defense and flows down the

slope on the landward side (EurOtop, 2018) which is the weakest part of a structure like a dike (Gerrit et al., 2019). The overtopping quantities may lead to erosion of the landward side of the structure and eventually lead to a breach (Bomers et al., 2018).

The EurOtop (2018) gives the latest equations regarding the overtopping discharge. The new manual version recommends equations with small differences compared to the older version (Allsop et al., 2007). The equations from the EurOtop (2018) read:

$$P_{ov} = exp[-(\sqrt{-ln0.02}\frac{R_c}{R_{u2\%}})^2 \tag{2.12}$$

Equation 2.12 calculates the probability that a wave can overtop the crest freeboard assuming $R_{u2\%}$.

$$\frac{q}{\sqrt{g \cdot H_{m0}^3}} = \frac{0.023}{\sqrt{tan\alpha}}\gamma_b \cdot \xi_{m-1,0} \cdot exp\left[-(2.7\frac{R_c}{\xi_{m-1,0} \cdot H_{m0} \cdot \gamma_b \cdot \gamma_f \cdot \gamma_\beta \cdot \gamma_v})^{1.3}\right] \tag{2.13}$$

with a maximum of:

$$\frac{q}{\sqrt{g \cdot H_{m0}^3}} = 0.09 \cdot exp\left[-(1.5\frac{R_C}{H_{m0} \cdot \gamma_f \cdot \gamma_\beta \cdot \gamma_v})^{1.3}\right] \tag{2.14}$$

where R_C is the crest freeboard and accounts for the height of the crest of the structure above the SWL and γ_v is the factor for a wall after the slope.

According to EurOtop (2018) and other readings like Gerrit et al. (2019), the allowable overtopping for different designs of dikes is given as:

- $q < 0.1$ l/s for low quality slopes
- $q < 1.0$ l/s for normal slopes
- $q < 10.0$ l/s for high-quality slopes

For the prediction of the percentage of the overtopping wave volumes, EurOtop (2018) suggests a two-parameter Weibull distribution as:

$$P_{V\%} = P(V_i \geq V) = \exp\left[-\left(\frac{V}{a}^b\right)\right] \cdot (100\%) \tag{2.15}$$

where, $P_{V\%}$ the overtopping percentage, $P(V_i \geq V)$ the probability that an individual overtopping event V_i surpasses a determined volume V, b and a a shape and a scale parameter respectively. These parameters found in Van der Meer et al., 2018 as:

$$\alpha = \left(\frac{1}{\Gamma(1+\frac{1}{b})}\right)\left(\frac{qT_m}{P_{ov}}\right) \tag{2.16}$$

where Γ is the mathematical function and b is the following shape factor:

$$b = 0.73 + 55\left(\frac{q}{gH_{m0}T_{m-1,0}}\right)^{0.8} \tag{2.17}$$

The maximum individual overtopping volume can be calculated using the number of overtopping waves N_{ow} (EurOtop, 2018; Koosheh et al., 2021) as:

$$V_{max} = a(\ln \cdot N_{ow})^{\frac{1}{b}} \tag{2.18}$$

The bibliography contains references on calculating the two factors based on various criteria, such as H_{m0} and the R_c (Koosheh et al., 2021; Mares-Nasarre et al., 2020; Molines et al., 2019).

3

Methodology

3.1. Experimental set-up

3.1.1. Wave flume

Experiments were conducted in the Deltares Delta Flume in Delft, the Netherlands. The Delta Flume is the largest wave flume in the world, being 291 m long, 5 m wide and 9.5 m deep.

A set-up comprising a foreshore, a salt marsh and a dike was installed in the flume. The concrete foreshore was constructed 51 m away from the wave board (x=0), with a 1:9 slope that changes to 1:45 (Figure 3.1). A 0.6 m high salt marsh cliff is located at the nearshore end of the foreshore, after which a 70.3 m salt marsh was constructed from blocks that were collected from the natural marsh in Peazemerlannen, Friesland in the north Netherlands Figure 3.2, Figure 3.3. At the end of the salt marsh, (x = 104 m) a concrete dike with a 1:3.6 slope and a crest height of 10.9 m was installed.

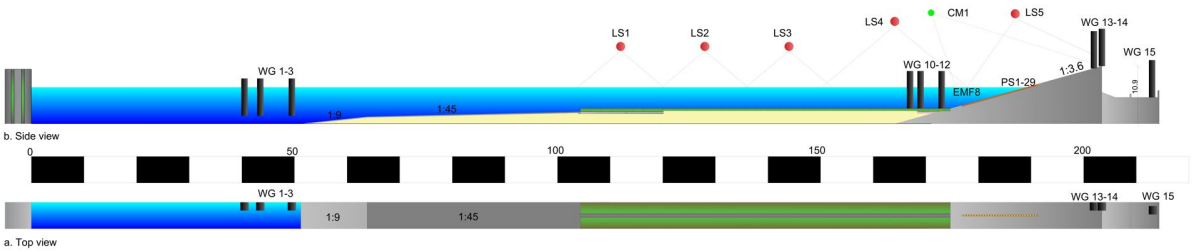

Figure 3.1: Cross section and top view of the experimental set-up.

The blocks consist of two categories, the steel blocks with a steel case of 2.0 m length, 2.0 m width, and 0.7 m height. The wooden blocks have a wooden case of 2.2 m in length, 2.0 in width, and 0.4 in height Figure 3.4.

The first marsh blocks close to the cliff, which are protected from a brushwood dam, consist of the thickest steel blocks with an average thickness of 67 cm. The steel blocks at the cliff are divided into two rows of 6 blocks and in the middle, there is a 47 cm footpath which helped in the experiments for the visual inspection or for potential service. These blocks were placed on top of compacted clay. Inside the clay, a drainage pipe was installed towards the front of the foreshore. This ensured no buildup of pore water pressures inside the blocks during the test. After the end of the steel blocks, 48 wooden blocks are again placed into two rows. These blocks are 47.6 cm thick and in between them, the pathway had a width of 46 cm. This time, the wooden blocks were positioned on the sand, with a layer of geotextile placed in between. Close to the dike, again 4 metal blocks were divided into two rows on top of compacted clay. The choice of placing the thicker blocks on the cliff and close to the toe of the dike was made assuming that the largest attack of the waves may occur at these locations. The last blocks, which come in contact with the dike are two thin wooden blocks, as the dike needs to be cut on the place that the blocks intercepts with it. Figure 3.5 shows a picture of the wave flume, where salt marsh blocks are located inside and the brushwood dam protects them from heavy wave attacks. The dike has a 1:3.6 slope of concrete and in the middle is located a wooden tube containing pressure cells for the measurement of the pressure on the dike. In this set-up, the salt marsh has a height of +2.9 m

Figure 3.2: Map of the Peazermelanen salt marsh field, Friesland, north Netherlands. The two locations marked in this picture are the seaward and landward locations of the excavation of the salt marsh blocks.

Figure 3.3: Salt marsh blocks located in the salt marsh field

from the flume bottom. The crest of the dike reaches 10.9 m. Behind the dike, there is an overtopping box to collect the overtopping volume. The box has a length of 10.6 m and one wall of 59 cm in height between them.

3.1.2. Vegetation

The vegetation is in different condition during different seasons. In spring vegetation starts growing and reaches a pick during Summer. During autumn, the stems start getting a woody profile and a brown color. The last condition of the cycle is the stems die and the stormy conditions of the winter carry them away so the new vegetation can sprout in spring (Eekman, 2021; Reents et al., 2022).

The vegetation blocks were gathered at the beginning of autumn (September) from the field and brought to the Delta Flume where they were preserved until the beginning of experiments in February 2024. This

Figure 3.4: Salt marsh blocks. a) Steel block of dimensions 2.0x2.0x0.7 m, b) Wooden block of dimensions 2.2x2.2x0.4 m

Figure 3.5: Salt Marsh blocks located in the flume with a brushwood dam on the cliff

means that the salt marshes had still a summer state when they were obtained and transitioned to autumn and winter profiles later on. The blocks comprised mainly of the genre Elymus Athericus, but the samples contain some Atriplex prostrata as well.

3.1.3. Test program

A summary of the test program is presented in Table 3.1. The experiments have centered around two primary principles, the condition of salt marsh vegetation and the intensity of wave conditions. The severity of wave conditions is categorized into low conditions with $H_s = 0.75m$ and $d = 4.4m$, mid (medium) conditions

with $H_s = 1.2m$ and $d = 5.4m$, and high (extreme) conditions with $H_s = 2.0m$ and $d = 6.9m$. For each level of wave intensity, two different deep water wave steepness values are under investigation, namely $S_0 = 2\%$ and $S_0 = 4\%$. The vegetation conditions can be categorized into three distinct groups. The salt marsh state is differentiated among fully vegetated conditions, damaged conditions with broken stems, and no-vegetation conditions (where the vegetation has been mowed). In Table 3.1 the first cycle of experiments was conducted with healthy vegetation (green), the second cycle assumed damaged vegetation due to biomass erosion (orange), and in the final cycle, the vegetation was mowed (red), and reference scenarios were carried out. An additional experiment was assumed so it will be possible to compare results with the experiments over salt marshes from Möller et al. (2014). This experiment had conditions of $H_s = 0.91m$, $d = 4.9m$ and $S_0 = 1.5\%$.

Table 3.1: Test program ID and values of water depth d, water depth above salt marsh d_m, wave height H_s, deep water steepness S_0, wave period T_p, and N the number of waves in the experiment.

ID	d [m]	d_m [m]	H_s [m]	S_0 [-]	T_p [s]	N [-]
SM-01	4.4	1.50	0.75	0.04	3.47	100
SM-02	4.4	1.50	0.75	0.02	4.90	100
SM-03	5.4	2.50	1.20	0.04	4.39	100
SM-04	5.4	2.50	1.20	0.02	6.20	100
SM-05	4.4	1.50	0.75	0.04	3.47	100
SM-06	4.4	1.50	0.75	0.02	4.90	1500
SM-07	4.4	1.50	0.75	0.04	3.47	1500
SM-08	4.4	1.50	0.75	0.02	4.90	100
SM-09	5.4	2.50	1.20	0.04	4.39	1000
SM-10	4.9	2.00	0.91	0.015	6.20	100
SM-11	5.4	2.50	1.20	0.02	6.20	1000
SM-12	6.9	4.00	2.00	0.02	8.01	100
SM-13	6.9	4.00	2.00	0.04	5.66	1000
SM-14	6.9	4.00	2.00	0.02	8.01	1000
SM-15	6.9	4.00	2.00	0.04	5.66	100
SM-16	4.4	1.50	0.75	0.04	3.47	100
SM-17	4.4	1.50	0.75	0.02	4.90	100
SM-18	5.4	2.50	1.20	0.04	4.39	100
SM-19	5.4	2.50	1.20	0.02	6.20	100
SM-20	4.4	1.50	0.75	0.04	3.47	100
SM-21	4.4	1.50	0.75	0.02	4.90	1500
SM-22	4.4	1.50	0.75	0.04	3.47	1500
SM-23	4.4	1.50	0.75	0.02	4.90	100
SM-24	5.4	2.50	1.20	0.04	4.39	1000
SM-25	5.4	2.50	1.20	0.02	6.20	1000
SM-26	6.9	4.00	2.00	0.02	8.01	100
SM-27	6.9	4.00	2.00	0.04	5.66	1000
SM-28	6.9	4.00	2.00	0.02	8.01	1000
SM-29	6.9	4.00	2.00	0.04	5.66	1000
SM-30	6.9	4.00	2.00	0.04	5.66	1000
SM-31	6.9	4.00	2.00	0.02	8.01	1000
SM-32	5.4	2.50	0.75	0.04	4.39	1000
SM-33	5.4	2.50	0.75	0.02	6.20	1000
SM-34	5.4	2.50	1.20	0.04	4.39	25
SM-35	5.4	2.50	1.20	0.04	4.39	25
SM-36	4.4	1.50	0.75	0.04	3.47	1000
SM-37	4.4	1.50	0.75	0.02	4.90	1000
SM-38	4.4	1.50	0.75	0.04	3.47	25
SM-39	4.4	1.50	0.75	0.04	3.47	25
SM-40	3.0	0.10	0.95	0.04	5.52	2000
SM-41	5.4	2.50	1.20	0.04	6.20	2000
SM-42	6.9	4.00	2.00	0.04	8.01	2000

3.2. Instumentation

For the calculation of the parameters of waves from the offshore position of the flume to the toe of the dike, this project uses a total of six wave gauges to record the water elevation time series offshore (WHM01 - WHM03) and close to the toe of the dike (WHM12A-WHM14A).

To capture wave run-up events along the dike slope in this study, a GoPro Hero 10 Black camera was employed. Throughout all experiments, consistent settings were maintained using a resolution of 3840 x 2160 pixels (4k) at 60 frames per second (fps) and a linear lens mode to mitigate any additional distortion. The camera was placed in two distinct positions for different wave conditions. For experiments with high water depth (e.g. SM-12, $H_s = 2.0m$ and $d = 6.9m$) the camera was positioned at x = 179 m from the wave board, 12 m from the flume bottom, while for experiments with $d < 6.9m$, the camera was positioned at x = 171 m from the wave board at the same height. The video recording in these settings can capture files up to 3.9 GB (around 9 minutes and 50 seconds) and then continuously save the recording in a new file. These were combined to create a total video for each experiment run.

The run-up and overtopping were also calculated by using data measured with a SICK LiDAR sensor model LD-LRS3611. The laser scanner (LS) was mounted above the dike at a height of 20.8 m and a distance of 187 m from the wave-board. The main principle a LiDAR sensor works is by emitting laser beams that reflect on objects, enabling us to calculate the distance by measuring the duration that the beam needs to reflect on the object and return to the scanner. The same sensor is used to calculate overtopping, as described later in section 3.4.

For the recording of the overtopping events, the laser scanner located above the slope of the dike was used once more. As the laser scanner is able to detect both the location of water but also the thickness of the layer of the wave, the calculation of the virtual overtopping was possible even for the experiments in which no overtopping was observed over the crest of the dike.

For the research of the run-up events it is important to differentiate the experiments by comparing some important wave characteristics. These characteristics need to be determined on the offshore location of the wave flume, where the waves have not yet been transformed from shoaling, or attenuated from the salt marsh vegetation. It is also important to measure the characteristics of incident and reflected waves near the toe of the dike, as the difference between them is crucial for assessing wave attenuation.

There are different methods to analyze the reflective and incident components of a wave in a flume. One of the most well-known is the method of Guza (Vos-Jansen, 2018). This method uses a wave gauge and an electromagnetic flow meter (EMF) to capture the water elevation and velocity in a specific area to separate the incoming from the reflected waves. Another commonly used method is the method of Zelt and Skjelbreia (1992) which uses an arbitrary number (2+) of wave gauges to identify the incoming and reflected components of a wave. This method assumes a one-dimensional wave field where the reflected waves are moving in the opposite direction of the incoming waves. By using Fourier analysis the water elevation equation can be expressed as Equation 3.1. Where $p = 1, 2, ..., P$ the locations of the different wave gauges. By analyzing the waves into reflected and incoming that moving in the opposite direction the waves can be expressed as Equation 3.2 (Zelt & Skjelbreia, 1992).

$$\eta_p(t) = \sum_{j=-N/2}^{N/2} A_{j,p} e^{i\omega j t} \tag{3.1}$$

$$\eta(x,t) = \sum_{j=-N/2}^{N/2} \alpha_{Lj} e^{i(kjx+\omega j t)} + \alpha_{Rj} e^{i(-kjx+\omega j t)} \tag{3.2}$$

A wave reflection analysis is performed to separate waves into incident and reflected. This is done using the method by Zelt and Skjelbreia (1992), using the three wave gauges WHM01 - WHM03 at the offshore and the three wave gauges WHM12A-WHM14A near the toe of the dike. The spacing between these wave gauges may lead to a variety of unwanted frequencies and phase errors. To avoid extreme variance densities and very low or very high frequencies that do not correspond to incident water elevations, the signal derived from this method needs to be filtered before being used in other methods. In this case, the signal was filtered using a band-stop filter, which is capable of attenuating a range of frequencies at very low levels. More details about the method and the procedure of the reflection analysis can be found in Appendix B

It is important to note that different methods and terms of the wave characteristics are being used in this thesis. In this work, the term of the significant wave height is assessed by using two different terms. The first term is associated with a zero-down crossing analysis of the time series recorded by the wave gauges. In this

case, the significant wave height is indicated by $H_{1/3}$. The second term is symbolized as H_{m0} and originated from the spectral analysis of the time series of surface elevation.

A zero-down crossing analysis (Figure 3.6.) is performed on the incoming wave signals to calculate the wave period and wave height of individual waves. This is done after subtracting the mean value of the incoming water elevation at the beginning of a test from the entire signal. The significant wave height ($H_{1/3}$) is calculated as shown in Equation 3.3.

$$H_{1/3} = \frac{1}{N/3} \sum_{j=1}^{N/3} H_j \tag{3.3}$$

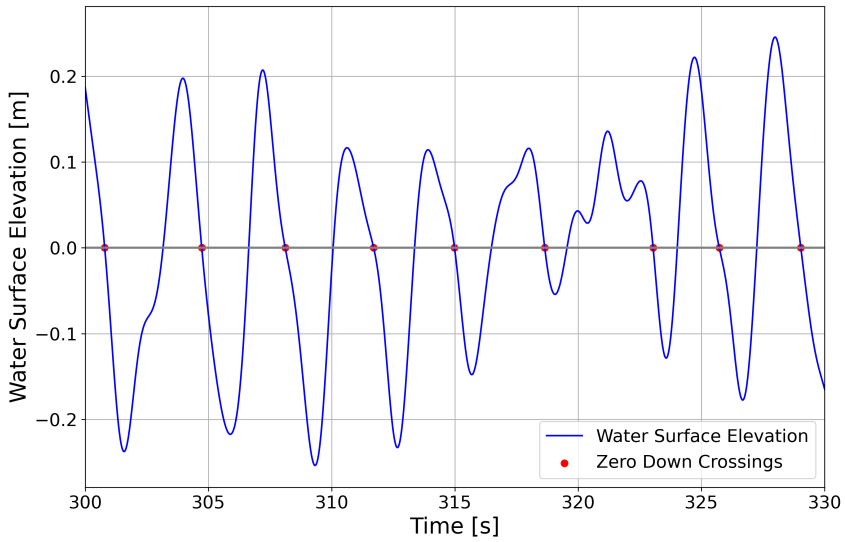

Figure 3.6: Zero-down crossing analysis of the incoming wave signal generated at the toe of the dike

Following, a spectral analysis is performed on the incoming wave signals the methodology outlined in Holthuijsen (2007). The spectrum is segmented into blocks, each subjected to Fast Fourier Transform (FFT) analysis, yielding 50-100 blocks, encompassing 20 waves. H_{m0} and $Tm-1,0$ are then calculated, using Equation 3.4-Equation 3.6.

$$H_{m0} = 4\sqrt{m_0} \tag{3.4}$$

$$m_n = \int_0^\infty f^n E(f) df, n \in \mathbb{Z} \tag{3.5}$$

$$T_{m-1,0} = \frac{m_{-1}}{m_0} \tag{3.6}$$

For the calculation of the Equation 3.5 a Fourier transform is used. To apply the Fourier Transform, the sampling frequency at which the spectrum was recorded has been used, as $F_s = 40Hz$. The method is first used to compute the variance density spectrum Equation 3.7, where $E\left\{\frac{1}{2}\alpha^2\right\}$ the variance. The variance density spectrum is considered one of the most important parameters in the ocean waves field as it is used to calculate the essential parameters of waves (Holthuijsen, 2007)

$$E(f) = \lim_{\Delta f \to 0} \frac{1}{\Delta f} E\left\{\frac{1}{2}\alpha^2\right\} \tag{3.7}$$

For both short and long-duration experiments, a sensitivity analysis for H_{m0} and $T_{m-1,0}$ is performed to assess the impact of the number of blocks (Figure 3.7). The confidence of the spectrum for the low-duration experiments has a significant difference between the upper and low intervals, while the high conditions give optimal results. The variance density spectrum of a short-duration experiment (SM-01) can be found in Figure 3.8, while the spectrum of a long-duration experiment (SM-06) can be visualized in Figure 3.9

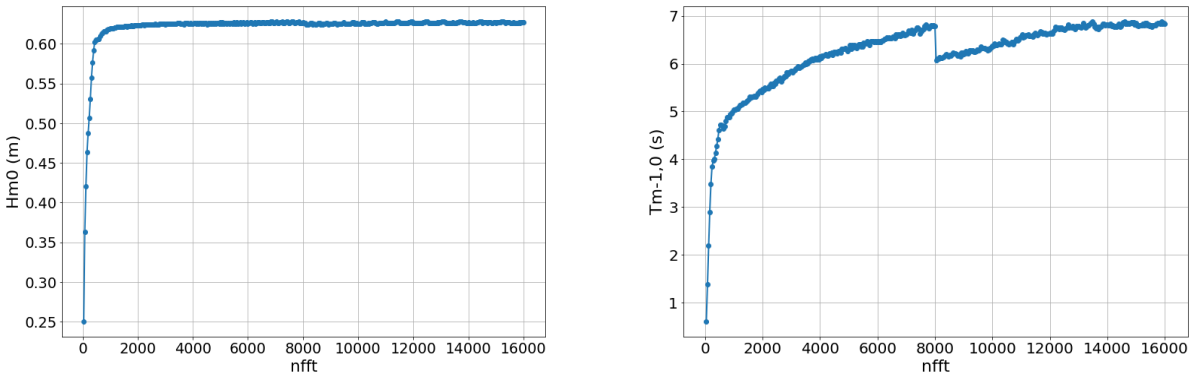

Figure 3.7: Sensitivity analysis for the test SM-01. H_{m0} and $T_{m-1,0}$ are plotted against the block length

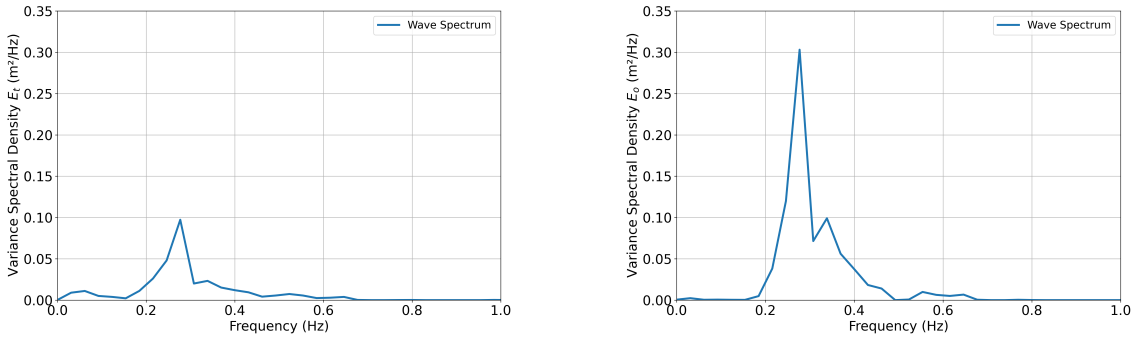

Figure 3.8: Wave spectrum of SM-01 with data obtained from the reflection and spectral analysis. a) Wave spectrum at the toe of the dike, b) Wave spectrum on the offshore

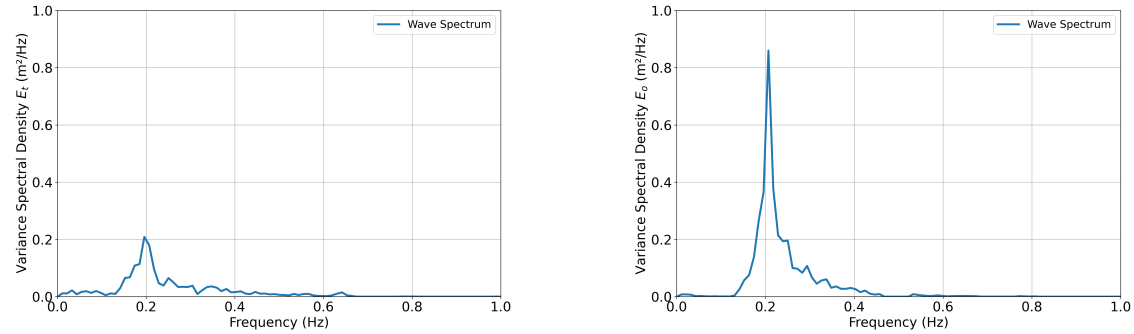

Figure 3.9: Wave spectrum of SM-06 with data obtained from the reflection and spectral analysis. a) Wave spectrum at the toe of the dike, b) Wave spectrum on the offshore

3.3. Wave Run-Up Measurements

To capture in detail all the run-up events on the slope of a dike it is essential to understand the mechanisms of the wave-dike interaction. As the waves reach the dike they break and/or run up the slope, but also some of the energy of these events is reflected towards the offshore location.

3.3.1. Video Camera

To ensure that the camera is providing accurate results it is necessary to calibrate the footage intrinsically and extrinsically to avoid any distortions and to ensure that the recordings provide a good pixel-to-distance correspondence for all the experiments. As the camera had to be repositioned for every experiment, calibration was needed for every single run individually to record experiments with different conditions.

For the needs of the camera calibration, a 2.25 by 1.5 m (8×5) black and white chessboard was painted on the slope of the dike. Detecting the corners of a chessboard is necessary for both calibration procedures Figure 3.11. The procedure of the Intrinsic calibration and extrinsic calibration can be found in section A.1 and section A.2 respectively. The first frame of the video is used to detect the chessboard Figure 3.10 left. When the intrinsic calibration is completed, then the first frame can be undistorted to see the results Figure 3.10 right.

Figure 3.10: Intrinsic calibration a) first frame of footage and b) undistorted first frame

Figure 3.11: Chessboard for the calibration of the camera. a) Painting of the chessboard on the dike slope, b) Finalized Chessboard on the slope

To optimize the processing of the video for the next stages, the original images (frames) are first undistorted by the intrinsic parameters, then the extrinsic parameters are applied to them and the frame is cropped in the minimum possible size to capture the run-up events. More details can be found in Appendix C.

The procedure that is being used in this thesis will be the same as it has been used previously by Lakerveld (2024). For the analysis of the retrieved signal, the moving water surface is identified in the cropped image by measuring the differences in intensities of consecutive frames, which is a common method in the field of computer vision (Migliore et al., 2006). The method from Lakerveld (2024) uses consecutive frames to find the variance in the intensity of pixels, which ranges from 0 to 255 according to the RGB colors (Red Green Blue). This leads to a separation of the moving water from the slope by creating a contrast. In this study, after applying the calibration matrices to the footage, an algorithm for the process of the video using the variances of six consecutive frames is used Equation 3.8 and calculates its mean value across the three colors. This produces a 2-D array for the variance. Furthermore, on this array, a blurring and a Gaussian filter are applied to the image to make the differences more visible and reduce noise. The area in which the median blur is applied is a 5x5 area of indices, while the Gaussian blurring filter has a standard deviation σ = 10 which was found to represent the best results. In the last step of the procedure, the median value of the variance on the x-axis (rows) is calculated in the 2-D array. To identify the front of the wave, the algorithm detects the first row of the picture where this median value exceeds the threshold. This point then is visualized as a (median) line and gives a 1-D array. Another method would be to pick the maximum value of the variance for the run-up, but this is prone to outliers, and the thickness of the layer of water running up the slope might not be detected. As the dike was made of concrete, the contrast to the water was not sufficient in cases where the dike was covered in vegetation. The size at which every video is cropped was manually detected to ensure that

the slope would be exposed in the process as little as possible to avoid detection of vegetation on the dike and residual movement of the camera from the wind. Moreover, the threshold that the median needs to surpass so the algorithm identifies the front of the wave was manually picked and may differ for different experimental runs. For runs in which the dike was clean and there was no significant movement of the camera, a low threshold for the median was chosen, leading to a good correlation between the median and the maximum of variance. For experiments in which the dike was full of vegetation and/or residual camera movement, a higher threshold was necessary to avoid noise detection. A higher threshold for the median value was chosen, which led to a poor correlation of the median and maximum variance points.

$$\left[\sigma^2\right]^i_{m,n} = var\left(\left[I^{i-5}_{m,n}\right],\left[I^{i-4}_{m,n}\right],\left[I^{i-3}_{m,n}\right],\left[I^{i-2}_{m,n}\right],\left[I^{i-1}_{m,n}\right],\left[I^{i}_{m,n}\right]\right) \tag{3.8}$$

where $I \in \{0,...,255\}$ for all colors.

$$\left[\mu_{med}\right]^i_{m,n} = med\left(\mu^i_{m-2,n-2},...,\mu^i_{m+2,n+2}\right) \tag{3.9}$$

Where $\mu^i_{m,n} = \left[\overline{\sigma^2}\right]^i_{m,n}$

Figure 3.12 shows an overview of the video process procedure that is applied to the run-up footage. The algorithm engages six video frames in a queue and subtracts the variance of their intensities over time. In the next step, the Median and Gaussian blur filters are applied. The final step includes the transformation of the variance in a median line over the y-axis, indicating the water movement over the slope. The algorithm runs in a loop so it moves to the next frame (t+1) and engages the six previous frames in the queue. More information on the method used for the video process can be found in section C.4

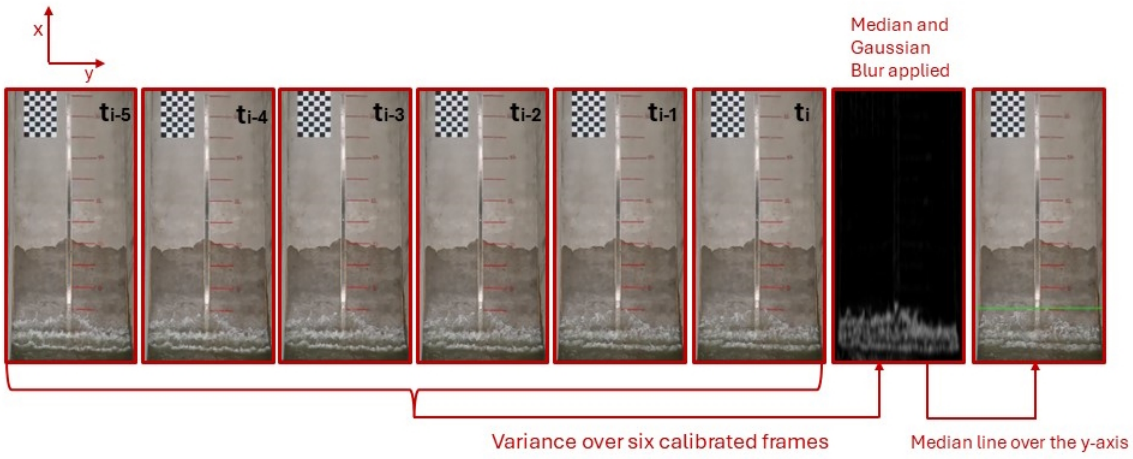

Figure 3.12: Video process procedure

The values of the median line are stored as pixel instances based on the zero coordinates of the frame O(0,0) (top left of the frame), which are translated to diagonal run-up on the slope. Next, the diagonal run-up is transformed into vertical run-up using a trigonometric transformation (Equation 3.10). More details about this procedure can be found in Appendix C

$$R_u = \frac{R_{u_{diagonal}}}{\sqrt{1^2+3.6^2}} - d_m \tag{3.10}$$

3.3.2. Laser Scanner

The laser scanner raw data was retrieved, calibrated and interpolated in spatial and temporal resolutions of d_x=0.1 m and d_t=0.02 s by D. Dermentzoglou. The retrieved signals are used later to calculate wave run-up and virtual overtopping on the dike.

3.3.3. Wave Run-Up Data processing

Video camera data processing

Initially, the pixel-to-meter correspondence is determined by opening the calibrated frames on their perspective sizes. The calibrated image is based on the chessboard pattern, so the real pixel-to-meter correspondence can be determined from that. Moreover, at this stage, it is essential to determine where the beginning coordinates are in the defined perspective size. The point (0,0) is always in the upper left corner of the frame. Details for the pixel-to-distance correspondence can be found in Appendix C

For the processing, several filters are applied. Based on the perspective size of the frame of the different videos, the maximum and minimum run-up on the slope are determined. This is mainly done to avoid noise coming from the parts of the dike where wave run-up is not to be expected. The signal that is acquired from the implementation of thresholds can be visualized for a sample of the run SM-01 Figure 3.13 top. A moving median filter is then applied to remove outliers from the signal that are greater than 1 standard deviation and by using a window of 21 frames (0.35 sec) Figure 3.13 middle. Lastly, a moving mean filter of 20 frames (0.33 sec) is applied, to smooth the signal that would otherwise have sharp unnatural peaks Figure 3.13 bottom.

In experiment SM-01, applying a moving mean filter resulted in an RMSE of 0.068 meters, which falls within the expected range. The bias was -0.017, indicating a 2% difference in the signals.

Laser scanner data processing

For processing the data acquired from the laser scanner, the layer thickness method was used (Hofland et al., 2015). First, the dry slope of the dike is identified as the mean value of the first few seconds of the interpolated LS signal, before waves are generated from the wave board. Furthermore, it is assumed that the vertical distance (run-up) that the water can cover in a time step (5 ms) cannot exceed 0.5 m Figure 3.14a. Finally, a minimum thickness threshold was applied to the water layer thickness data to eliminate noise caused by minor displacements of the laser scanner. Multiple thresholds, ranging from 1 to 5 cm, were tested to determine the optimal value. To assess the wave run-up the peaks of the run-up signal are identified Figure 3.14 b.

3.3.4. Wave run-up Validation

Video camera run-up validation

In order to validate the retrieved signals, a manual detection of the peaks is performed by visually monitoring the footage of experiments.

For the manual detection of the run-up, short two minute samples of three experiment's video footage were used, each consisting of 7200 frames. For each frame, the maximum value of run-up is hand picked. As a result, higher values of run-up are expected from this method, as in the video process method, the median line is used to estimate the run-up values for every frame. The results of this comparison are found in Figure 3.15. Table 3.2 shows the Pearson correlation coefficient (R), the root mean square error (RMSE), and the bias between the two signals.

Table 3.2: Comparison of the video process and the manual peak detection

Experiment	R	RMSE (m)	Bias
SM-01	0.951	0.068	-0.017
SM-03	0.947	0.078	-0.022
SM-20	0.949	0.073	-0.020

Another useful method in validating the run-up results is comparing them with the dike flotsam measurements. Flotsam, which is debris floating on water and subsequently deposited on the dike, creates a visible line on the dike. In these experiments, flotsam was measured after the end of the day, while data is missing for multiple experiments that were conducted the same day. In Figure 3.16 the measured run-up is plotted against the measured flotsam on the dike. From the value of the coefficient of determination R^2 = 0.85, it can be concluded that there is a strong agreement between the run-up results and the flotsam measurements on the dike. The flotsam values are higher than the run-up values in almost all cases, which is expected as flotsam can be used for the estimation of the maximum run-up on a dike, while here it is compared with the 2% exceedance.

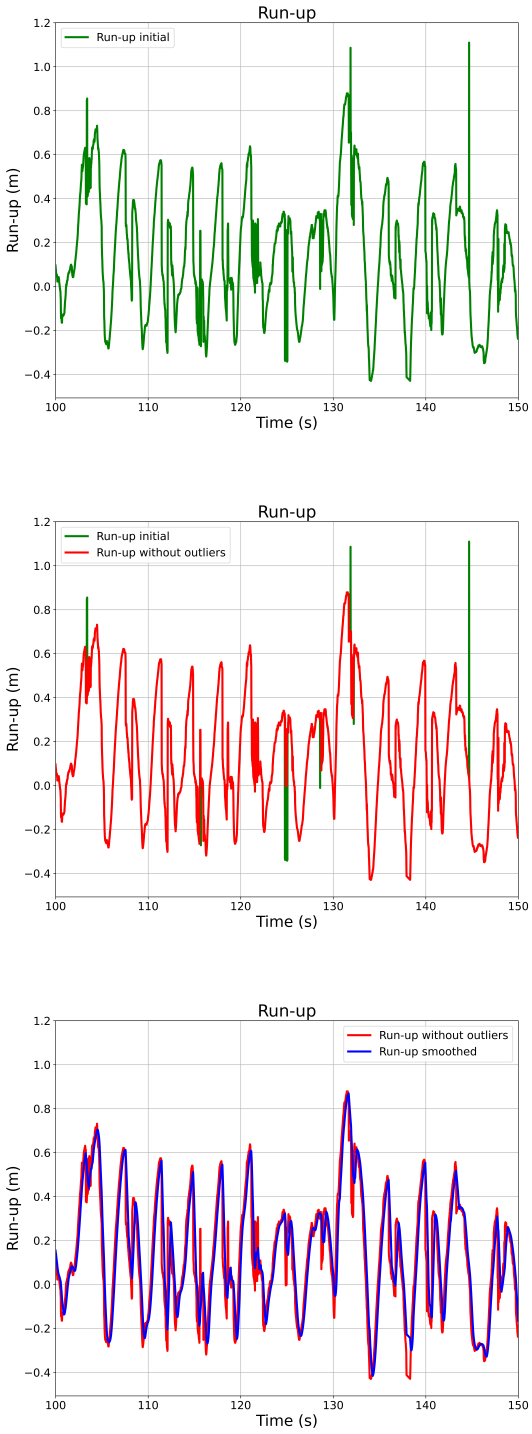

Figure 3.13: Run-up signal from SM-01, the subfigures show a) initial Signal, b) modified signal with removal outliers, c) modified signal with moving mean

The number of incoming waves that become run-up events (N_w) is different than the measured number of waves reaching the toe of the dike, resulting from the zero-down crossing analysis (N_{wm}). This is due to the reflection of waves from the dike slope and waves which are not detected by the video process due to their size. The number of waves detected by the process N_w, is commonly preferred (EurOtop, 2018) to be used. The number of waves in long-duration experiments is an order of magnitude larger than that of short-

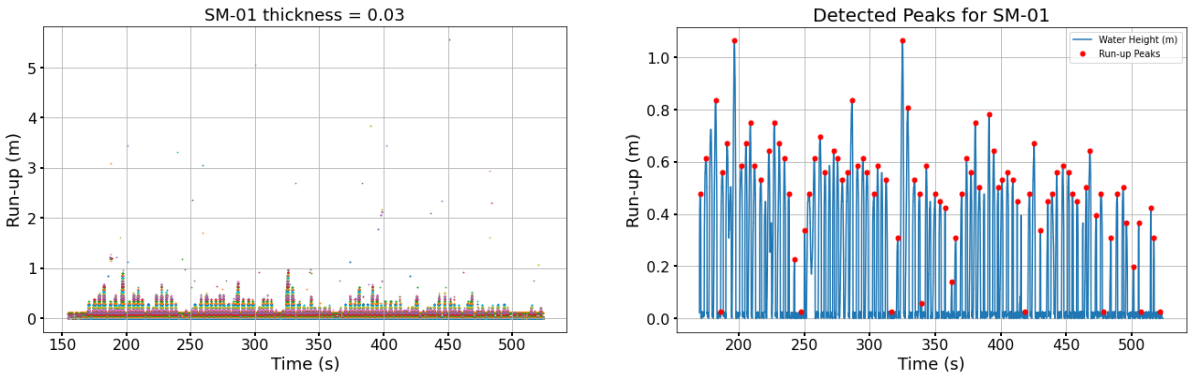

Figure 3.14: Laser scanner run-up signal from SM-01. a) Run-up signal filtering, b) Detection of peaks

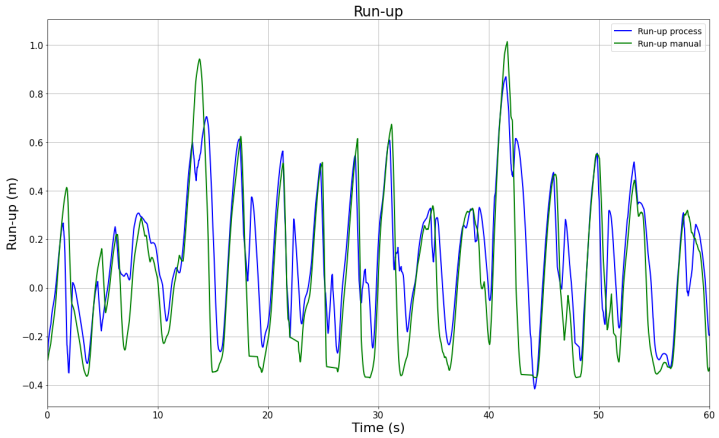

Figure 3.15: Comparison of the run-up signals of the video and the manual process of test SM-01

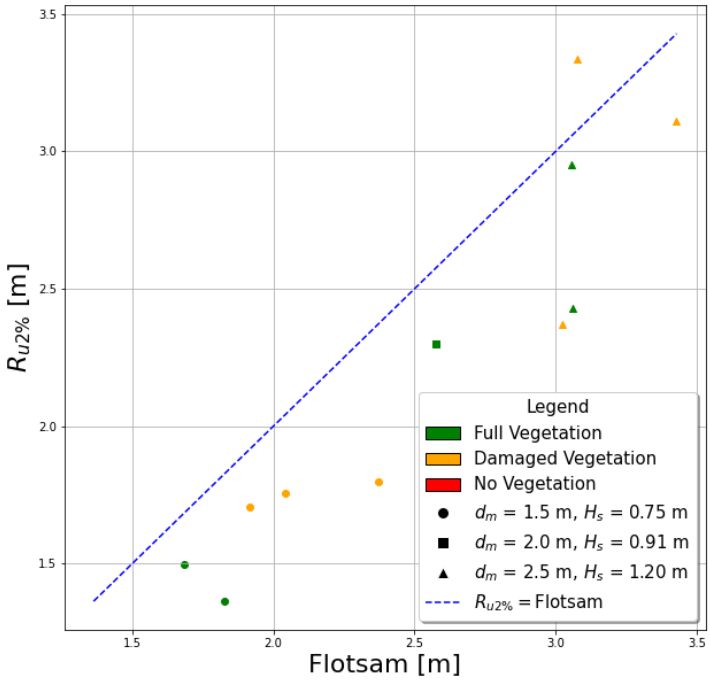

Figure 3.16: Comparison of the run-up with the flotsam measurements on the dike and their correlation

duration experiments. This leads to different results in the run-up statistics. This is visible in Figure 3.17 and Figure 3.18, where the histograms and the empirical cumulative distribution function (eCDF) of the peaks of the experiments SM-01 and SM-06 are visible. The two experiments have the same wave characteristics but differ in number of waves.

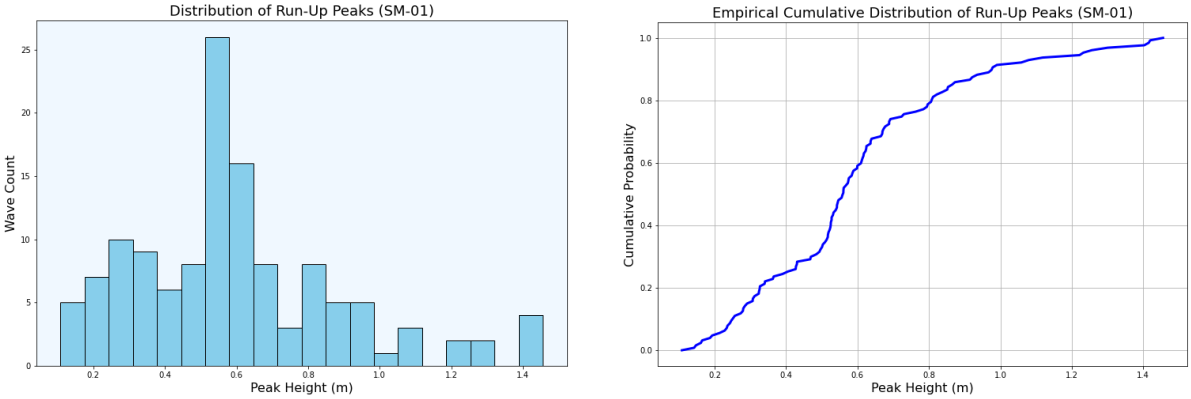

Figure 3.17: Distribution of run-up peaks of SM-02. a) Histogram of run-up peaks, b) empirical cumulative distribution function plot of run-up peaks

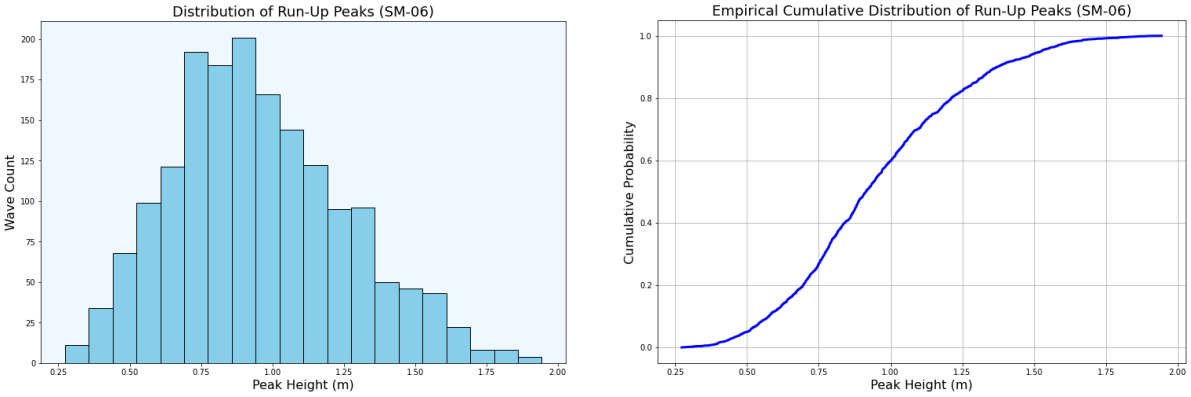

Figure 3.18: Distribution of run-Up peaks of SM-06. a) histogram of run-up peaks, b) empirical cumulative distribution function plot of run-up peaks

Laser scanner run-up validation

The thickness threshold was determined by analyzing the bias between the laser scanner and the visual detection method. A threshold of 3 cm consistently resulted in the lowest bias, making it the optimal choice (Figure 3.19,Table 3.3).

Table 3.3: Results of validation of the video process by comparison with the manual peak detection

Thickness (m)	SM-01	SM-03	SM-20
0.01	0.202	0.322	0.268
0.02	0.069	0.124	0.111
0.03	0.033	0.032	0.037
0.04	0.050	0.074	0.079
0.05	0.053	0.108	0.091

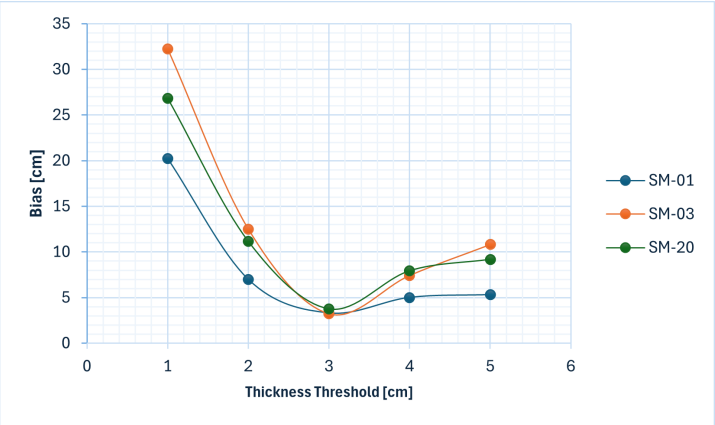

Figure 3.19: Validation of the laser scanner signal by comparison with the manual peak detection for five different thicknesses

3.4. Wave Overtopping Measurements

Apart from wave run-up, it is also possible to measure virtual overtopping using a LS, by measuring the volumes that exceed a specific height. The height investigated was a range of virtual crests. A volume can be measured by calculating the thickness of the waves on the slope for each time step of the experiment. The thickness time series is later multiplied by the front velocity time series of the waves. The velocity of each wave is calculated as the derivative of the front displacement. For this calculation, it is assumed that the front velocity is constant and acts as the velocity at which the water flows over the virtual crest (Oosterlo et al., 2019). This method approximates the volume above the virtual crest level and is applied in cases where real overtopping events occur. A more direct approach to determining virtual overtopping volumes would be to measure the water volume above the virtual crest line directly, without relying on velocity estimation. The cumulative volume for every experiment is calculated by the summation of the individual virtual overtopping events. From this volume, it is possible to derive the mean discharge as Equation 3.11 shows, where D is the duration of every experiment. The virtual crest values were picked in a range from 0 to 5.5 m above still water level. It is important to note that for experiments without real overtopping the water quantities are expected to run-up the slope and then run-down. For this reason, the negative velocities are calculated as run-down and are not included in the calculations of overtopping.

$$q = \frac{\Sigma V_i}{D} \tag{3.11}$$

4

Results

This chapter presents the results obtained from the measurements and methods detailed in chapter 3.

section 4.1 is an analysis of the characteristics retrieved from the analysis of the waves. Several parameters are compared to understand the influence of salt marsh on mitigating the magnitude of the spectral and wave characteristics. The subscripts used in this chapter are classified as offshore conditions (subscript o) and nearshore conditions at the toe of the dike (subscript t). In section 4.2, the wave run-up results from the video footage are presented. The primary aim of this chapter is to understand the variations in wave run-up across different vegetation and storm conditions scenarios and to compare these findings with existing results and equations from the literature. It is important to note that the results of the long-duration experiments (1000+ waves) are expected to lead to a better estimation of reality than the short-duration experiments (100 waves). For this reason, the results of the long-duration experiments are going to be analyzed, while the results of the short-duration experiments can be found in section D.1.

In section 4.3 the results derived from the laser scanner data processing are investigated. In the first part of this section, the results of run-up from the laser scanner measurements are calculated and compared with the results of run-up from the video process method. In the second part, the overtopping discharges are calculated and compared with equations found in the literature. Moreover, an attempt is made to quantify the decrease of the overtopping quantities according to vegetation conditions.

4.1. Wave Analysis

Comparing the significant wave height $H_{1/3}$ and the spectral wave height H_{m0} provides insights into whether these two metrics reflect different characteristics of the wave field. In Figure 4.1a the comparison of the two parameters for the offshore location is presented. At this location, the two parameters have similar values, with the majority being slightly higher for H_{m0}. The bias between the two parameters is 0.04 m. In Figure 4.1b, the results for the location near the toe of the dike have a greater difference between the two parameters, with the bias reaching 0.06 m. This is due to the presence of lower-energy wave components in the energy spectrum, which do not influence the highest one-third of the waves ($H_{1/3}$) but contribute to the total energy, leading to higher values of the spectral parameter (H_{m0}).

Another important comparison for wave analysis is that of the spectral and peak periods. The peak period, T_p, is calculated as the period corresponding to the highest density in the spectrum. This comparison is important as an initial comparison of the two periods before the effect of the vegetation. The estimated relation for the two parameters in deep waters for a JONSWAP single peaked spectrum is $T_{m-1,0} = 1.1T_p$. In Figure 4.2a, the comparison of these two periods is analyzed for the offshore location. The graph results are scattered between the lines $T_{m-1,0} = T_p$ and $T_{m-1,0} = 0.8T_p$ so the initial assumption for the deep water relation proves not to be valid. From a first analysis, it is evident that the worse the vegetation conditions, the higher the values of the peak period compared to the spectral period. This can be explained by the small difference in the spectrum between experiments with different vegetation conditions. In Figure 4.2b the spectrum between good and damaged vegetation is almost identical. On the other hand, the scenario without vegetation has lower values of energy.

Investigating these parameters near the dike toe is also of great importance. Understanding the change of wave period between offshore and the dike toe can provide insight on how vegetation affects the wave

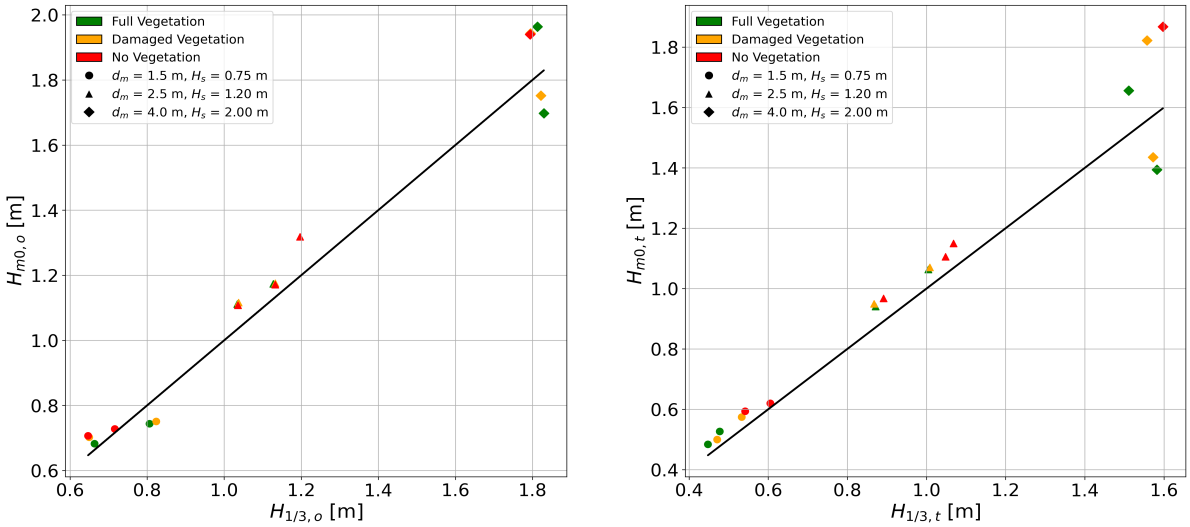

Figure 4.1: Comparison of the spectral wave height H_{m0} and the significant wave height $H_{1/3}$ for: a) the offshore location and b) the toe of the dike.

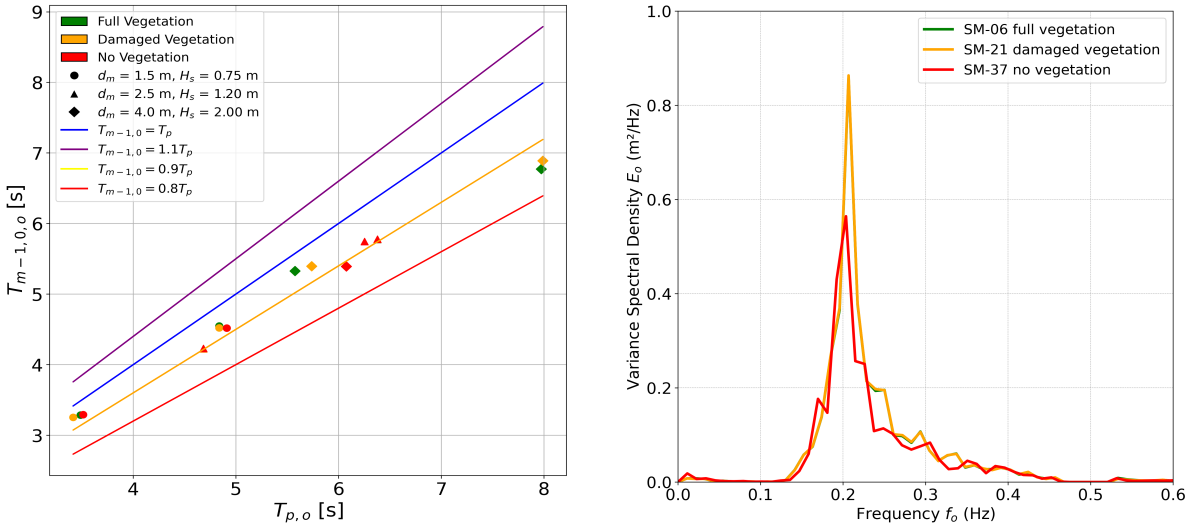

Figure 4.2: Comparison of spectral period and peak period at the offshore and the explanation based on their energy density spectrum for the incoming waves

spectrum and contributes to wave attenuation. Figure 4.3a shows a comparison of $T_{m-1,0}$ and T_p at the toe of the dike. For this case, $T_{m-1,0} \approx 0.8 - 1.1\,T_p$. Here, it is clear that for different storm conditions, vegetation quality is of great importance. In general, the results reveal that the better the quality of vegetation, the higher the spectral period $T_{m-1,0}$ measured in the experiments. In Figure 4.3b it is evident that for frequencies above 0.1 Hz the better the vegetation conditions the greater the decrease in spectral density. This means that a higher dissipation of energy results in higher values of the spectral period $T_{m-1,0}$. At the same time, low-frequency peaks are formed for frequencies lower than 0.1 Hz.

Figure 4.4 shows the reduction of the significant wave height H_{m0} from offshore to the toe of the dike. This graph reveals various aspects of attenuation based on both vegetation and water depth. The highest reduction in H_{m0} is recorded for the low-condition experiments. The presence and condition of vegetation in these experiments significantly affect the reduction of this parameter. Under low storm conditions, the reduction in H_{m0} ranges from 14% without vegetation to nearly 30% with good and damaged vegetation. The range of values decreases for medium storm conditions between 5 and 15%, meaning that the reduction has halved from low to mid conditions. In high storm conditions, the reduction range is between 4 and 19% showing a similar dissipation pattern with the mid conditions. It is once again visible that the higher storm

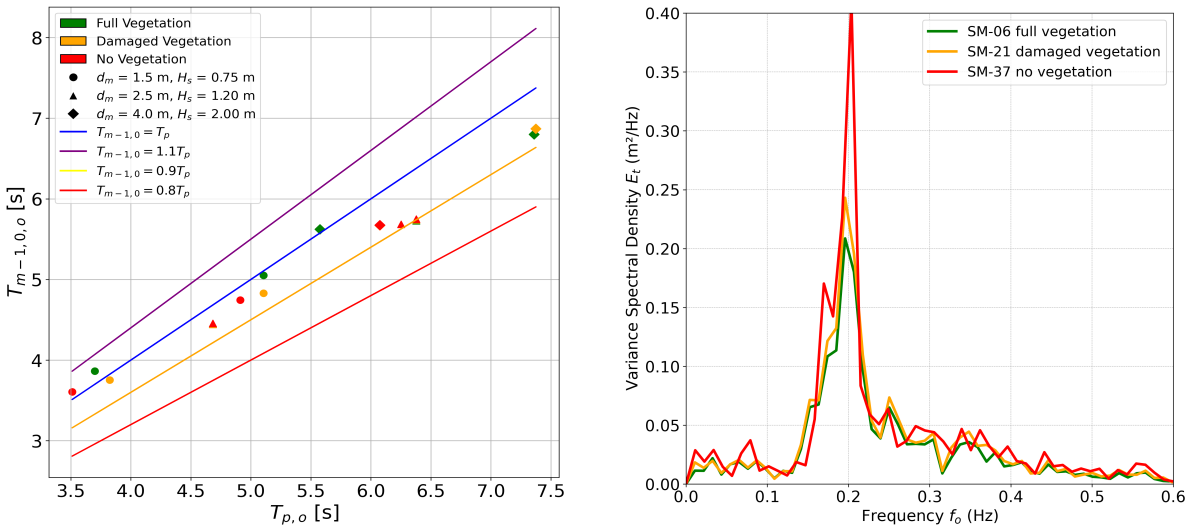

Figure 4.3: Comparison of spectral period and peak period at the toe of dike and the explanation based on their energy density spectrum for the incoming waves

conditions and water depth lead to a different pattern of attenuation. The same hypothesis has been made in Vuik et al. (2016) where the reduction in the significant wave height is in the range of 25 to 50%.

In general, for lower wave conditions, the reduction in H_{m0} is the highest, indicating that vegetation plays an important role in wave attenuation. For increased water depths, the reduction decreases, suggesting that the attenuation from the vegetation has a diminished effect. Under the highest water depth and largest wave height, there is increased dissipation once again, because of the large wave height, leading to waves that are dissipated more efficiently by the salt marsh and the foreshore. The results of this study are consistent with results on attenuation from previous research conducted in a large-scale wave flume, where for low conditions (H_s=0.2-0.4 m) the dissipation of energy was up to 17.9%, for mid conditions (H_s=0.6 m) the dissipation dropped to 14.7% before increasing again to 16.9% for the highest conditions (H_s=0.7 m) (Möller et al., 2014).

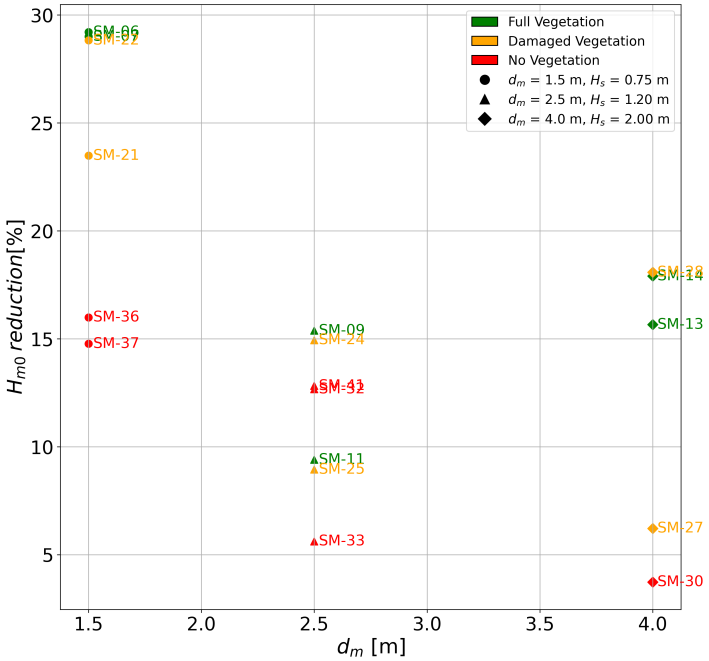

Figure 4.4: Reduction of H_{m0} in % from the offshore to the dike. The reduction is calculated as $(H_{m0,t} - H_{m0,o}) \times 100 / H_{m0,t}$

4.2. Wave Run-up

In this chapter, the results of run-up from the experiments are initially discussed in subsection 4.2.1. In subsection 4.2.2 the run-up results are compared with existing empirical equations from the literature to assess whether these equations accurately predict run-up on a living dike. It is crucial to note that the experiments of the highest storm (H_s = 2.00 m and d_m = 4.00 m) are not included in the analysis. These conditions resulted in a significant number of overtopping events during the experiment, in some cases exceeding 1 in 10 waves. This made it impossible to calculate key run-up parameters such as $R_{u2\%}$. For this reason, only the results from low- and mid-condition storms are investigated for their run-up events. Another important observation is that short-duration experiments (100 waves) yield significantly different results than long-duration experiments (≥ 1000 waves). The average difference between the short- and long-duration experiments is 0.15 m. This difference is likely due to the significant variation in the number of waves, even though the waveboard operates with the same stirring file. The short-duration experiments correspond to the initial 100 waves of the long-duration experiments, indicating that the analysis of the longer experiments provides a representative understanding of both categories. For this reason, this study focuses on analyzing the results of 1000 waves. In the final part of this chapter, the results of the run-up measured by the laser scanner device are compared with empirical equations from the literature and the results of the video process method to assess the difference in accuracy.

4.2.1. Wave run-up comparison between experiments

Figure 4.5 shows the probability of exceedance for run-up heights under low and mid storm conditions. Each graph compares these probabilities for experiments with the same storm conditions but different vegetation quality. The nearly parallel lines indicate that poorer vegetation quality is associated with higher run-up for the same probability of exceedance. In Figure 4.5a the 2% exceedance run-up difference between good and damaged vegetation conditions is 0.15 m, while the difference between damaged vegetation and no vegetation scenarios is 0.28 m. Here it is evident that the difference between the two vegetated scenarios is lower than the difference between the damaged vegetation and no vegetation scenarios. The same behavior is observed in Figure 4.5b where the difference in exceedance run-up 2% between good and damaged vegetation is 0.20 m, and the difference between damaged vegetation and no vegetation conditions is 0.60 m. These results reveal a significant relationship between run-up and vegetation conditions. The run-up increases with poorer vegetation, and the rate of increase is greater with lower vegetation quality.

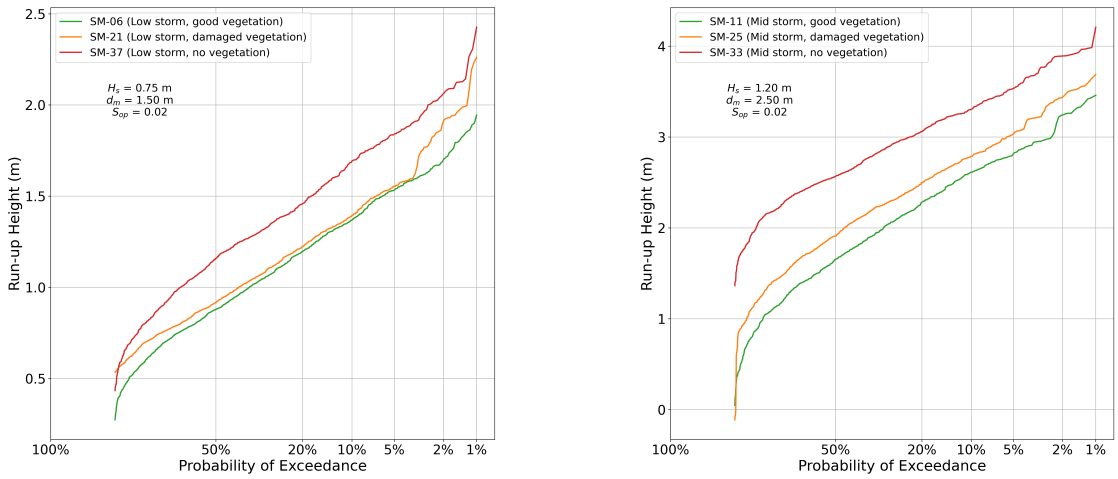

Figure 4.5: Run-up heights and their probability of exceedance for a)experiments with low storm conditions and b)experiments with mid storm conditions

In Figure 4.6 the measured run-up is plotted against H_{m0} for an initial comparison of the two parameters, with the significant wave height measured at the toe of the dike. According to the equations in section 2.3, $R_{u2\%}$ is proportional to H_{m0}, so a pattern of increase is expected for higher conditions. The general relationship between the two values can be partly explained by the linear regression fitlines that were produced for

each of the vegetation conditions. These lines show a linear trend for each category, with the strongest linear relationship observed for good vegetation conditions. By comparing the run-up of experiments conducted under identical storm conditions, but with different vegetation quality, it can be concluded that lower vegetation quality results in a higher wave height at the toe and, as a result, a higher wave run-up on the dike. The same conclusion is drawn in Keimer et al. (2021), where the run-up levels decreased as the height of the vegetation increased. Regarding the initial hypothesis that water depth may play a crucial role, these cases do not provide sufficient evidence to substantiate it. The results analyzed above were consistent with the results found in Marin-Diaz et al. (2023), where the run-up and the wave height for a foreshore covered in salt marshes also revealed a strong linear trend.

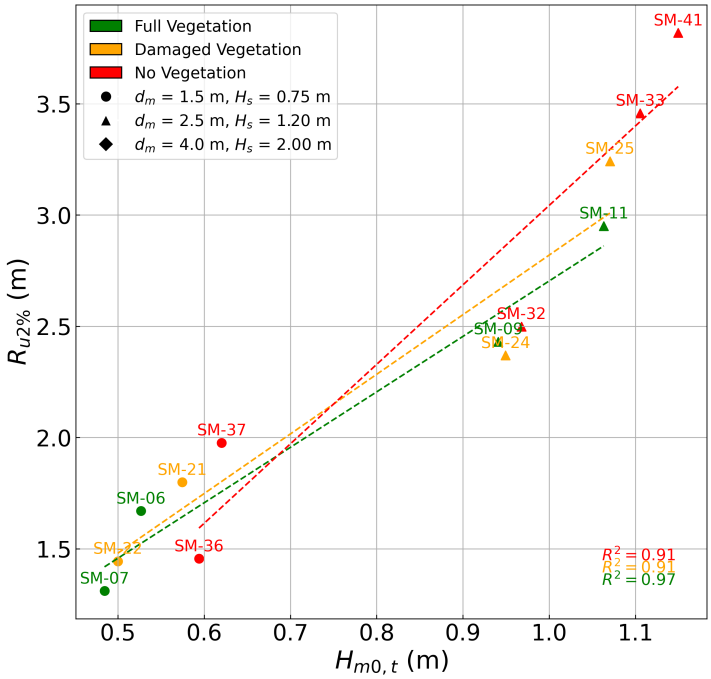

Figure 4.6: $R_{u2\%}$ *vs* $H_{m0,t}$. The significant wave height is calculated for a location close to the toe of the dike

In Figure 4.7 wave run-up is plotted in the form of box plots. The experiments are categorized according to the wave characteristics at the offshore location. Every category reveals the results of the same wave conditions and water depth for the three vegetation conditions. The difference in run-up between the various types of vegetation is noticeable. The better the condition of the vegetation, the lower the run-up values. This is evident from the fact that 50% of the run-up values (represented by the boxes) in experiments with full vegetation are lower compared to those in experiments with damaged vegetation, while the scenarios with damaged vegetation have lower values than the scenarios without vegetation. Furthermore, the $R_{u2\%}$ and the median run-up values are generally higher in experiments with damaged vegetation compared to the full vegetation, while the conditions without vegetation lead to the highest values. The only exceptions are the SM-09 and SM-24 experiments, with SM-09 exhibiting particularly high values, comparable to those of SM-32.

Box plots are also used to compare the dimensionless run-up values between experiments. The dimensionless run-up is calculated as the ratio of the run-up height to the significant wave height, H_{m0}, measured at the toe of the dike. In Figure 4.8 the results for the dimensionless run-up exhibit very similar values for waves with a mild slope (S_{op} = 0.04) across both categories of storm conditions (H_s = 0.75 m and H_s = 1.20 m). This demonstrates that the reduction in run-up is not directly attributed to the presence of vegetation itself, but rather to the decrease in H_{m0} caused by the vegetation. It also suggests that run-up primarily depends on the wave height at the dike toe. A similar conclusion can be drawn by analyzing the mild steepness waves (S_{op} = 0.02). In this case, nearly all the experiments, regardless of the wave and depth conditions, yield similar results. Only the highest conditions examined (H_s = 1.20 m) show a gradual change in dimensionless run-up based on the quality of the vegetation.

In Figure 4.9 a comparison of dimensionless run-up can be found for different water depths at the off-

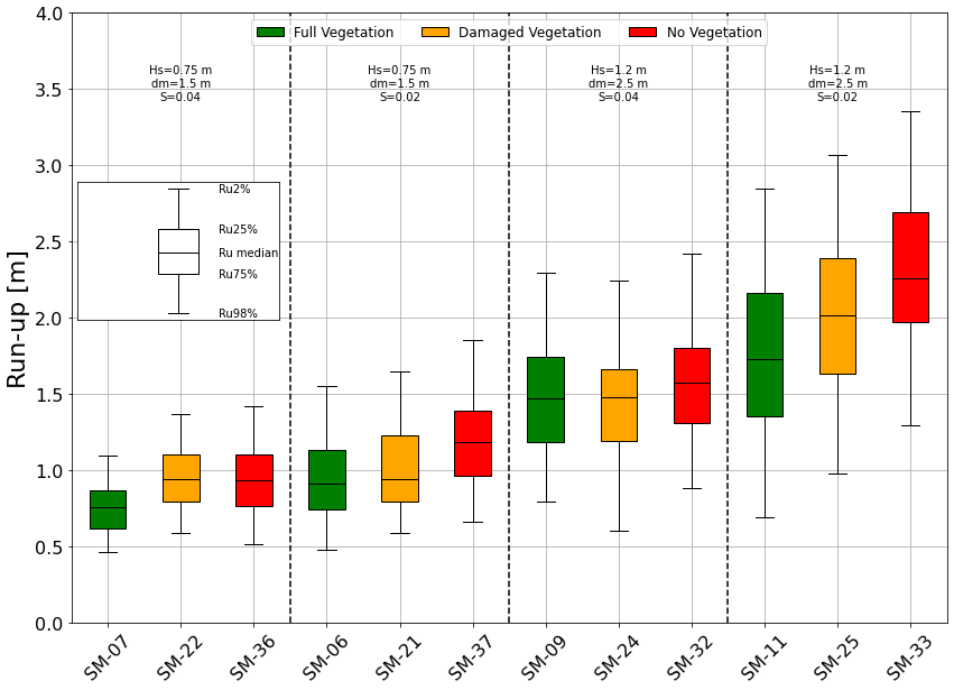

Figure 4.7: Run-up values compared for the same conditions of storm with different conditions of vegetation

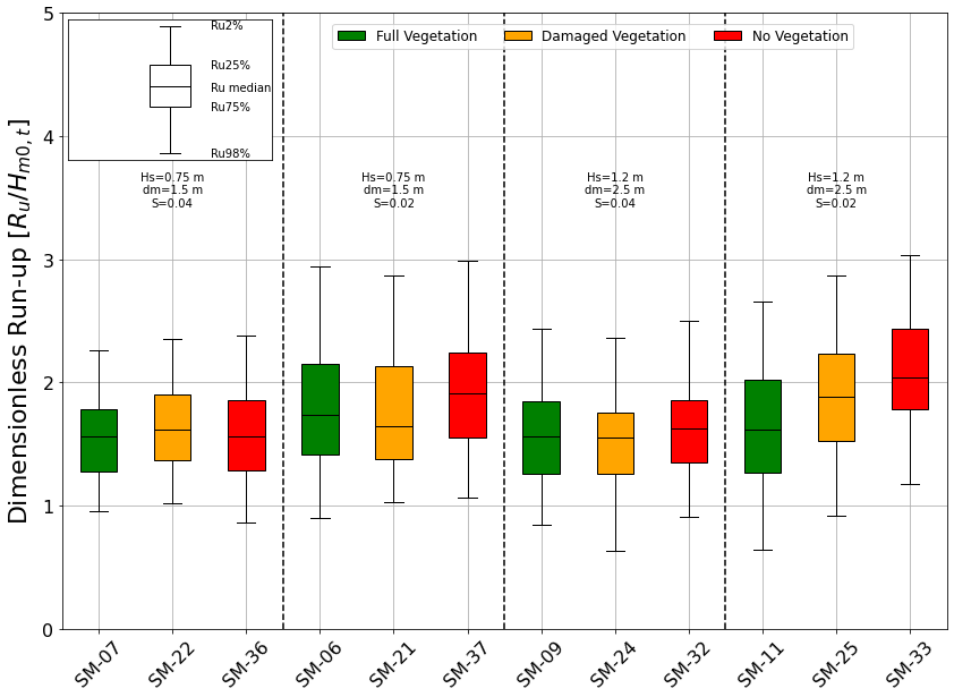

Figure 4.8: Dimensionless run-up values compared for the same conditions of storm with different conditions of vegetation

shore location. This comparison is important as it enables us to identify the influence of water depth in the attenuation of waves and thus the reduction of the run-up heights. The graph reveals that a fully vegetated foreshore leads to lower run-up values than at the same conditions with less vegetation. The water depth heavily influences the results. As the water depth increases, differences in run-up results between various vegetation conditions decrease. Moreover, the higher the wave conditions in the same water depth (increased wave steepness) leads to a higher difference in run-up between fully vegetated, damaged, and no vegetation scenarios. The difference between SM-06 and SM-37 is 0.47, while the difference for the experiments SM-07

and SM-36 is 0.14.

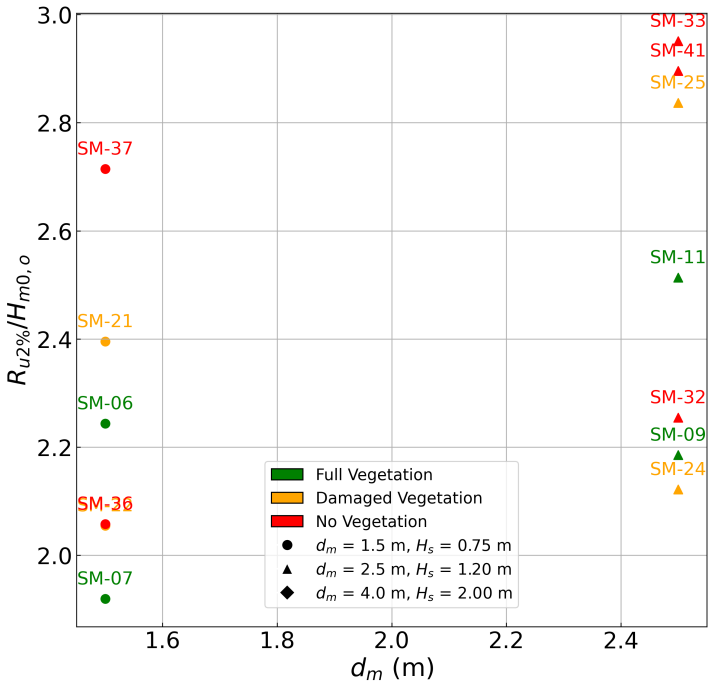

Figure 4.9: Dimensionless run-up against the water depth above the salt marsh d_m for the offshore location

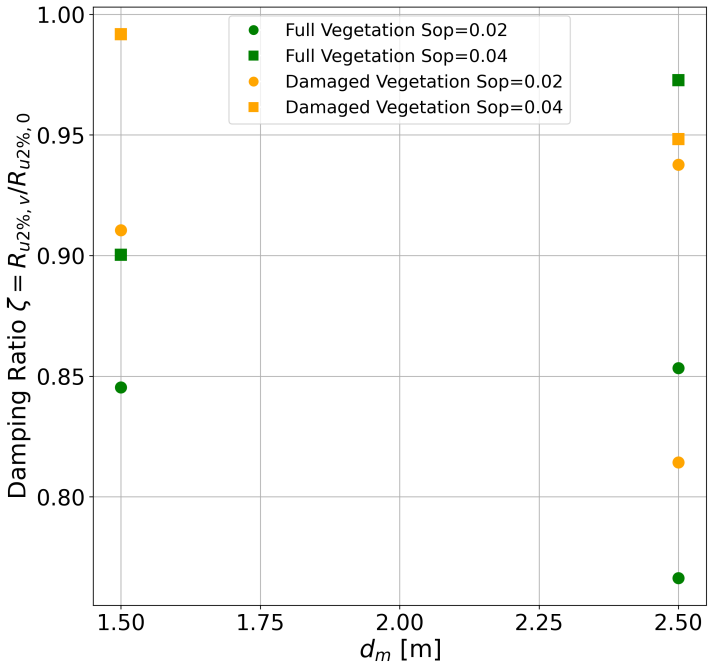

Figure 4.10: Damping ratio of the run-up for full and damaged vegetation conditions

At this stage of the study, the relationship between vegetation and run-up reduction is evident. A parameter that has been used in previous research to assess the efficacy of vegetation in mitigating run-up is the damping ratio ζ, as mentioned in section 2.3 (Manousakas et al., 2022). This parameter is the ratio of $R_{u2\%}$ in tests with vegetated foreshore conditions to tests with a bare foreshore (mowed vegetation scenarios). Comparison of the ratios between the full and damaged vegetation conditions can be crucial to understanding the mitigation properties of vegetation on waves and calculating the differences in wave run-up. In Figure 4.10

it is visible that the damping ratio of fully vegetated foreshores is in most of the cases lower than the ratio of damaged vegetated foreshores for both low and mid-storm conditions. In mid-storm conditions (H_s = 1.20 m, d_m = 2.50 m), it is visible that the damping ratio has lower values than in the low storm conditions (H_s = 0.75 m, d_m = 1.50 m). Furthermore, in low storm conditions, the percentage difference between the ratios of good and damaged vegetation reaches 7.1% and 9.1%. These findings indicate that the well-vegetated foreshores led to significant reductions in run-up events, up to 9%, which could directly influence the design and enhancement of sea dikes. For the medium storm conditions the percentage difference in the ratio ranges between 6% and 9%. The average difference between vegetated to non-vegetated foreshores for run-up is 10.3%. These findings are consistent with previous research on artificial vegetation, which demonstrated an average run-up reduction of 9.6% (Keimer et al., 2021). On the other hand, the average difference between damaged vegetation to a fully vegetated foreshore is at 7.7% revealing that the difference between the two vegetated categories is lower than the difference between vegetated and non-vegetated foreshores.

4.2.2. Wave run-up comparison with literature

In this part, it is crucial to undertand if the calculated run-up results can be accurately estimated using empirical equations available in the literature. In Figure 4.11 the comparison between the measured and the predicted values according to EurOtop (2018) is presented. The results reveal that all of the data points, except one, are located within the 90% confidence band of the equations. The test that is located outside the upper confidence interval is an experiment with no vegetation, mid-storm conditions (H_s = 1.20 m), and d_m = 2.5. Its run-up 2% value is significantly higher than the other experiments. Finally, it is noteworthy that the results from the mild steepness waves (S_{op} = 0.02) are located above the predicted values while the results of the steep waves (S_{op} = 0.04) are located below it.

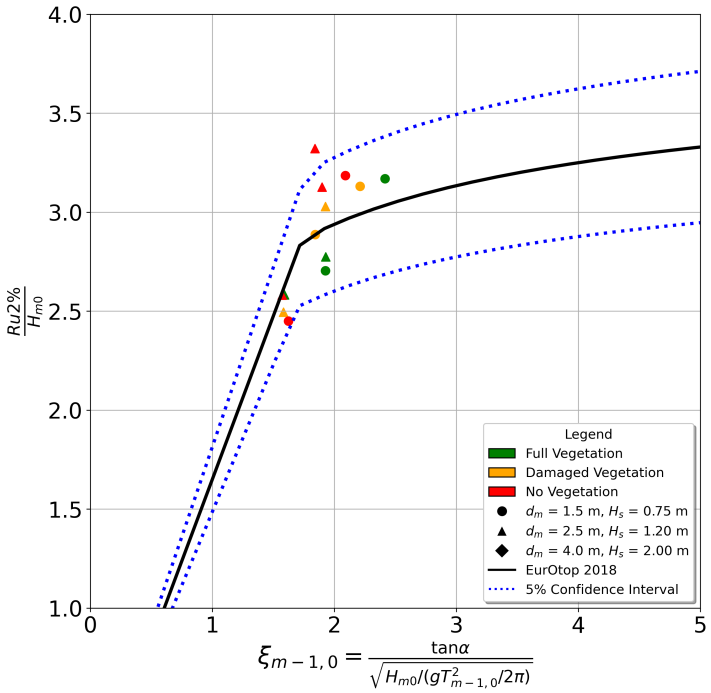

Figure 4.11: Dimensionless run-up using the spectral parameters at the Toe of the dike. The results are compared with the empirical equations from EurOtop (2018).

Figure 4.12 is a plot of the same equations, using $H_{1/3}$ in the place of H_{m0} for the calculation of the dimensionless run-up and $\xi_{m-1,0}$. This is done in order to check if the results are in better agreement with the equations, as suggested by Lakerveld, 2024. This results in multiple points falling outside the 5% upper confidence band.

To verify whether the results align with reality, the correlation between the dimensionless run-up and $\xi_{m-1,0}$ and the root mean square error (RMSE) between measured and expected values are calculated. These results can be found in Table 4.1, where its shown that using H_{m0} as initially suggested in the formulas leads to a higher correlation and lower RMSE in comparison to the case when $H_{1/3}$ is used. The relative error between

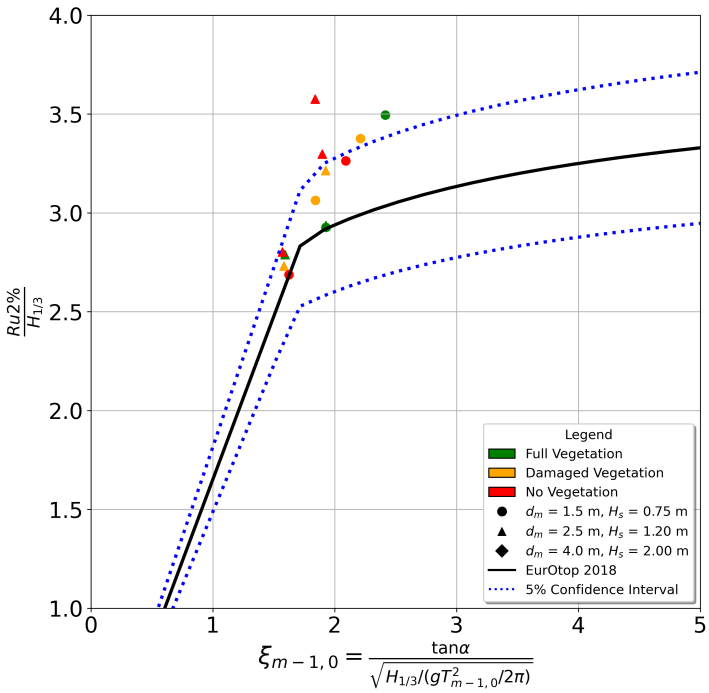

Figure 4.12: Dimensionless run-up using $H_{1/3}$ instead of H_{m0} at the toe of the dike. This attempt was made to enable comparison with the results presented in Lakerveld (2024)

the predicted and measured values for this case is 5%.

Table 4.1: Correlation of dimensionless run-up with ξ and RMSE between predicted and calculated values for different conditions

Method	Correlation	RMSE
H_{m0}	0.85	0.18
$H_{1/3}$	0.77	0.30

The results of run-up are also compared with the equation proposed by Van Gent et al. (1999) (Figure 4.13). Equation 2.10 which is derived from results generated from a computational model, does not describe well the measured run-up. On the other hand, the predicted values from Equation 2.10 agree with the results of this study. The root mean square error between the calculated and predicted values using the equation is RMSE = 0.19. It is also evident that for values of $\xi_{m-1,0} < 2$ the equations from EurOtop (2018) and Van Gent et al. (1999) are very close.

4.3. Wave run-up and wave overtopping from the laser scanner

4.3.1. Wave run-up from the laser scanner

The run-up results derived from the laser scanner procedure as mentioned in subsection 3.3.3 are compared with the results from the video camera procedure. In Table 4.2 the results of $R_{u2\%}$ measured with the laser scanner are compared with the results measured with the video camera. The results reveal an average difference of 7% (0.13 m) between the two devices. In previous studies in the Delta Flume, the difference between the two methods reaches 13.5% (Cete, 2019) and 13.0% between visual and laser scanner measurements (Hofland et al., 2015).

The results in Figure 4.14 show that the majority of the experiments exist within the 90% confidence interval of EurOtop (2018). Three of the experiments in the low-condition tests are not included in the error band 90%. The measured run-up of the laser scanner was in general smaller in comparison to the predicted values from the equations, which is attributed to the thin layer of water forming at the edge of a run-up wave and is untraceable with the used method. The root mean square error of the predicted and calculated values is RMSE=0.31.

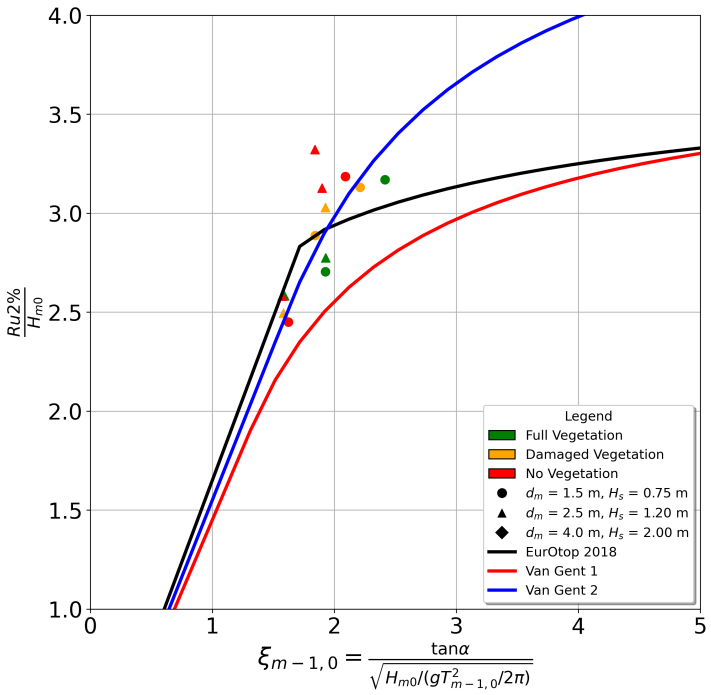

Figure 4.13: Dimensionless run-up using H_{m0} at the toe of the dike and the predicted values from Van Gent et al. (1999)

Table 4.2: Results of run-up from the camera and laser scanner procedure and their comparison

Experiment	h	Hm0 [m]	Tm-1,0 [s]	CM Run-Up 2%	LS Run-Up 2%	Difference [m]	Difference %
SM-01	4.40	0.56	3.36	1.03	1.09	0.06	5.54
SM-02	4.40	0.64	4.65	1.50	1.25	0.24	16.29
SM-03	5.40	1.05	4.27	2.29	2.58	0.29	12.56
SM-05	4.40	0.55	3.37	1.27	1.15	0.11	9.07
SM-06	4.40	0.74	4.55	1.67	1.48	0.18	11.06
SM-07	4.40	0.68	3.29	1.08	1.04	0.04	3.44
SM-08	4.40	0.64	4.63	1.36	1.46	0.09	6.93
SM-09	5.40	1.11	4.23	2.43	2.45	0.03	1.03
SM-10	4.90	0.81	5.62	2.30	2.15	0.14	6.25
SM-11	5.40	1.17	5.77	2.95	2.81	0.14	4.86
SM-16	4.40	0.57	3.35	1.27	1.37	0.10	8.16
SM-17	4.40	0.65	4.63	1.76	1.59	0.16	9.30
SM-18	5.40	1.06	4.27	2.43	2.48	0.05	2.17
SM-19	5.40	1.23	5.76	3.11	2.95	0.16	5.25
SM-20	4.40	0.56	3.36	1.19	1.20	0.01	0.53
SM-21	4.40	0.75	4.52	1.80	1.62	0.18	9.91
SM-22	4.40	0.70	3.25	1.44	1.15	0.30	20.60
SM-23	4.40	0.64	4.64	1.69	1.62	0.07	4.12
SM-24	5.40	1.12	4.22	2.37	2.45	0.08	3.55
SM-25	5.40	1.18	5.78	3.24	2.92	0.32	9.88
SM-32	5.40	1.11	4.23	2.50	2.56	0.07	2.66
SM-33	5.40	1.17	5.78	3.46	3.15	0.30	8.74
SM-36	4.40	0.71	3.29	1.46	1.37	0.08	5.80
SM-37	4.40	0.73	4.52	1.98	1.92	0.05	2.67
					Average:	0.13	7.00

4.3.2. Wave overtopping from the Laser Scanner

To calculate the virtual overtopping volumes, the water layer thickness time series from the run-up is used. According to EurOtop (2018) for the equations from section 2.4 a distinction has to be made according to the Irribaren number $\xi_{m-1,0}$. If $\xi_{m-1,0} > 2$ then the waves enter the surging category and are assumed to be

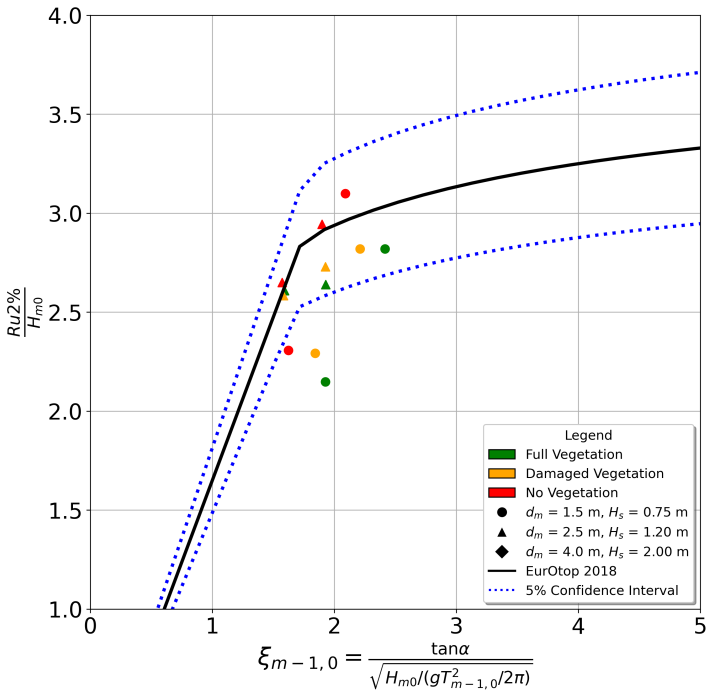

Figure 4.14: Laser scanner dimensionless run-up using the spectral parameters for the toe of the dike. Comparison with quations from EurOtop (2018).

non-breaking waves.

In Figure 4.15 the results of the approach for low and mid conditions are compared with the EurOtop (2018) equations. In Figure 4.15a the results are positioned within the confidence limits, showing that the empirical equations accurately predict virtual overtopping. In Figure 4.15b, for low values of freeboard, the results have higher values than the equation and its exceedance values. However, for medium and high freeboard values, the results are well within the 90% confidence band.

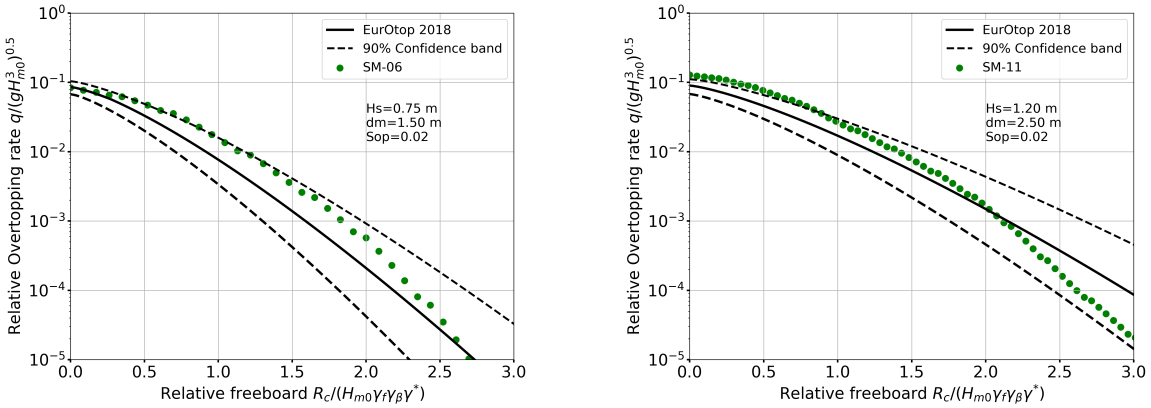

Figure 4.15: Virtual overtopping results compared to EurOtop (2018) equations for experiments with full vegetation. a) low storm conditions for non-breaking waves and b) mid storm conditions for non-breaking waves.

For the high storm conditions, the predicted values from the equations do not align well with the calculated values Figure 4.16. This is attributed to the large volumes of water splashing on the dike, which likely caused the laser scanner to overestimate the thickness of the water layer.

To understand the influence of vegetation on the decrease in virtual overtopping discharge, the overtopping discharge is plotted against the freeboard values. In Figure 4.17a, the results of low-storm condition experiments with the three vegetation conditions can be found. The difference in discharge between the veg-

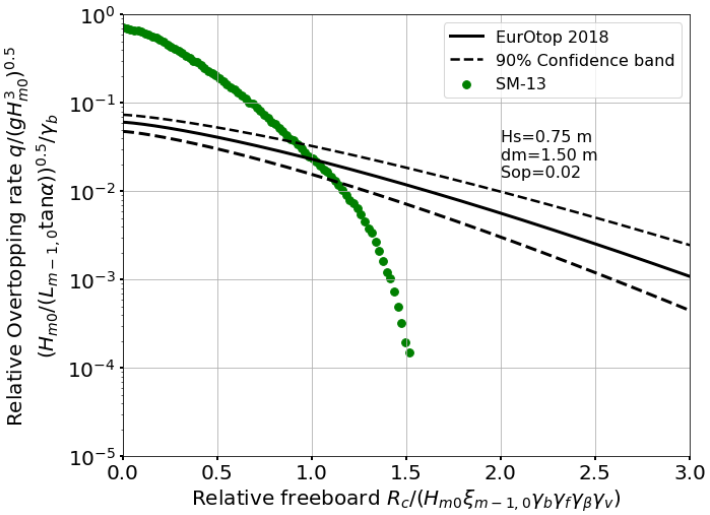

Figure 4.16: Virtual overtopping results compared to EurOtop (2018) equations for experiments on high storm conditions with full vegetation.

etation categories is evident, the lower the quality of vegetation, the higher the virtual overtopping discharge in all freeboard values. In Figure 4.17b, the results of mid-storm condition experiments with the same vegetation show the same pattern. For low freeboard values the discharges have similar values, but for medium to higher freeboard, the difference is evident. Once more, the discharge values get higher with lower vegetation conditions. For the high storm conditions, only one storm condition scenario was available for assessment. In Figure 4.18 it is evident that the good and damaged vegetation conditions lead to similar results, while the no vegetation scenario has increased values of overtopping discharge for all the values of freeboard.

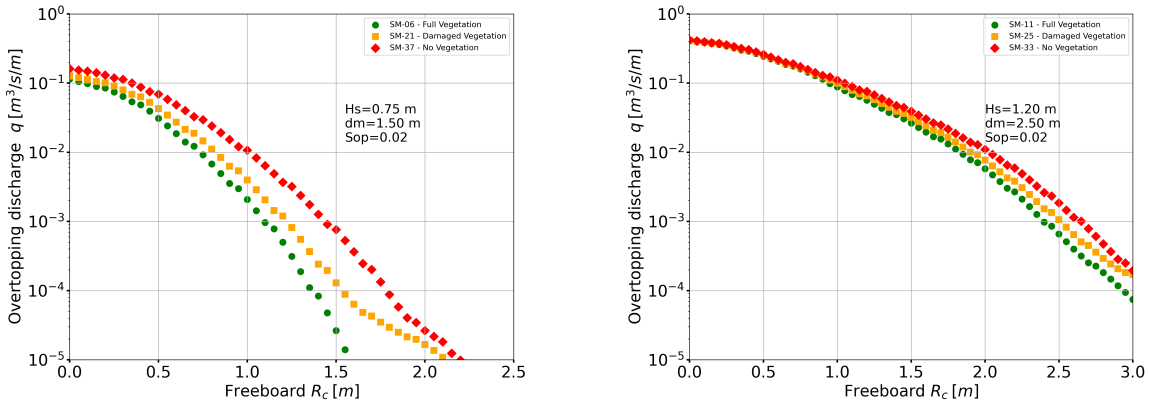

Figure 4.17: Overtopping discharge against the freeboard values for the three vegetation conditions. a) low storm conditions and b) mid storm conditions.

To calculate the effect of vegetation on the overtopping volumes, it is essential to compare the virtual volumes for the different categories of vegetation. The virtual cumulative volumes for different virtual crest values are found in Table 4.3. From this, it is possible to calculate the overtopping reduction ratio of overtopping volumes between experiments with and without vegetation as:

$$\kappa_i = \frac{\Sigma V_{v,i}}{\Sigma V_{o,i}} \tag{4.1}$$

with i = 0.5, 1.0, 1.5, 2.0, 2.5 and 3.0 the virtual crest height.

The results of the overtopping reduction ratio calculated for the different virtual freeboards and the percentage decrease between the vegetated and the reference scenario can be found in Table 4.4. The results

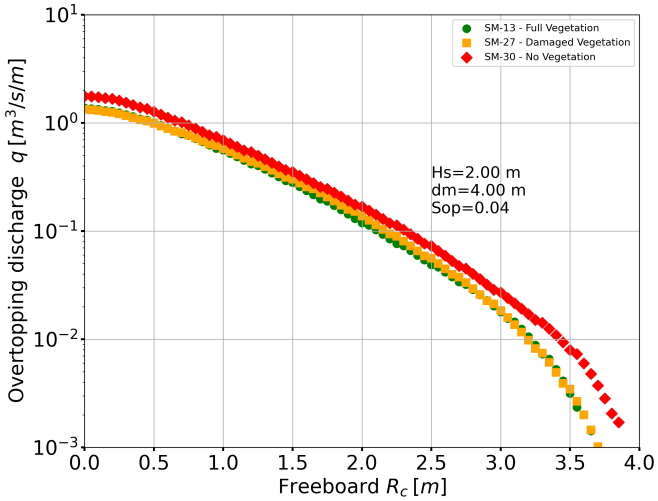

Figure 4.18: Overtopping discharge against the freeboard values for high storm conditions and the three vegetation conditions.

Table 4.3: Cummulative overtopping volumes for different virtual crest heights

Experiment	$\Sigma V_{0.5}[m^3/m]$	$\Sigma V_{1.0}[m^3/m]$	$\Sigma V_{1.5}[m^3/m]$	$\Sigma V_{2.0}[m^3/m]$	$\Sigma V_{2.5}[m^3/m]$	$\Sigma V_{3.0}[m^3/m]$
SM-01	3	3	3	3	3	3
SM-03	57	75	81	82	83	83
SM-06	232	251	252	252	252	252
SM-07	62	63	63	63	63	63
SM-09	420	592	636	647	653	655
SM-11	378	1113	1372	1438	1448	1456
SM-13	4823	7513	8855	9424	9657	9742
SM-16	7	7	7	7	7	7
SM-18	88	112	116	117	117	118
SM-21	303	337	339	340	340	340
SM-22	98	101	101	101	101	101
SM-24	576	726	760	768	771	772
SM-25	2063	2886	3171	3242	3256	3261
SM-27	5095	8082	9636	10348	10637	10732
SM-30	6608	10221	12054	12932	13312	13452
SM-32	627	814	864	876	879	880
SM-33	2233	3184	3533	3631	3649	3652
SM-36	115	125	125	125	125	125
SM-37	310	365	370	371	371	371

reveal a decrease of up to 50% for the low conditions, a 55% decrease in overtopping volumes for the mid conditions and a maximum decrease of 28 % for the high conditions.

By finding the percentage difference between the overtopping reduction ratios for the same storm conditions, it is also possible to assess the reduction between good and damaged vegetation. These results for low conditions range from 13.1 to 13.6% for the steep waves and from 23.3 to 25.8% for the mild steepness waves. For mid-storm conditions, these results have a wider range with a percentage difference of 13.8 to 18.4% for the steep waves and 15.3 to 27.1% for the mild steepness waves. Under high storm conditions, the two vegetation states resulted in a difference ranging from 5.3% to 9.2%.

Table 4.4: Overtopping reduction ratio and percentage of overtopping decrease between vegetated and reference scenario

Experiments	d_m [m]	H_s [m]	S_{op} [-]	Vegetation (/no-vegetation)	κ	Reduction [%]
SM-06/SM-37	1.5	0.75	0.04	Full Vegetation	0.68-0.75	25-32
SM-21/SM-37	1.5	0.75	0.04	Damaged Vegetation	0.91-0.98	2-9
SM-07/SM-36	1.5	0.75	0.02	Full Vegetation	0.50-0.51	49-50
SM-22/SM-36	1.5	0.75	0.02	Damaged Vegetation	0.57-0.58	42-43
SM-09/SM-32	2.5	1.20	0.04	Full Vegetation	0.46-0.51	49-54
SM-24/SM-32	2.5	1.20	0.04	Damaged Vegetation	0.86-0.90	10-14
SM-11/SM-33	2.5	1.20	0.02	Full Vegetation	0.77-0.78	22-23
SM-25/SM-33	2.5	1.20	0.02	Damaged Vegetation	0.88-0.95	5-11
SM-13/SM-30	4.0	2.00	0.04	Full Vegetation	0.72-0.73	27-28
SM-27/SM-30	4.0	2.00	0.04	Damaged Vegetation	0.77-0.80	20-23

5

Discussion & Recommendations

5.1. Wave analysis

The method by Zelt and Skjelbreia (1992) was used to perform a reflection analysis offshore and at the toe of the dike. In this method, it is important to ensure that the spacing between the wave gauges is not proportional to the wavelength. This problem occurred in the experiments for the offshore location as it is visible in Figure 5.1a. For this reason, a Bandstop filter is applied to overcome this issue ensuring that no more than 5% of the total spectral energy is removed Figure 5.1b.

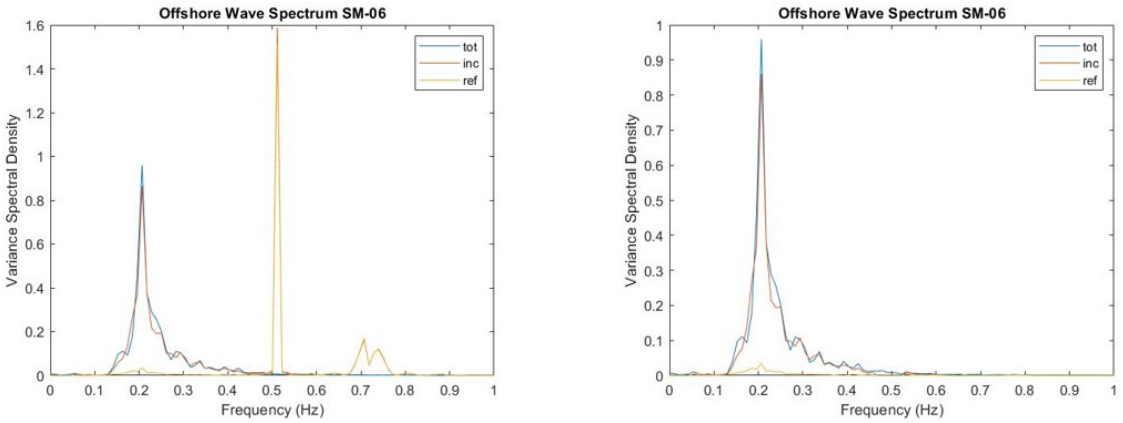

Figure 5.1: Variance density spectra of experiment SM-06 with and without a bandstop filter.

5.2. Wave run-up

5.2.1. Video camera run-up

For the calculation of the wave run-up on the dike, this study uses a computer vision algorithm that detects the water running up on the slope of the dike on the video footage that was acquired during the experimental runs. This algorithm engages consecutive frames of the video and calculates the movement of water on the slope. The videos captured during the experiments had a variety of lengths depending on the number of waves running on the experiment. Due to the different depth conditions and the scale of the experiment, the camera had to be repositioned after every experiment to be prepared for the initiation of the next one. This was a big challenge for the callibration of the video footage. For every footage, a separate extrinsic calibration procedure was needed to transform the data into real dimensions. Due to the large amount of flotsam on the slope of the dike, processing the footage from several experiments turned out to be a challenge. Initially, the chessboard that was painted on the slope for detection purposes was not detectable due to the vegetation gathered in the area. In these cases, the detection has been completed manually. The video processing required additional filters for accurate run-up detection, along with increased threshold values. The higher

threshold values increased the run-up values detected by the process. Moreover, the concentration of vegetation on the slope of the dike and the difference in light exposure led the processing of the video to require several modifications so the recognition of run-up from the algorithm to be completed.

To validate the results of the run-up a visual detection method is used to identify the run-up from the video footage. The results of the visual detection are in good correspondence with the results from the video process. The small difference that exists between the two signals is due to the camera's incapability to record the very thin water layers. The video process calculates the variance of the consecutive frames over the width of the flume but the results are produced based on the median line of these results, thus the results of the video process might be underestimated in some events Figure 5.2. For the visual detection method, the movement of the waves on the dike was picked in the middle of the dike as the waves were observed to get the highest values around the center of the flume. The variation of the run-up over the width was assumed insignificant as the processing algorithm calculates the run-up only of the axis that the waves move. The camera was recording at 60 fps, making it impossible to manually detect the run-up for the whole experiment frame by frame. For this reason, the detection was made for a part of the experiments.

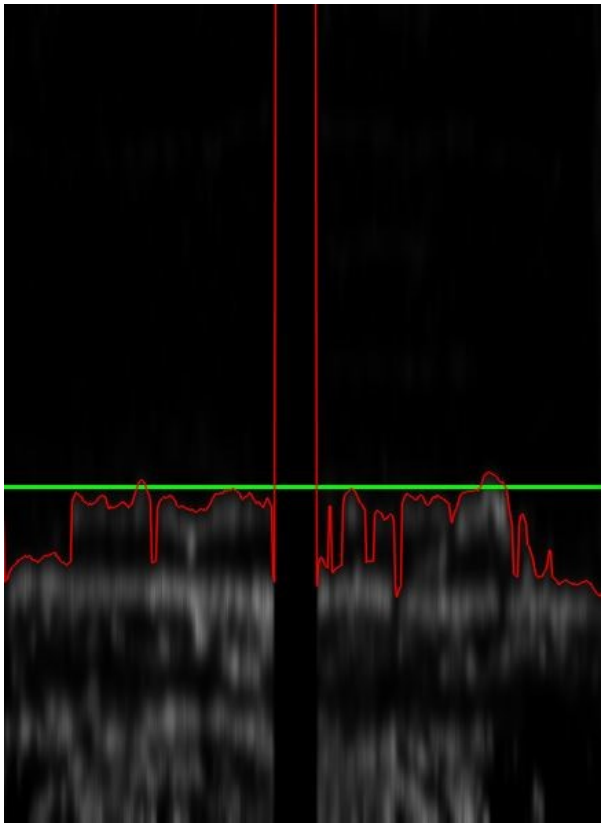

Figure 5.2: Detection of the run-up from the video process, red line is the variance of the consecutive frames over the width of the flume and green line is the median line of the variance.

The results of the run-up exceedance analysis point out that the condition of vegetation is of great importance. Experiments with identical hydrodynamic conditions show higher run-up levels when there is damaged or no vegetation in the flume. This is visible in Figure 5.3, where all the experiments have low wave conditions but have the same vegetation condition, a fully vegetated marsh. SM-01 and SM-05 (experiments with H_s = 0.75 m, dm = 1.5 m and S_{op} = 0.04) were carried out with only 3 experiments between them, which was enough to damage vegetation and increase run-up. The same is true between experiments SM-02 and SM-08 (experiments with H_s = 0.75 m, dm = 1.5 m and S_{op} = 0.02).

The wave setup was calculated at the toe of the dike for all experiments conducted in this study. The results indicated that the setup values were very low (0.1–2 cm), with the 100-wave experiments even resulting in negative values. In Figure 5.4, the results for relative setup, expressed as $\eta_s/L_{m-1,0}$, are compared with empirical equations from Keimer et al. (2021). It is evident that the calculated setup values are negligible compared to the predicted values.

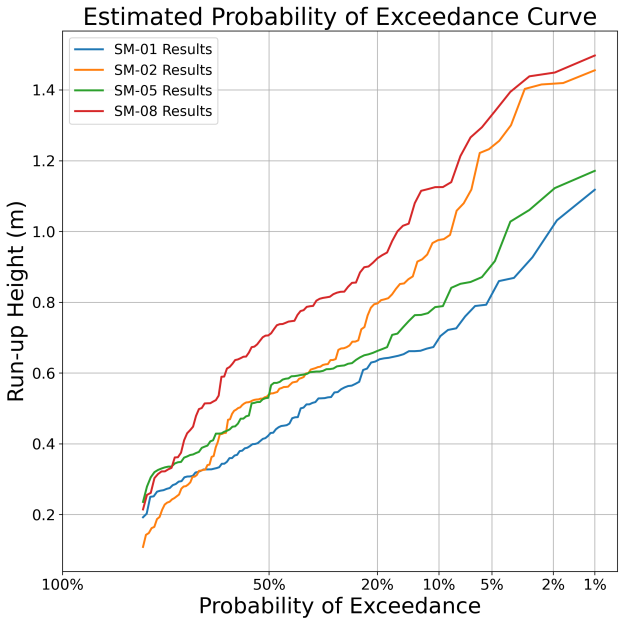

Figure 5.3: Exceedance probability of run-up for experiments with low storm conditions and good quality of vegetation

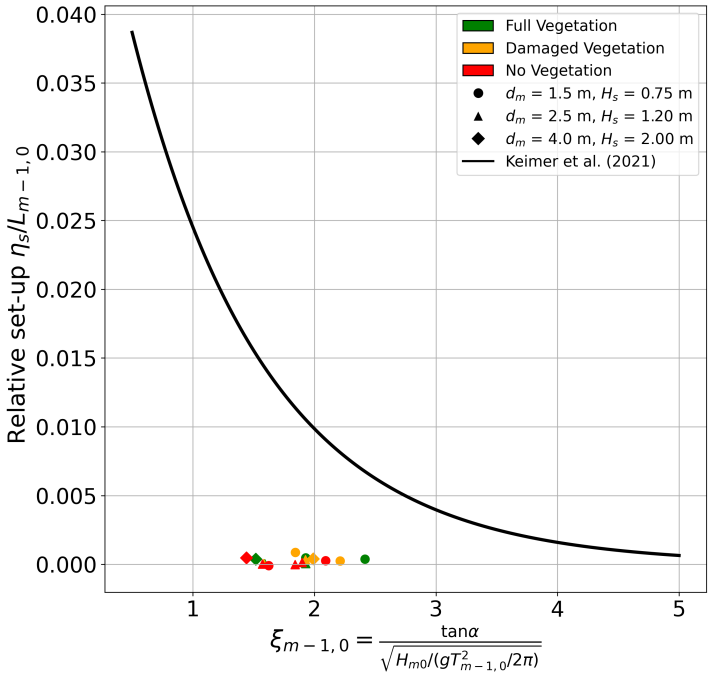

Figure 5.4: Relative set-up for different values of the Irribaren number. Comparison with empirical equations found in Keimer et al. (2021).

5.2.2. Laser scanner run-up

A LIDAR laser scanner is used to acquire elevation data for every flume experiment. A further investigation of the RSSI values would have been useful as the data tends to be more accurate than the distance data (Hofland et al., 2015), but the RSSI values were not recorded. The results of the laser scanner run-up were acquired for five different values of the water layer thickness threshold to determine which is the best predicting value. A thickness of 0.03m was chosen as it leads to the lowest bias between the laser scanner and the video footage

tracking. The lower thickness thresholds would overestimate the run-up. The laser scanner signal was also compared with the manual detection signal, and a bias of 0.13 m or 7% was calculated. Figure 5.5 illustrates a comparison between the laser scanner and the video processing signals. It is evident that the two methods show good agreement for lower run-up events, but the laser scanner fails to detect higher run-up values. This is because the laser scanner is unable to accurately measure thin layers of water.

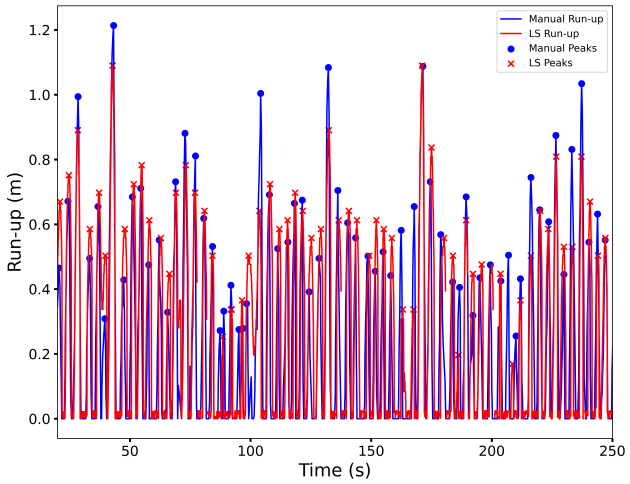

Figure 5.5: Comparison of laser scanner and manual run-up signal

5.3. Wave overtopping

To calculate the overtopping events, the data derived from the laser scanner measurements were used. The layer thickness of each wave was multiplied by the velocity of the wave. In this study, the assumption that the velocity of the wave represents the frontal velocity on the virtual crest was made as recommended in Oosterlo et al. (2019).

The results analyzed in subsection 4.3.2 are results of the low and mid storm conditions. The data from the highest storm conditions were not processed as the intense breaking of the waves on the dike slope led to splashing of water, which the laser scanner device unidentified as the thickness of the wave run-up. This led to an overestimation of the virtual volumes of water.

5.4. Recommendations

Regarding the set-up of the experiment, several recommendations are made:

- It is important to have instruments that can measure the elevation of the water successfully both offshore and near the dike. If its planned to perform a reflection analysis using a 3 wave gauge method (Zelt and Skjelbreia (1992)), it is essential to have a good spacing between the wave gauges to avoid errors in the signal;
- In the case of a laser scanner, it is important to understand the settings of the device and measure all the important parameters which are data of distance, RSSI, and the time that the pulse is received from the device.
- If the use of the camera is necessary the camera must remain in the same position and not be removed to avoid the calibration for every experiment.
- In the case of using both a camera and a laser scanner, the velocities can also be calculated from the displacement of the water during a frame. In this way to comparison of the results from the laser scanner and the camera will work as validation of the method.
- In the case that the experiments include real vegetation, it is important to clean the surface of the dike before every experiment to avoid problems with the measurements. The same actions need to be done for all the underwater equipment in the flume.

The recommendations for the test program are:

- It is suggested that the test program includes the same experiments for all vegetation conditions. Moreover, for the completion of a study with a sufficient sample of data, it is important to include a variety of wave conditions for several water depths to capture all the vital points of the mechanisms that are investigated.
- Avoid having irregular wave experiments with very few waves. A minimum of 500 waves in every experiment is essential for the analysis of wave run-up and a statistical description of the variables.

6

Conclusions

This research provides insight into the efficacy of salt marsh vegetation conditions in reducing the run-up and wave overtopping over a real scale dike under extreme storm conditions. The experiments were conducted in the Deltares Delta Flume.

How do salt marshes affect the run-up on a dike?

The existence of salt marsh vegetation on the foreshore of a dike leads to a reduction in the wave run-up. This reduction is not attributed directly to the presence of vegetation but rather to the decrease in the significant wave height H_{m0} caused by vegetation. Furthermore, the reduction diminishes when the vegetation is assumed to be in a damaged state compared to the fully vegetated conditions. The importance of setup on wave run-up could not be assessed, as the setup results were negligible compared to the run-up values.

The reduction rate due to salt marsh vegetation was assessed by calculating the damping ratio of $R_{u2\%}$ of the vegetated foreshore for good and damaged vegetation conditions and the $R_{u2\%}$ to the bare foreshore scenario. The results of the damping ratio for the mid-storm conditions (H_s = 1.20 m and d_m = 2.50 m) are lower than the low-storm conditions (H_s = 0.75 m and d_m = 1.50 m). The ratios reveal that the vegetated foreshores can decrease the run-up from 2 to 16% for low conditions and from 4 to 24% for mid-storm conditions.

Furthermore, the results of the damping parameters were compared for experiments with the same wave conditions but different vegetation quality. By calculating the percentage difference between the damping ratio of good and damaged vegetation it is possible to assess the difference in run-up according to the quality of salt marsh. The results show that for low storm conditions, the reduction ranges from 7.1 to 9.1 %, while for mid-storm conditions from 6.0 to 9.0 %. These findings are consistent with previous research on artificial vegetation, which demonstrated an average run-up reduction of 9.6% (Keimer et al., 2021).

In general, the average reduction from vegetated to non-vegetated foreshores is at 10.3%, while the average difference between the two categories of vegetation is on average at 7.7%. From this, it is evident that the existence of vegetation is important even if the salt marsh has already eroded.

This research question breaks down into two sub-questions.

What is the difference in accuracy between measuring wave run-up using a video camera and a laser scanner?

To measure wave run-up in this study, a GoPro video camera was mounted during the experiments to record the run-up events on the dike. The footage of the experiments was processed with a method of computer vision to acquire the run-up data Lakerveld (2024). The method identifies the wave's front position by analyzing the difference between frames. When compared to a visual method, the results showed a bias ranging from 0.017 to 0.022 m.

Furthermore, a LIDAR laser scanner was also used to record the run-up events. After the initial processing of the data, to remove the baseline of the dry slope, several layers of thickness were picked to see which gave the optimal results. A layer thickness of 0.03 m produces the best results, which have a bias of 0.032-0.037 with the manually detected signal.

The $R_{u2\%}$ results are generally higher when using the video processing method, leading to an average difference in run-up between the two methods of 0.13 m (7%). For this reason, the video camera leads to more reliable results. A reason why the video process method is a better choice for recording the run-up on the dike is the easy set-up and preprocessing that require only mounting and calibration. A laser scanner is also more expensive and cannot be used in many cases.

How well can wave run-up be predicted with existing empirical formulas?

To compare the results of run-up derived by the measurements with the video camera and the laser scanner with equations found in the literature is it essential to start with the equations found in EurOtop (2018) and Van Gent et al. (1999). The equations from EurOtop (2018) are intended for the spectral conditions close to the toe of the dike. In addition to these parameters, the results were compared with these equations using $H_{1/3}$ instead of H_{m0} for the conditions at the toe of the dike. In this case, the results of $H_{1/3}$ lead to lower values of run-up compared to the predicted values from the equation, and there are many experiments outside the acceptable margins. In the case H_{m0} is used as suggested by the manual, the equations can accurately describe the results. Steep waves (S_{op} =4%) are underestimated, while waves with lower steepness (S_{op} =2%) were overestimated by the equations. Furthermore, the RMSE between measured and predicted values from this equation is 0.18 m, and the relative error is 5%. This shows overall a good agreement of the results with the EurOtop manual equations and means that it is possible to predict the run-up values on a living dike under storm conditions.

In addition, the equations of Van Gent et al. (1999) are found to be in good agreement with the measured run-up values from the experiments. Equation 2.10 from Van Gent et al. (1999), predicts very low values of run-up that do not correspond with the measured values. By using Equation 2.10 it is possible to predict the measured results accurately. The RMSE between the measured and predicted values is at 0.19 m.

The run-up was also calculated using the laser scanner, showing that the lower conditions cannot be measured accurately due to the thin layers of water. The majority of the results are within the confidence intervals of the equation with an RMSE = 0.31 m. The relative error between the predicted and the measured values is 12%.

How do salt marshes affect overtopping on a dike?

It is evident that the worse the vegetation conditions the higher the virtual overtopping discharges and virtual overtopping volumes. To define the intervals of the virtual overtopping volume reduction, a virtual crest with R_c = 0.5 was used for the low and R_c = 3.0 for the high intervals. For low storm conditions (H_s = 0.75 m and d_m = 1.5 m), a well-vegetated foreshore can lead to a reduction of 49 to 50 % for the steep waves (S_{op} = 0.04) and a reduction of 25 to 32 % for the mild steepness (S_{op} = 0.02). For the same wave conditions and damaged vegetation, virtual overtopping is significantly reduced. The steep wave experiments have a reduction between 2-9 % while the milder steepness wave experiments between 42 to 43%. Here, the results reveal that the existence of vegetation may have a lower impact on the reduction of overtopping for mild steepness waves compared to the steep waves, but the lower quality of vegetation may lead to a reduction that is three times lower than the reduction from good quality vegetation. In medium storm conditions (H_s = 1.20 m and d_m = 2.5 m), the results are somewhat similar. The mild steepness wave experiments have a lower decrease in overtopping from 22 to 23%, while the other experiments drop from 49 to 54%. The quality of vegetation is important once again, as for damaged vegetation conditions the reduction falls to 5-11% and 10-14%, respectively. For the high storm conditions (H_s = 2.00 m and d_m = 4.0 m), where only one scenario is available (S_{op} = 0.04), the results showed a 20 to 23 % decrease. The results are similar to the other two storm conditions.

To understand further the impact of vegetation in overtopping it is important to evaluate the decrease in overtopping from good to damaged vegetation. This is possible by calculating the percentage difference in individual overtopping reduction ratios for low- and medium-storm conditions. For low conditions and steep waves, the reduction ranges from 13.1 to 13.6 %, while for the mild steepness waves, it ranges from 27.0 to 29.1 %. For medium wave conditions, the same conditions lead to a decrease of 13.8 to 18.4 % and a decrease of 39.9 to 48.6% respectively. These results reveal that the higher the wave conditions, the greater the reduction in good vegetation compared to damaged vegetation. For the highest storm conditions, the comparison of the two vegetated scenarios revealed a decrease of 5.3% to 9.2%, indicating that the importance of vegetation conditions is reduced under the most extreme conditions.

In general, the results of the reduction of the virtual overtopping volumes from the existence of vegetation reveal that the higher the wave conditions the lower the reduction of overtopping. At the same time, the

results indicate that a good-quality vegetated foreshore is more crucial under mid-wave conditions, as it leads to a greater decrease compared to low conditions. However, for the highest storm conditions, this importance diminishes significantly.

which breaks down into an additional sub-question.

How well can wave overtopping be predicted with existing empirical formulas?

Comparison of the results of overtopping with the equations from EurOtop (2018) shows a strong agreement between the calculated and predicted values for the low and mid conditions. These equations can be used well for the case of salt marsh vegetated foreshores under these storm conditions. For the highest storm conditions, the results exhibit a different behavior compared to the predicted values, with significantly higher results observed for low freeboard levels. This overestimation is likely caused by splashing water being detected by the laser scanner.

Bibliography

Allsop, W., Bruce, T., & Schüttrumpf, H. (2007). Eurotop wave overtopping of sea defences and related structures: Assessment manual. https://www.researchgate.net/publication/256197945

Astorga-Moar, A., & Baldock, T. E. (2023). Assessment of wave overtopping models for fringing reef fronted beaches. Coastal Engineering, 186. https://doi.org/10.1016/j.coastaleng.2023.104395

Augustin, L. N., Irish, J. L., & Lynett, P. (2009). Laboratory and numerical studies of wave damping by emergent and near-emergent wetland vegetation. Coastal Engineering, 56, 332–340. https://doi.org/10.1016/j.coastaleng.2008.09.004

Baker, S., Murphy, E., Cornett, A., & Knox, P. (2022). Experimental study of wave attenuation across an artificial salt marsh. Frontiers in Built Environment, 8. https://doi.org/10.3389/fbuil.2022.893664

Bomers, A., Lopez, J. P. A., Warmink, J. J., & Hulscher, S. J. (2018). Modelling effects of an asphalt road at a dike crest on dike cover erosion onset during wave overtopping. Natural Hazards, 93, 1–30. https://doi.org/10.1007/s11069-018-3287-y

Calvin, K., Dasgupta, D., Krinner, G., Mukherji, A., Thorne, P. W., Trisos, C., Romero, J., Aldunce, P., Barrett, K., Blanco, G., Cheung, W. W., Connors, S., Denton, F., Diongue-Niang, A., Dodman, D., Garschagen, M., Geden, O., Hayward, B., Jones, C., … Ha, M. (2023). Ipcc, 2023: Climate change 2023: Synthesis report. contribution of working groups i, ii and iii to the sixth assessment report of the intergovernmental panel on climate change [core writing team, h. lee and j. romero (eds.)]. ipcc, geneva, switzerland. (P. Arias, M. Bustamante, I. Elgizouli, G. Flato, M. Howden, C. Méndez-Vallejo, J. J. Pereira, R. Pichs-Madruga, S. K. Rose, Y. Saheb, R. S. Rodríguez, D. Ürge-Vorsatz, C. Xiao, N. Yassaa, J. Romero, J. Kim, E. F. Haites, Y. Jung, R. Stavins, … C. Péan, Eds.). https://doi.org/10.59327/IPCC/AR6-9789291691647

Cete, C. (2019). Quantifying the effect of woody vegetation on the wave loads on a dike using remote sensing large scale physical model tests. http://repository.tudelft.nl/.

Duarte, C. M., Losada, I. J., Hendriks, I. E., Mazarrasa, I., & Marbà, N. (2013). The role of coastal plant communities for climate change mitigation and adaptation. https://doi.org/10.1038/nclimate1970

Eekman, I. L. ((2021). Seasonal variation in salt marsh vegetation impact of physical stressors on the development, decay and seed retention of salicornia europaea.

Esselink, P., van Duin, W., Bunje, J., Cremer, J., Folmer, E., Frikke, J., Glahn, M., de Groot, A., Hecker, N., Hellwig, U., Jensen, K., Körber, P., Petersen, J., Stock, M., & de AV Groot. (2017). Wadden sea quality status report salt marshes wadden sea quality status report-salt marshes 2 colophon.

EurOtop. (2018). Eurotop manual on wave overtopping of sea defences and related structures an overtopping manual largely based on european research, but for worldwide application second edition 2018. www.overtopping-manual.com

Franklin, G. L., & Torres-Freyermuth, A. (2022). On the runup parameterisation for reef-lined coasts. Ocean Modelling, 169. https://doi.org/10.1016/j.ocemod.2021.101929

Gerrit, J., Henk, S., & Verhagen, J. (2019). Engineering the interface of soil and water.

Hofland, B., Diamantidou, E., van Steeg, P., & Meys, P. (2015). Wave runup and wave overtopping measurements using a laser scanner. Coastal Engineering, 106, 20–29. https://doi.org/10.1016/j.coastaleng.2015.09.003

Holthuijsen, L. H. (2007). Waves in oceanic and coastal waters. Cambridge University Press. https://doi.org/10.1017/CBO9780511618536

Keimer, K., Schürenkamp, D., Miescke, F., Kosmalla, V., Lojek, O., & Goseberg, N. (2021). Ecohydraulics of surrogate salt marshes for coastal protection: Wave–vegetation interaction and related hydrodynamics on vegetated foreshores at sea dikes. Journal of Waterway, Port, Coastal, and Ocean Engineering, 147. https://doi.org/10.1061/(asce)ww.1943-5460.0000667

Koch, E. W., Barbier, E. B., Silliman, B. R., Reed, D. J., Perillo, G. M. E., Hacker, S. D., Granek, E. F., Primavera, J. H., Muthiga, N., Polasky, S., Halpern, B. S., Kennedy, C. J., Kappel, C. V., & Wolanski, E. (2016). Non-linearity in ecosystem services: Temporal and spatial variability in coastal protection.

Koftis, T., Prinos, P., & Stratigaki, V. (2013). Wave damping over artificial posidonia oceanica meadow: A large-scale experimental study. Coastal Engineering, 73, 71–83. https://doi.org/10.1016/j.coastaleng.2012.10.007

Koosheh, A., Etemad-Shahidi, A., Cartwright, N., Tomlinson, R., & van Gent, M. R. (2021). Individual wave overtopping at coastal structures: A critical review and the existing challenges. https://doi.org/10.1016/j.apor.2020.102476

Lakerveld, S. (2024). Quantifying the influence of salt marshes on wave run-up on a dike during extreme wave conditions, an experimental study.

Li, Y., Zhao, D., Yu, G., & Xie, L. (2023). Wave height attenuation over a nature-based breakwater of floating emergent vegetation. Sustainability (Switzerland), 15. https://doi.org/10.3390/su151410749

Ma, Y., Zhu, L., Peng, Z., Xue, L., Zhao, W., Li, T., Lin, S., Bouma, T. J., Hofland, B., Dong, C., & Li, X. (2023). Wave attenuation by flattened vegetation (scirpus mariqueter). Frontiers in Marine Science, 10. https://doi.org/10.3389/fmars.2023.1106070

Manousakas, N., Salauddin, M., Pearson, J., Denissenko, P., Williams, H., & Abolfathi, S. (2022). Effects of seagrass vegetation on wave runup reduction – a laboratory study. IOP Conference Series: Earth and Environmental Science, 1072. https://doi.org/10.1088/1755-1315/1072/1/012004

Mares-Nasarre, P., Molines, J., Gómez-Martín, M. E., & Medina, J. R. (2020). Individual wave overtopping volumes on mound breakwaters in breaking wave conditions and gentle sea bottoms. Coastal Engineering, 159. https://doi.org/10.1016/j.coastaleng.2020.103703

Marin-Diaz, B., van der Wal, D., Kaptein, L., Martinez-Garcia, P., Lashley, C. H., de Jong, K., Nieuwenhuis, J. W., Govers, L. L., Olff, H., & Bouma, T. J. (2023). Using salt marshes for coastal protection: Effective but hard to get where needed most. Journal of Applied Ecology, 60, 1286–1301. https://doi.org/10.1111/1365-2664.14413

Maza, M., Lara, J. L., Losada, I. J., Ondiviela, B., Trinogga, J., & Bouma, T. J. (2015). Large-scale 3-d experiments of wave and current interaction with real vegetation. part 2: Experimental analysis. Coastal Engineering, 106, 73–86. https://doi.org/10.1016/j.coastaleng.2015.09.010

Migliore, D., Matteucci, M., & Naccari, M. (2006). A revaluation of frame difference in fast and robust motion detection. https://doi.org/10.1145/1178782.1178815

Molines, J., Herrera, M. P., Gómez-Martín, M. E., & Medina, J. R. (2019). Distribution of individual wave overtopping volumes on mound breakwaters. Coastal Engineering, 149, 15–27. https://doi.org/10.1016/j.coastaleng.2019.03.006

Möller, I., Kudella, M., Rupprecht, F., Spencer, T., Paul, M., van Wesenbeeck, B. K., Wolters, G., Jensen, K., Bouma, T. J., Miranda-Lange, M., & Schimmels, S. (2014). Wave attenuation over coastal salt marshes under storm surge conditions. Nature Geoscience, 7, 727–731. https://doi.org/10.1038/NGEO2251

Möller, I., & Spencer, T. (2002). Wave dissipation over macro-tidal saltmarshes: Effects of marsh edge typology and vegetation change. Journal of Coastal Research, 36, 506–521. https://doi.org/10.2112/1551-5036-36.sp1.506

Oosterlo, Hofland, B. ; Meer, J. ; V. D., Overduin, M. ; Steendam, G. J., Nieuwenhuis, J.-W. ; Vledder, G. ; V., Steetzel, H. ; & Reneerkens, M. (2019). Measuring (oblique) wave run-up and overtopping with laser scanners. Citation. https://doi.org/10.18451/978-3-939230-64-9_045

Paul, M., & Amos, C. L. (2011). Spatial and seasonal variation in wave attenuation over zostera noltii. Journal of Geophysical Research: Oceans, 116. https://doi.org/10.1029/2010JC006797

Reents, S., Möller, I., Evans, B. R., Schoutens, K., Jensen, K., Paul, M., Bouma, T. J., Temmerman, S., Lustig, J., Kudella, M., & Nolte, S. (2022). Species-specific and seasonal differences in the resistance of saltmarsh vegetation to wave impact. Frontiers in Marine Science, 9. https://doi.org/10.3389/fmars.2022.898080

Rupprecht, F., Möller, I., Paul, M., Kudella, M., Spencer, T., van Wesenbeeck, B. K., Wolters, G., Jensen, K., Bouma, T. J., Miranda-Lange, M., & Schimmels, S. (2017). Vegetation-wave interactions in salt marshes under storm surge conditions. Ecological Engineering, 100, 301–315. https://doi.org/10.1016/j.ecoleng.2016.12.030

Spalding, M. D., Mcivor, A. L., Beck, M. W., Koch, E. W., Möller, I., Reed, D. J., Rubinoff, P., Spencer, T., Tolhurst, T. J., Wamsley, T. V., van Wesenbeeck, B. K., Wolanski, E., & Woodroffe, C. D. (2014). Coastal ecosystems: A critical element of risk reduction. Conservation Letters, 7, 293–301. https://doi.org/10.1111/conl.12074

Stockdon, H. F., Holman, R. A., Howd, P. A., & Sallenger, A. H. (2006). Empirical parameterization of setup, swash, and runup. Coastal Engineering, 53, 573–588. https://doi.org/10.1016/j.coastaleng.2005.12.005

Thompson, B. F. E., & Vincent, C. L. (1985). Significant wave height for shallow water design.

Van den Hoven, K., Kroeze, C., & van Loon-Steensma, J. M. (2022). Characteristics of realigned dikes in coastal europe: Overview and opportunities for nature-based flood protection. Ocean and Coastal Management, 222. https://doi.org/10.1016/j.ocecoaman.2022.106116

Van der Meer, J. W. (1998). Wave run-up and overtopping.

Van der Meer, J. W., Hoven, A. V., Steendam, G. J., & Hoffmans, G. (2018). Hydraulic simulators on real dikes and levees.

Van Gent, M. R. A., der Werf, V., & M., I. (1999). Physical model investigations on coastal structures with shallow foreshores.

Van Loon-Steensma, J. M. (2015). Salt marshes to adapt the flood defences along the dutch wadden sea coast. Mitigation and Adaptation Strategies for Global Change, 20(6), 929–948. https://doi.org/10.1007/s11027-015-9640-5

Van Wesenbeeck, B. K., Wolters, G., Antolínez, J. A., Kalloe, S. A., Hofland, B., de Boer, W. P., Çete, C., & Bouma, T. J. (2022). Wave attenuation through forests under extreme conditions. Scientific Reports, 12. https://doi.org/10.1038/s41598-022-05753-3

Vos-Jansen, L. (2018). Physical modelling of reflection on gentle coasts comparing methods to analyse long waves and optimising the lay-out for a wave absorber to minimise reflection in a wave flume.

Vuik, V., Jonkman, S. N., Borsje, B. W., & Suzuki, T. (2016). Nature-based flood protection: The efficiency of vegetated foreshores for reducing wave loads on coastal dikes. Coastal Engineering, 116, 42–56. https://doi.org/10.1016/j.coastaleng.2016.06.001

Zelt, J. A., & Skjelbreia, J. E. (1992). Estimating incident and reflected wave fields using an arbitrary number of wave gauges.

Zhao, Y., Peng, Z., He, Q., & Ma, Y. (2023). Wave attenuation over combined salt marsh vegetation. Ocean Engineering, 267. https://doi.org/10.1016/j.oceaneng.2022.113234

A

Appendix: Calibration

A.1. Intrinsic Calibration

Intrinsic calibration refers to the process of correcting the distortion caused by the internal characteristics of a camera. This distortion primarily arises from inaccuracies in the curvature of the camera lens and the way images are captured and processed. Intrinsic calibration typically involves determining a 3x3 matrix and 5 distortion coefficients. Various methods and algorithms can be used to find these coefficients. One commonly used method is the CameraCalibrator app in MATLAB. This algorithm requires a minimum number of images of a chessboard captured from different angles by the camera undergoing calibration. The intrinsic calibration parameters need to be found only once for all the experiments.

The intrinsic calibration parameters were found by using 20 pictures of a chessboard of 10x7 squares, of 35x35 mm. The results can be found in the Table A.1 and Table A.2

Table A.1: 3x3 Matrix for Intrinsic calibration

$$\text{Internal camera matrix}$$
$$\begin{bmatrix} f_x & 0 & c_x \\ 0 & f_y & c_y \\ 0 & 0 & 1 \end{bmatrix} = \begin{bmatrix} 2587.3520 & 0 & 2792.93682 \\ 0 & 2614.2888 & 2212.9157 \\ 0 & 0 & 1 \end{bmatrix}$$

Table A.2: Distortion Coefficients for Intrinsic calibration

$$\begin{bmatrix} k_1 & k_2 & p_1 & p_2 & k_3 \end{bmatrix} = \begin{bmatrix} 0.05943822 & -0.08327561 & 0.00 & 0.00 & 0.00 \end{bmatrix}$$

The script for the intrinsic calibration algorithm can be found in Table A.1.

```
% Define images to process
imageFileNames = {};
% Detect checkerboards in images
[imagePoints, boardSize, imagesUsed] = detectCheckerboardPoints(imageFileNames);
imageFileNames = imageFileNames(imagesUsed);

% Read the first image to obtain image size
originalImage = imread(imageFileNames{1});
[mrows, ncols, ~] = size(originalImage);

% Generate world coordinates of the corners of the squares
squareSize = x;  % x in units of 'millimeters'
worldPoints = generateCheckerboardPoints(boardSize, squareSize);
```

```
% Calibrate the camera
[cameraParams, imagesUsed, estimationErrors] = estimateCameraParameters(imagePoints, worldPoints,
    'EstimateSkew', false, 'EstimateTangentialDistortion', false, ...
    'NumRadialDistortionCoefficients', 2, 'WorldUnits', 'millimeters', ...
    'InitialIntrinsicMatrix', [], 'InitialRadialDistortion', [], ...
    'ImageSize', [mrows, ncols]);

% View reprojection errors
h1=figure; showReprojectionErrors(cameraParams);

% Visualize pattern locations
h2=figure; showExtrinsics(cameraParams, 'CameraCentric');

% Display parameter estimation errors
displayErrors(estimationErrors, cameraParams);

% For example, you can use the calibration data to remove effects of lens distortion.
undistortedImage = undistortImage(originalImage, cameraParams);

% See additional examples of how to use the calibration data.  At the prompt type:
% showdemo('MeasuringPlanarObjectsExample')
% showdemo('StructureFromMotionExample')
%%

% Specify the path to the image you want to undistort
imageToUndistort = 'Image.JPG';

% Read the specified image
originalImage = imread(imageToUndistort);

% Undistort the image using the camera parameters
undistortedImage = undistortImage(originalImage, cameraParams);
```

A.2. Extrinsic Calibration

The extrinsic calibration of a camera depends on the position of the camera. As the camera is dismounted for each experimental run, an equal number of extrinsic calibration matrices is required for each run. To find the extrinsic calibration matrices, a script in Python was developed. The script uses the findHomography command of the OpenCV library. This command requires two pictures with the same size (points) chessboard. The first picture was the first frame of the footage (or any other frame that the chessboard was visible) and the second picture was a theoretically created picture with a chessboard. The theoretical picture was created by using open picture editing apps. The algorithm then would match all the points of the chessboard of the two pictures and would bring the frame from the footage to real dimensions. As the dike was sometimes covered with mud and vegetation the algorithm could not detect all of the chessboard. In these cases, by trial and error, a different size of pattern was chosen.

In the algorithm that was developed to extract the extrinsic transformation matrix for the videos, the perspective size of transformation was also included. By trial and error, the optimal size of the video frames was picked and embodied into the transformation matrix. This was later used in the process of the video.

There were in total 41 experimental runs and so 41 different extrinsic transformation matrices. An example of such a matrix is shown in Table A.3, which depicts the extrinsic transformation matrix for test SM-01.

Table A.3: Extrinsic transformation matrix of SM-01

Extrinsic Transformation Matrix

$$\begin{bmatrix} 8.13297073e-01 & 9.64573897e-02 & -1.59754846e+03 \\ -1.07931707e-01 & 1.45634949e+00 & -2.25126966e+02 \\ -6.43005070e-05 & 5.09496738e-04 & 1.00000000e+00 \end{bmatrix}$$

B

Appendix: Reflection Analysis

In the method for the reflection analysis from Zelt and Skjelbreia (1992) the exact position of the wave gauges for the two sets of wave gauges must be known. The input in this method is the location of every wave gauge according to the first wave gauge that is used. This means that in these experiments the wave gauge locations would be $w_{gx_{offshore}} = 0, 3, 9$ m for the offshore location and $w_{gx_{nearshore}} = 0, 7.719, 9.397$ m for the near-shore location. As mentioned in the main report, the spacing leads to additional frequencies that are not representative of the incident waves. Very low frequencies were filtered as they produced unrealistic scenarios of spectral variance as shown in Figure B.1. The time series of the elevation captured from the wave gauges was once again cropped before the reflection analysis to represent only the time that waves populate the domain of the wave gauges. The higher frequencies that result in extreme spectra were filtered using the band-stop filter in MATLAB Figure B.2. To make sure that this filtering will not result in the loss of a significant area of the spectra, the error was calculated for all the experiments and found to be 5%. This is considered to be acceptable.

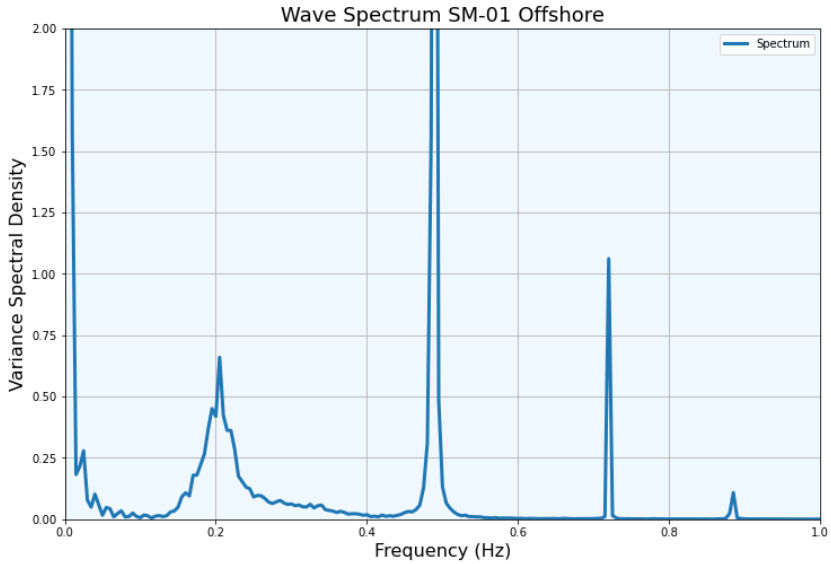

Figure B.1: Spectrum of SM-06 before filtering the frequencies

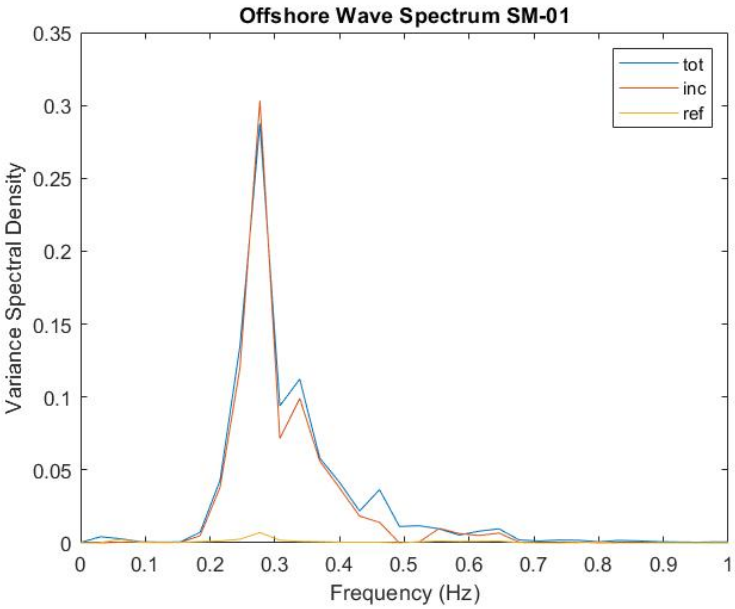

Figure B.2: Offshore wave spectrum with filtered frequencies

C

Appendix: Procedure

C.1. Video editing

As mentioned above, the videos are combined and cropped in the optimal way to have a minimal size for video processing . All these actions were made using ffmpeg through the Command Prompt window of Windows.

C.2. Video Process

The video process method was the same as that used in Lakerveld (2024). Initially, the characteristics of the video are engaged in the algorithm (time, frames per second, etc.). Then the intrinsic parameters and the extrinsic transformation matrix are applied to the frames of the video according to the perspective size that was assumed. At this point, the variance of the six consecutive frames is calculated and the filters are applied. Then the median line over the y is created and stored in a CSV file together with the time of the video.

C.3. Data Processing

As it is mentioned above the pixel-to-meter correspondence is determined by opening the calibrated frames on their perspective sizes Figure C.1. The chessboard is the area of the image that was used in the method to transform the image in real-world distances. Moreover, the chessboard has known dimensions and coordinates. For these reasons, the chessboard was used to find the correspondence of pixels-to-meters for every perspective image of the different experiments. The results are visible on Table C.1.

Based on known locations on the dike (chessboard coordinates) it is possible to determine the starting point and base all the measurements on that. Figure C.2 depicts how is a frame divided into pixels.

To calculate the run-up from the results acquired by the video processing, the data need to be transformed into a diagonal run-up and then later on the vertical run-up before applying filters.

In the algorithm developed, the diagonal run-up is being calculated by the single pixel to meters transformation in Equation C.1, where $R_{u_{diagonal}}$ is the run-up in the diagonal, O is the zero coordinates (0,0), M is the number of pixels that the median line exists on the vertical (height) of the frame and C is the correspondence of pixel-to-meters.

$$R_{u_{diagonal}} = O - \frac{M}{C} \tag{C.1}$$

For the calculation of the vertical Run-up R_u Equation 3.10 was used as mentioned before.

To find the individual waves of every experimental run and the peak of the Run-up, the local maxima with a custom prominence were used depending on the results of the run. The prominence was used to avoid double results from occurring from the same wave. An alternative method would be to assume a period that the maximum value of a wave can occur and peak only one value from this. For the wave period, the best results are occurring for the peak period calculated from the wave spectra recorded by the wave gauges. Both methods work significantly well as no double results of run-up occurred on the signals that were analyzed.

The peaks of the run-up signal were later sorted from maximum to minimum and the $R_{u2\%}$ by multiplying the number of waves by 0.02 and finding this position of wave on the sorted list. For example, if the run had

Figure C.1: Calibrated-cropped first frame of SM-01

1000 waves, the $R_{u2\%}$ would be the 20th value on Run-up on the sorted list.

As the tests are taking place in a wave flume, the wave board needs some time to initiate its movement at the start of the experiment and then to stop at the end of the experiment. This means that the first and last waves of the experiment will not be in stationary conditions as they were supposed to. In this thesis, the assumption is that the first 5 waves and the last 5 waves are to be ignored.

C.4. Manual Video Process

To validate the results of the video process, a manual method was also developed. The logic of this method is simple, as the video is playing in the background it requires a click per frame where the water appears to be on the slope. The clicks are saved in a CSV file as vertical distances from the zero coordinates point O(0,0). The same data processing as before can be applied to these results as well.

Table C.1: Test Program ID and pixel-to-distance correspondence on the diagonal and vertical

ID	Pix/m Diagonally	Pix/m Vertically
SM-01	80	21,41
SM-02	81	21,65
SM-03	80	21,53
SM-04	81	21,77
SM-05	145	38,81
SM-06	80	21,41
SM-07	70	18,74
SM-08	70	18,68
SM-09	55	14,75
SM-10	61	16,29
SM-11	40	10,71
SM-12		0,00
SM-13		0,00
SM-14		0,00
SM-15		0,00
SM-16	68	18,20
SM-17	66	17,66
SM-18	85	22,72
SM-19	84	22,36
SM-20	81	21,77
SM-21	105	28,01
SM-22	120	32,12
SM-23	100	26,76
SM-24	82	21,95
SM-25	61	16,45
SM-26		0,00
SM-27		0,00
SM-28		0,00
SM-29		0,00
SM-30		0,00
SM-31		0,00
SM-32		0,00
SM-33	90	24,09
SM-34	68	18,08
SM-35	135	36,13
SM-36	95	25,29
SM-37	95	25,29
SM-38	65	17,40
SM-39	71	19,00
SM-40	65	17,40
SM-41		0,00
SM-42	73	19,54

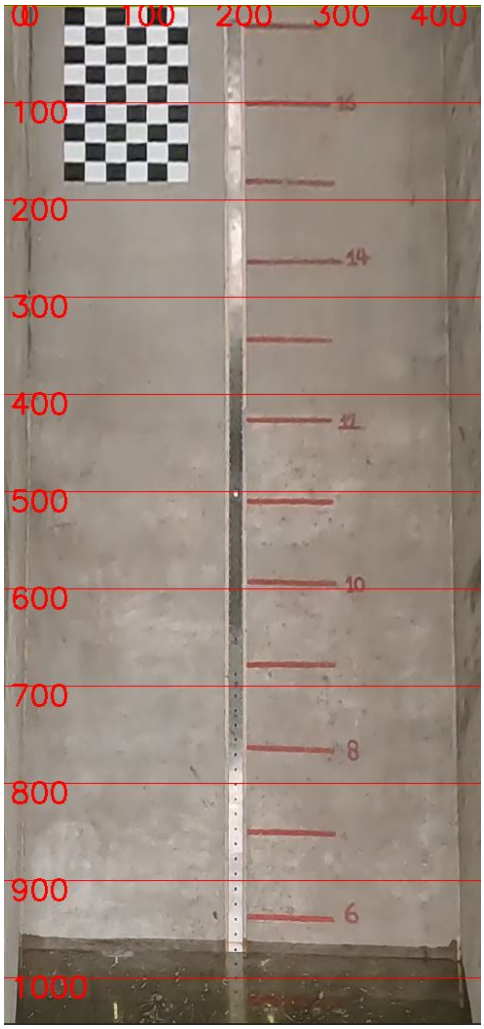

Figure C.2: Pixel divided frame

D

Appendix: Additional results

D.1. Additional results from the wave analysis

According to Table 3.1, the wave conditions are speculated to have a target wave height. By comparing this target parameter with the significant wave height derived from the spectrum analysis at the offshore location, it is possible to assess the deviation of the experiments due to the wave-board's operation. In Figure D.1, this difference is noticeable, with an average absolute difference of 0.034 m between the two parameters. Most of the results fall below the equality line, indicating that the measured significant wave heights tend to underestimate the target values. During the experiments it was noticed that some waves for mid and high conditions may break before reaching the location of the wave gauges, this may explain the lower values measured.

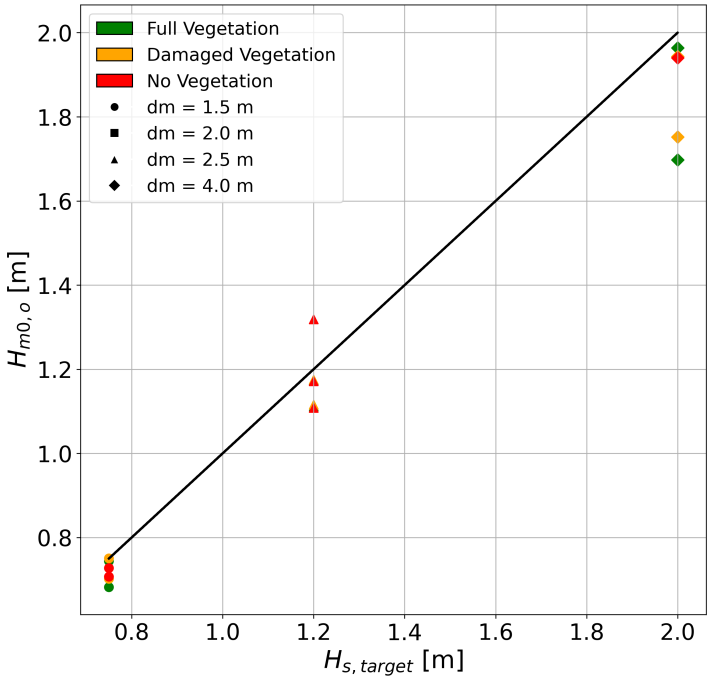

Figure D.1: Comparison of significant wave heights H_{m0} and the target H_s for the offshore location

For the 100 waves Figure D.2, the results reveal a small deviation of the values for low and high conditions. The average absolute difference of the calculated and theoretical wave height is 0.025 m.

In Figure D.3 the results reveal that the comparison of the two parameters is scattered in a small range of values between $T_{m-1,0} = T_p$ and $T_{m-1,0} = 0.8T_p$.

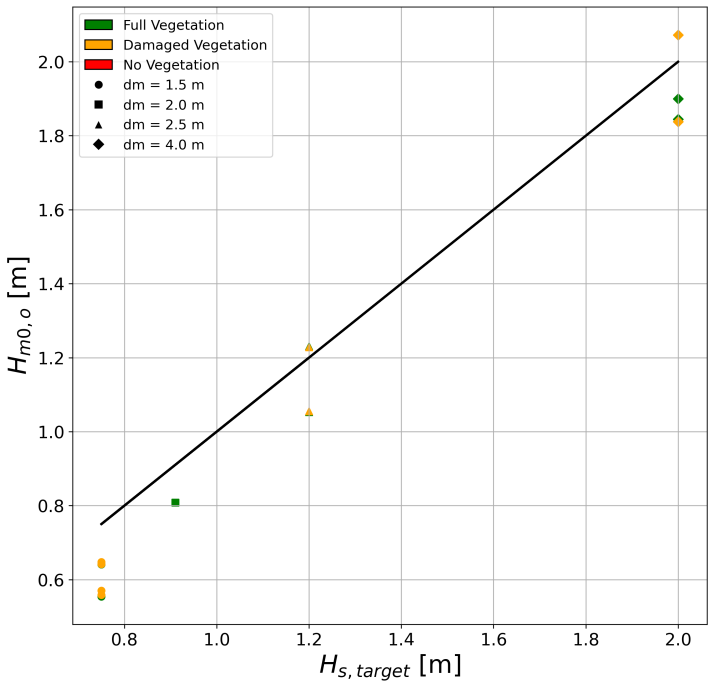

Figure D.2: Comparison of significant wave heights H_{m0} and H_s for the offshore location and 100 waves

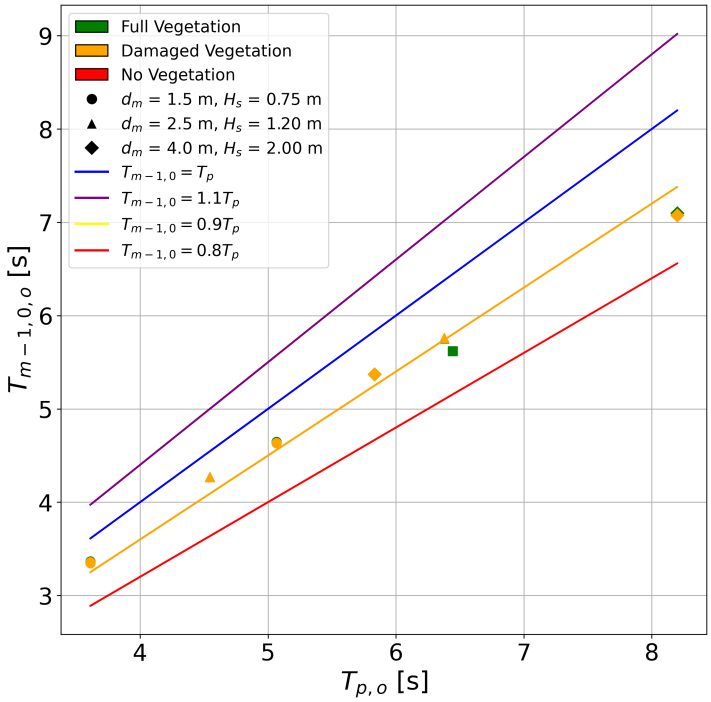

Figure D.3: Comparison of spectral period and peak period offshore for 100 waves

For experiments containing 100 waves Figure D.4, the toe of the dike conditions includes values that extend outside of the range of the values measured offshore. The range extends from $T_{m-1,0} = 0.8T_p$ and beyond $T_{m-1,0} = 1.1T_p$.

Figure D.5 shows the reduction of the significant wave height H_{m0} from offshore to the toe of the dike for short-duration experiments. In experiments with good vegetation conditions under low wave action, a reduction in H_{m0} of up to 28% is observed, with a minimum reduction of approximately 21%, indicating that

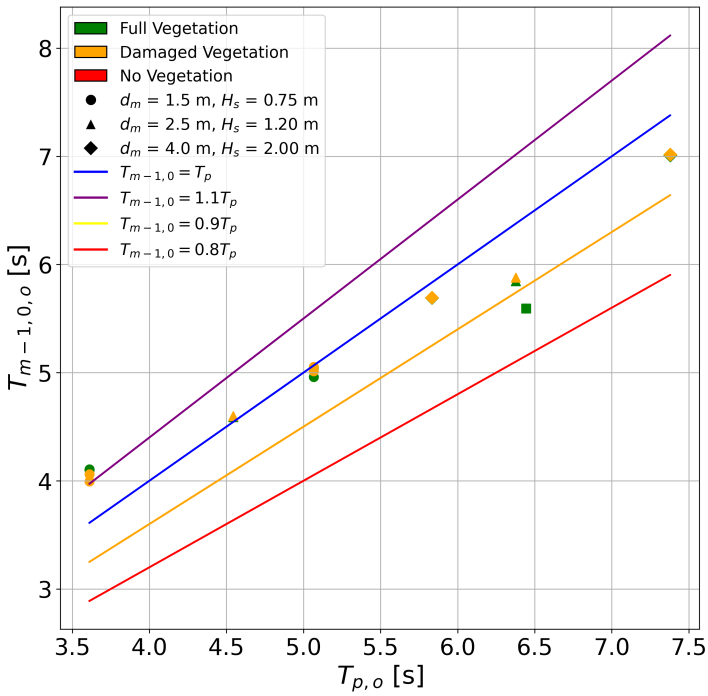

Figure D.4: Comparison of spectral period and peak period at the toe of dike for 100 waves

the vegetation condition is a key factor in wave attenuation in shallow waters. Experiments on damaged vegetation show that the reduction is in a closer and lower range of 16 to 17% reduction in wave height. Intermediate storm conditions experiments show a maximum reduction of only 23% and a range of 10 to 23% for good vegetation. In low and mid conditions, there is a clear pattern that good vegetation leads to a higher wave height reduction than damaged conditions. Furthermore, the reduction decreases from the low to mid conditions and even more to the high conditions, meaning that depth is an important aspect of this decrease. In the highest storm conditions, the range of values has decreased from 8% to a maximum of 15%. In this case, damaged vegetation has a higher decrease, meaning that the influence of the quality of vegetation is not significant for high water depths.

An additional experiment was conducted to allow comparison with previous research on wave attenuation. The wave conditions in this experiment match the studies of Möller et al., 2014. Regardless of the low depth, this scenario reveals only a decrease in 11% in H_{m0}.

Figure D.6 is used in a variety of studies but also attempts to design coastal structures and constitutes a robust method to calculate the significant wave height $H_{1/3}$ by using the known parameters of peak period and water depth. This empirical graph consists of two known lines depicting the maximum values and the pre-breaking values. The values that are below the pre-breaking line are considered post-braking. The lower the values in this graph the shallower the waters. The parameter indicated in the graph as ε is the wave steepness s_{op} that has been recorded in different laboratory experiments for waves in the breaking zone (Thompson & Vincent, 1985). In this case, both significant heights and the relative depth can be calculated for all the different experiments, and the graph can be used to understand the wave breaking due to water depth and different conditions of vegetation. With this knowledge, it is possible to acquire important insight into the tests that have been conducted in this study.

For the offshore location of the flume, the two graphs in Figure D.6 are used. In the case of 100 waves Figure D.6a most of the experiments follow the pre-breaking line trend but are located lower than it. This means that some breaking has already occurred in most of the tests before the waves reach the offshore location of the wave gauges. The values are scattered in a wide range of values of relative depth, ranging from 0.01 to almost 0.05, while the ratio of significant wave heights has a range from 0.95 to 1.05. Some results seem to have values higher than the maximum H_s/H_{m0}, which means that they have not reached their breaking point. These results have a higher ratio of wave heights around 1.15. The experiments that reveal no breaking at this point are the experiments of low-intensity storms. On the tests running for 1000 or more waves Figure D.6b most of the experiments are located even lower on the graph with values of the ratio between 0.9 to

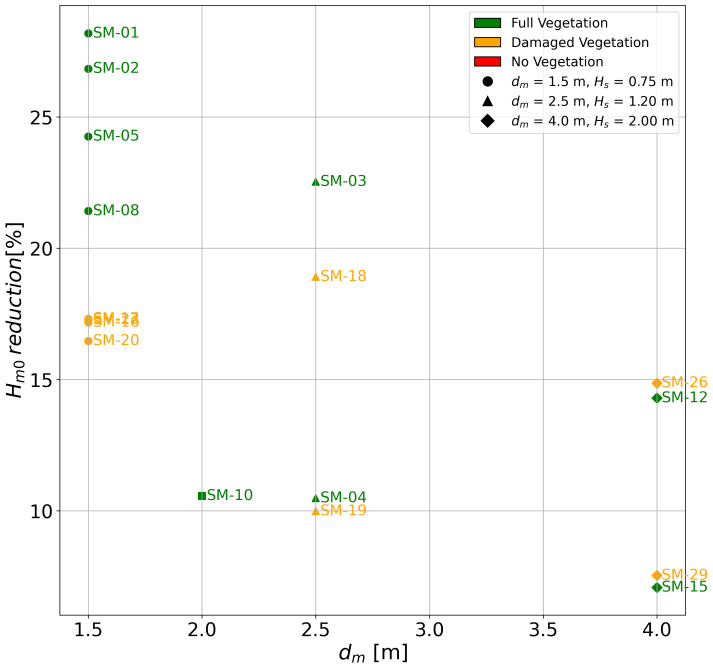

Figure D.5: Reduction of H_{m0} in % from the offshore to the dike for 100 waves

1.00, revealing that there is even more breaking at this point, while the range of the depth values is the same as before. Once again some low-condition tests seem not to have reached the breaking point yet.

When the waves reach the location where the wave gauges are placed close to the toe of the Dike the results from Figure D.7 reveal that there is even more breaking than before. In Figure D.7a this is visible in the lower values of the ratio $H_{1/3}/H_{m0}$ that is located around and mainly below the value of 1.0 for the ratio of the wave heights. The values of the relative water depth have also been decreased, ranging for this shallower part of the flume from $4 \cdot 10^{-3}$ to $1.5 \cdot 10^{-2}$. Although the good vegetation conditions fluctuate with different values of the significant height ratio, there is a clear distinction between the no vegetation conditions compared to the damaged vegetation conditions. The range of the ratio of the significant heights seems to be wider reaching from 0.9 to 1.06. Concerning the long-duration experiments in Figure D.7b the values are located lower than 1.0. Only one experiment with good vegetation conditions appears not to have reached the breaking point, which contrasts with the other data. In those cases, it is evident that damaged vegetation and mainly tests without vegetation have higher values of the ratio, suggesting that the breaking occurred at a lower ratio.

D.2. Additional results for wave run-up

In this part, the additional results from the estimated probability of exceedance graphs are located.

Figure D.8 presents the probability of exceedance for run-up heights under low and medium storm conditions for a run of 100 waves. In Figure D.8a experiment SM-01 features a fully vegetated foreshore, whereas experiment SM-16 involves a foreshore with damaged vegetation. The difference in the 2% exceedance run-up between these two experiments is 0.24 cm. The same behavior is observed in Figure D.8b for mid storm conditions. The two lines show a parallel trend, with a 0.20 cm difference in the 2% exceedance run-up. These experiments, involving only 100 waves, are sensitive to small increases in the run-up. From these results it is evident that the difference between damaged and good vegetation has decreased for the higher conditions, this is possibly due to the influence of the water depth in the attenuation of the wave height.

For experiments running 100 waves, the results reveal a linear trend for both the fully vegetated foreshore and experiments with damaged vegetation, while their linear regressions have values of $R^2 = 0.91$ and $R^2 = 0.95$, respectively.

In Figure D.13 the results are very similar to the results of the long-duration experiments. The experiments with damaged vegetation led to higher run-up values (Ru2%, Ru mean and R50%) in all conditions. A comparison of the experiments with the full and damaged vegetation reveals a clear pattern of higher run-up

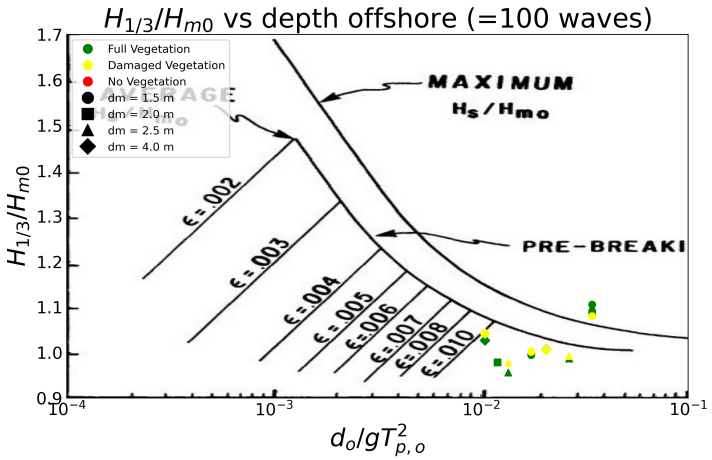

(a) Offshore 100 waves

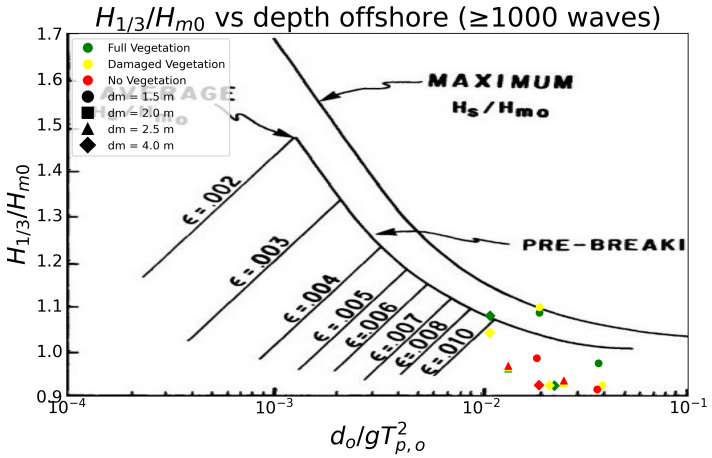

(b) Offshore 1000 or more waves

Figure D.6: Maximum and Average values of $H_{1/3}/H_{m0}$ for irregular waves as a function of the relative depth and steepness on the offshore for 100 and 1000 or more waves. A modified version of the diagram from Thompson and Vincent (1985)

values in the experiments with damaged vegetation. By comparing the boxes that reveal 50% of the results, it is evident that the results have the same number of events, but the worse the conditions in the vegetation, the higher these results appear on the graph. The only exceptions are the experiments SM-05 and SM-20 where the good quality vegetation leads to a higher run-up than the damaged vegetation scenario.

In Figure D.14 the dimensionless run-up for 100 waves is plotted in the form of a box plot. From this it is evident that the majority of the results lead to similar results in the dimensionless run-up, proving that the run-up depends on the $H_{m)}$ and not on the vegetation.

In Figure D.16 the short-duration experiments are plotted. The results generally show a scatter around the lines predicted by the equations. There is no clear distinction between the experiments with good and damaged vegetation. An important distinction can be observed in experiments with different wave conditions. Below the line depicting the equation, the low and mid conditions correspond to a wave steepness of $S_{op} = 0.04$, while above the line, the same experiments with a higher steepness, $S_{op} = 0.02$, can be seen. All of the experiments with higher wave steepness are scattered within the 5% confidence interval of the equations, with some results closely matching the predicted values. However, lower wave conditions tend to underestimate the equations, two of the samples fall outside the 5% confidence interval. These two samples consist of tests with 100 waves and low storm conditions. The results of these tests could be underestimated as the volume of water, and hence the layer of water, running up the slope is very small and the algorithm of the video process cannot distinguish the highest positions of the water on the dike, which leads to lower $R_{u2\%}$ values.

In Figure D.17 the same parameters are plotted for a location at the offshore. For the experiments with

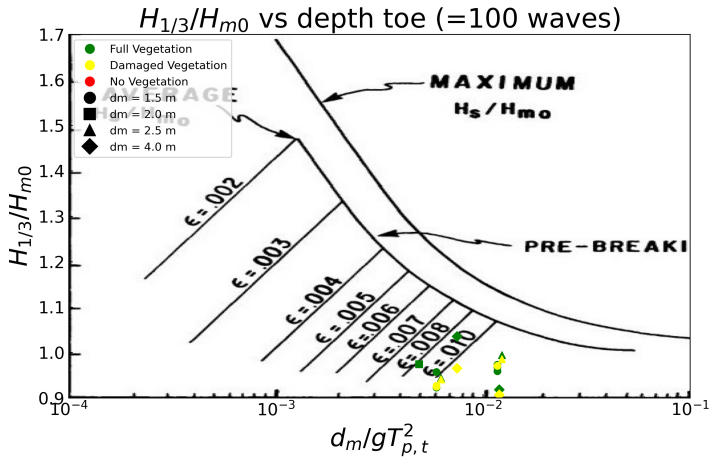

(a) Toe of the dike 100 waves

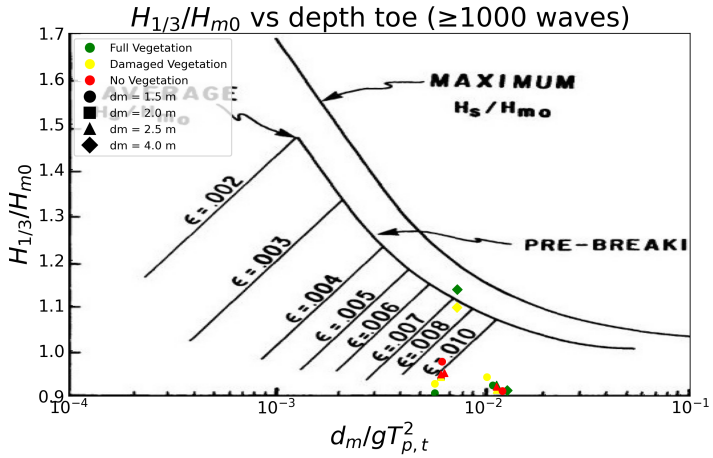

(b) Toe of the dike 1000 or more waves

Figure D.7: Maximum and Average values of $H_{1/3}/H_{m0}$ for irregular waves as a function of the relative depth and steepness at the toe of the dike for 100 and 1000 or more waves. A modified version of the diagram from Thompson and Vincent (1985)

100 waves shown in Figure D.17a, the results tend to underestimate the equations from EurOtop. There appears to be no clear connection, since only a few experiments fall within the confidence interval 5%. The same conclusion can be drawn from Figure D.17a, where more results fall within the confidence interval 5%. Furthermore, the scatter appears to follow a linear trend, with worse vegetation conditions corresponding to higher run-up values that align with the estimated values. The values of ξ for the offshore conditions have been changed to lower values. For the 100 waves, ξ ranges from 1.4 to 2.2, while for the 1000 waves, from 1.3 to 1.9.

The alternation of the equations for the significant wave height is important for a previous similar attempt has been made from Lakerveld, 2024. The results in Figure 4.12 reveal that the use of $H_{1/3}$ instead of H_{m0} leads to higher values of dimensionless run-up.

In Figure D.18 the dimensionless run-up of the 100 waves experiments has been plotted. There are no significant differences between these results and the results using the H_{m0} in Figure D.16 except that the higher conditions deviate more than the milder condition tests out of the interval 5%. The ξ values are again between $\xi = 1.5$ and $\xi = 2.5$.

Table D.1: Correlation of dimensionless run-up with ξ and RMSE between predicted and calculated values for different conditions

Correlation	100 waves	≥1000 waves	RMSE
Toe H_{m0}	0.70	0.85	0.23
Offshore H_{m0}	0.66	0.80	0.40
Toe $H_{1/3}$	0.69	0.77	0.26

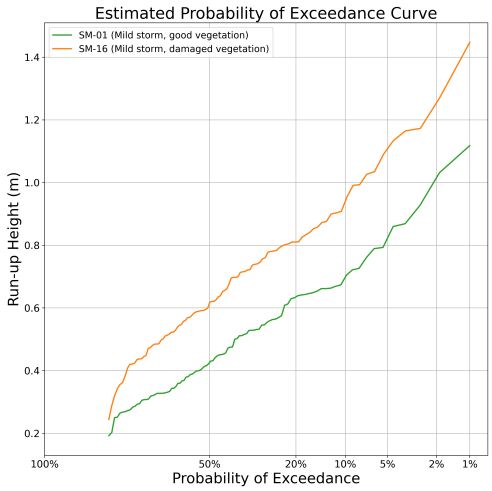

(a) Run-up heights and their probability of exceedance for experiments with low storm conditions and 100 waves

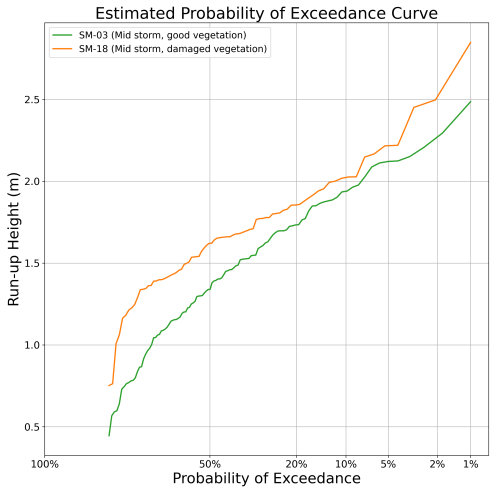

(b) Run-up heights and their probability of exceedance for experiments with medium storm conditions and 100 waves

Figure D.8: Run-up heights and their probability of exceedance for a)experiments with low storm conditions and 100 waves and b)experiments with medium storm conditions and 100 waves

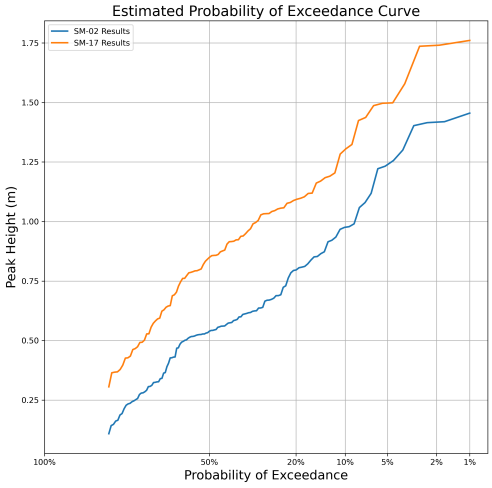

(a) Run-up heights and their probability of exceedance for experiments with low storm conditions and 100 waves

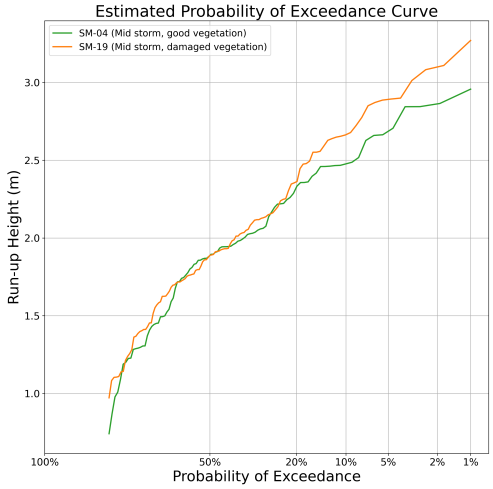

(b) Run-up heights and their probability of exceedance for experiments with medium storm conditions and 100 waves

Figure D.9: Run-up heights and their probability of exceedance for a)experiments with low storm conditions and 100 waves and b)experiments with medium storm conditions and 100 waves

In Figure D.19 the results of 100 waves are analyzed as these equations have a good match with them. The trend of the first equation, which depicts the results of the computation model, matches the lower values of the results derived from the experiments. However, the results of the second equation, which depict the calibrated results of Van Gent et al. (1999), have the same trend as the majority of the higher scatter derived from the experiments in the Delta Flume with 100 waves.

By comparing the results of the laser scanner and the video camera in Figure D.20a it is visible that there is a better correlation of the laser scanner results with the equations for the experiments with 100 waves.

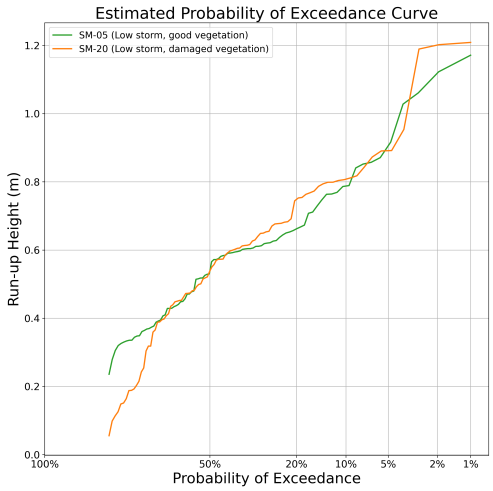

(a) Run-up heights and their probability of exceedance for experiments with low storm conditions and 100 waves

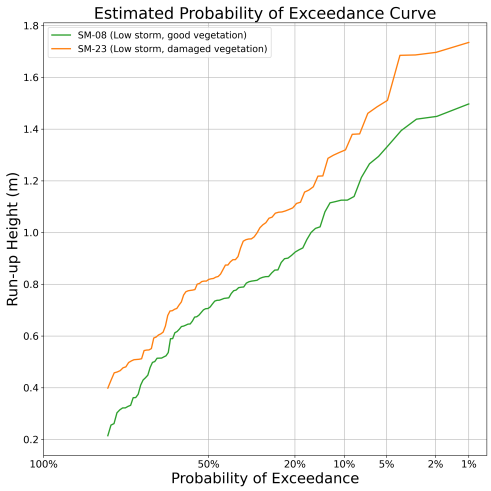

(b) Run-up heights and their probability of exceedance for experiments with low storm conditions and 100 waves

Figure D.10: Run-up heights and their probability of exceedance for a)experiments with low storm conditions and 100 waves and b)experiments with low storm conditions and 100 waves

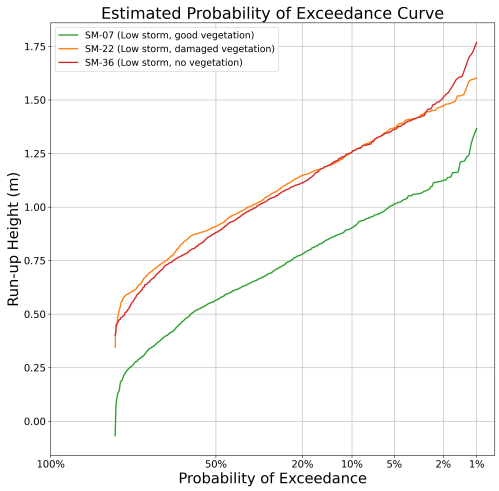

(a) Run-up heights and their probability of exceedance for experiments with low storm conditions and 1500 waves

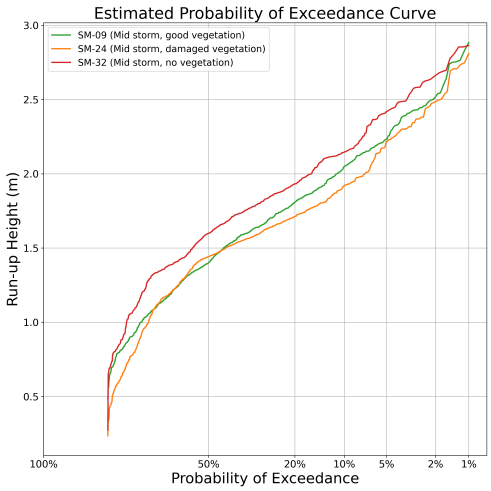

(b) Run-up heights and their probability of exceedance for experiments with medium storm conditions and 1500 waves

Figure D.11: Run-up heights and their probability of exceedance for a)experiments with low storm conditions and 1500 waves and b)experiments with medium storm conditions and 1500 waves

D.3. Additional results for wave overtopping

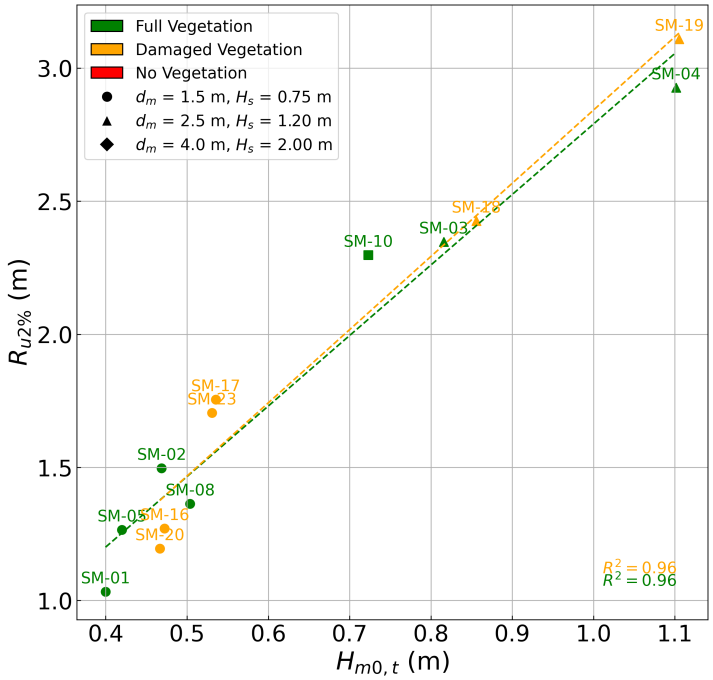

Figure D.12: $R_{u2\%}$ *vs* $H_{m0,t}$ 100 waves

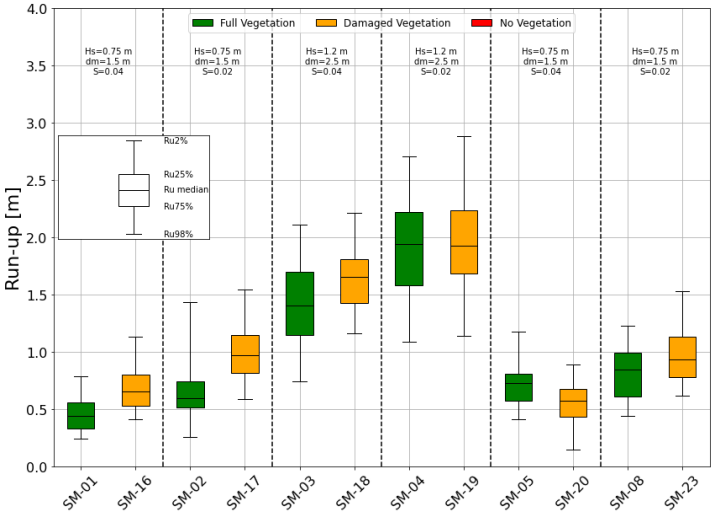

Figure D.13: Run-up from the experiments with 100 waves

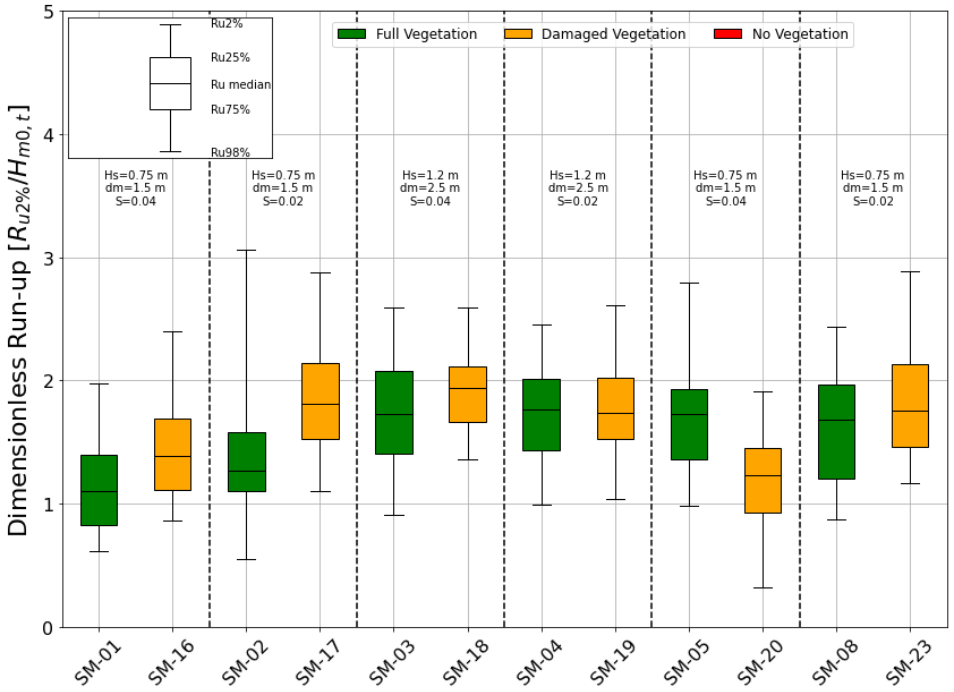

Figure D.14: Dimensionless run-up values compared for the same conditions of storm with different conditions of vegetation for 100 waves

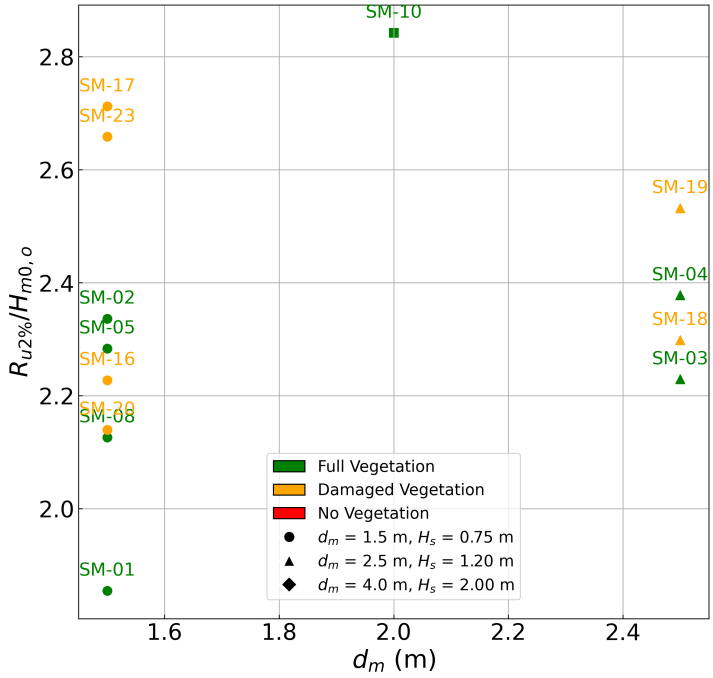

Figure D.15: Dimensionless run-up against d_m toe

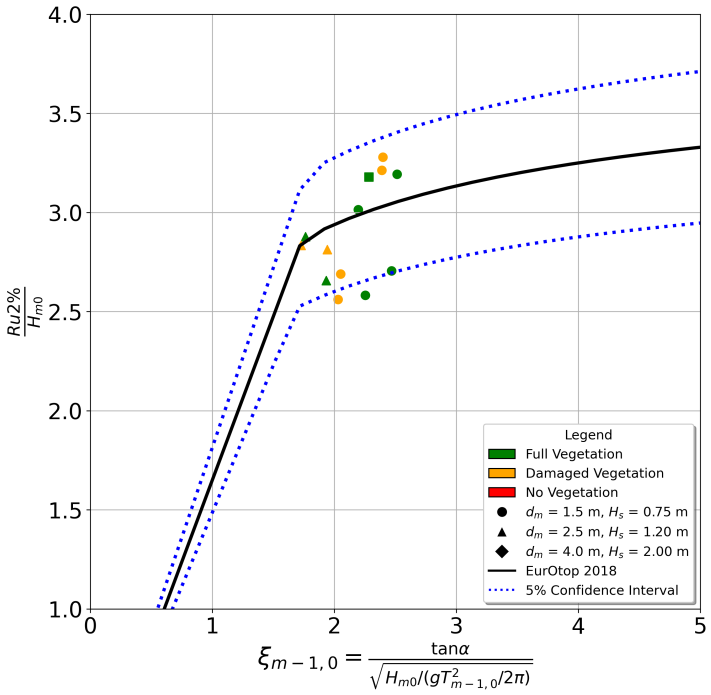

Figure D.16: Dimensionless run-up using the spectral parameters at the Toe of the dike for 100 waves

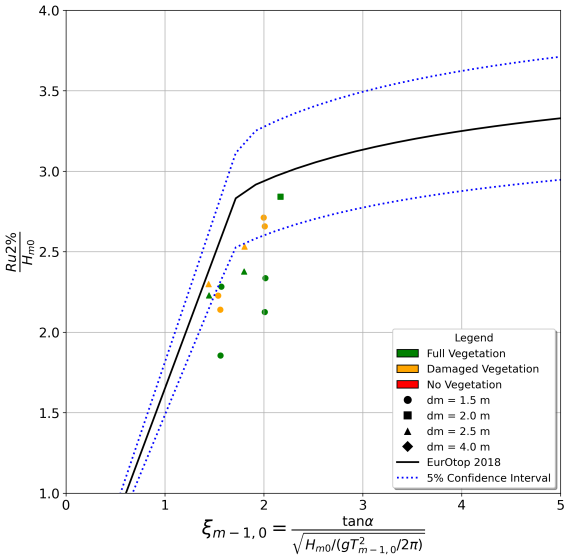

(a) Dimensionless run-up using the spectral parameters offshore for 100 waves

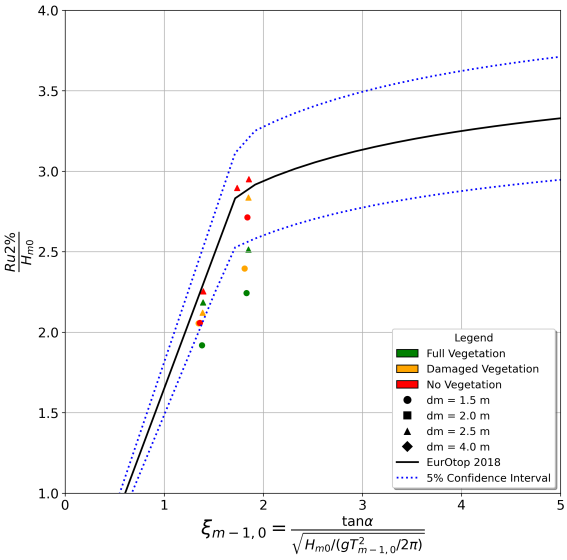

(b) Dimensionless run-up using the spectral parameters offshore for 1000 or more waves

Figure D.17: Comparison of the Delta Flume results with the equations from the EurOtop manual for the spectral parameters H_{m0} and $\xi_{m-1,0}$ for a location at the offshore, for experiments of 100 and 1000 or more waves

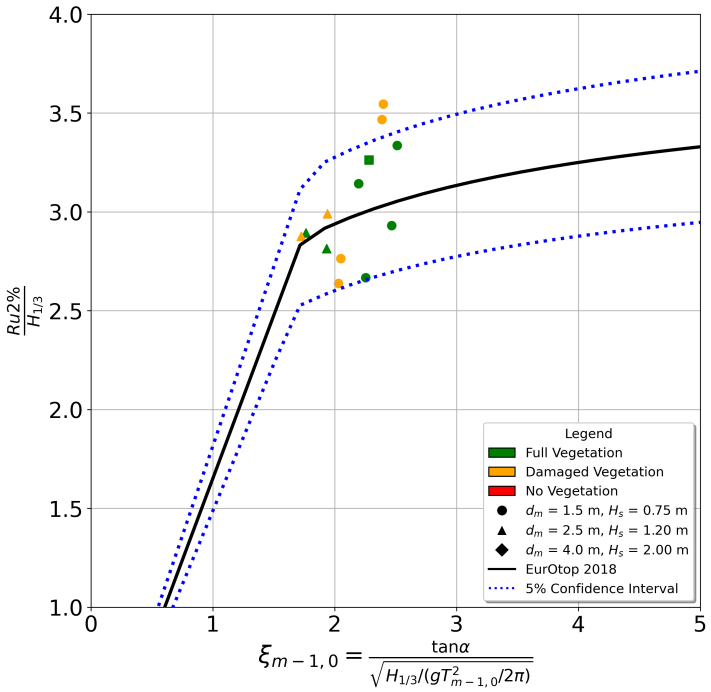

Figure D.18: Dimensionless run-up using $H_{1/3}$ offshore for 100 waves

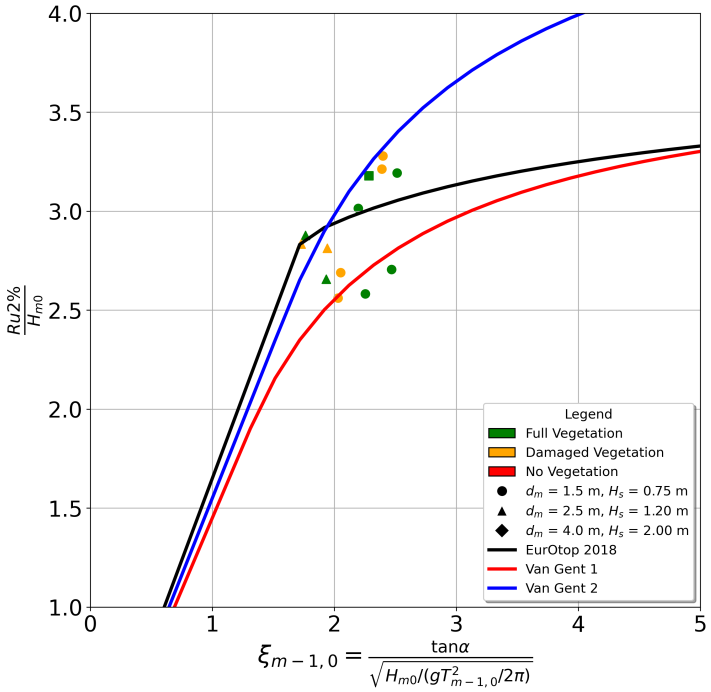

Figure D.19: Dimensionless run-up using H_{m0} close to the toe of the dike for 100 waves

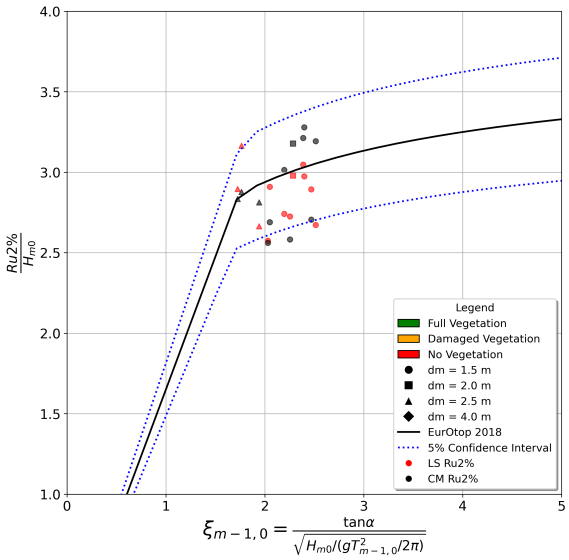

(a) Comparison of $R_{u2\%}$ results derived from the video camera and the laser scanner for experiments with 100 waves at the toe of the dike

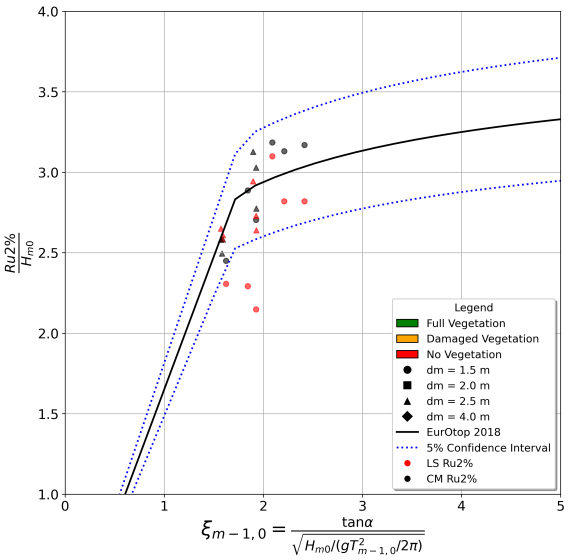

(b) Comparison of $R_{u2\%}$ results derived from the video camera and the laser scanner for experiments with ≥ 1000 waves at the toe of the dike

Figure D.20: Comparison of $R_{u2\%}$ results derived from the video camera and the laser scanner for experiments with 100 and 1000 or more waves at the toe of the dike.

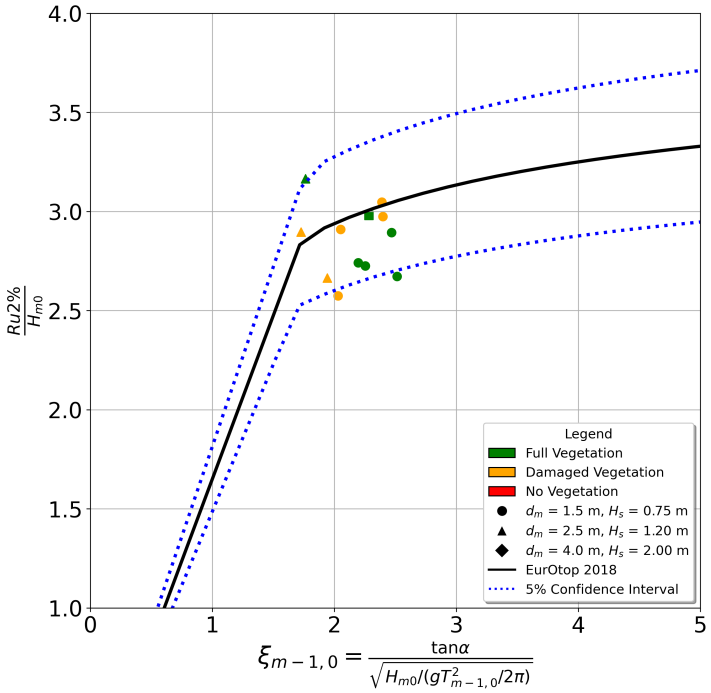

Figure D.21: Dimensionless run-up using the spectral parameters for the toe of the dike for 100 waves

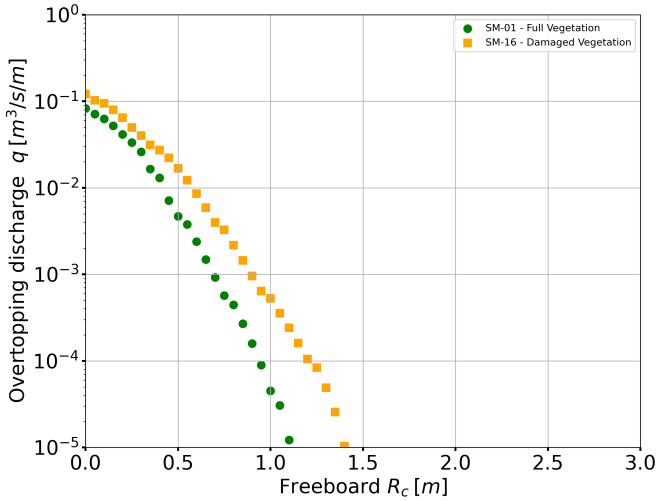

Figure D.22: Experiments with 100 waves and low storm conditions

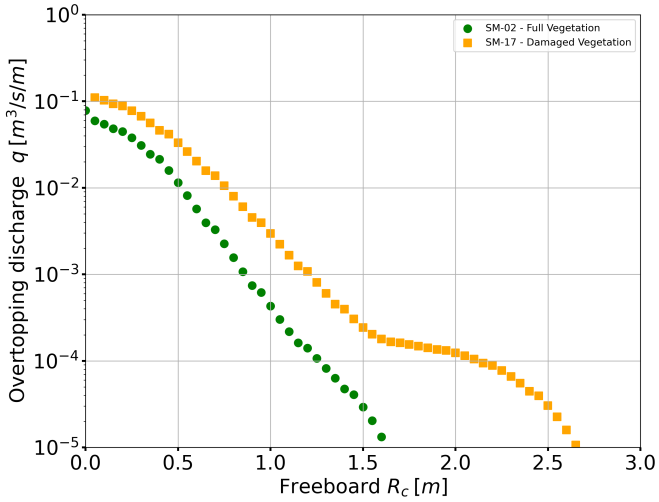

Figure D.23: Experiments with 100 waves and low storm conditions

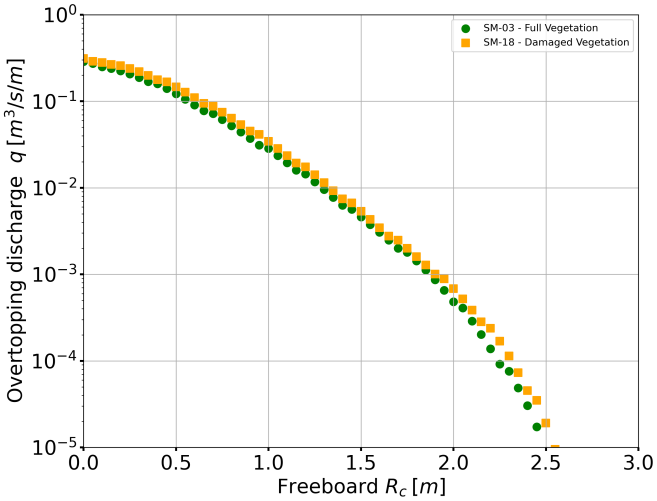

Figure D.24: Experiments with 100 waves and mid storm conditions

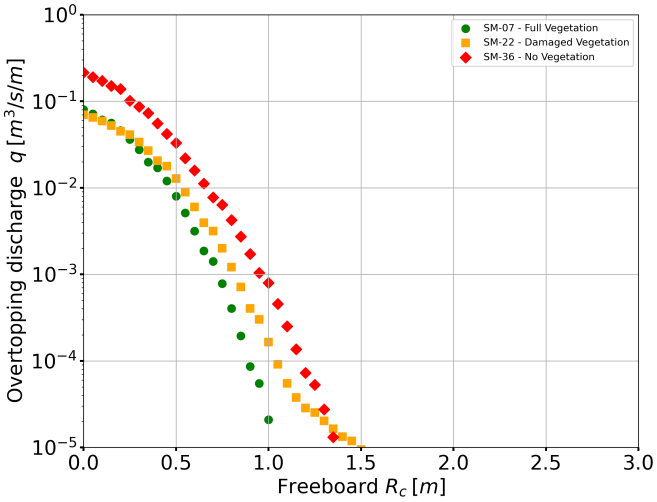

Figure D.25: Experiments with 1000 waves and low storm conditions

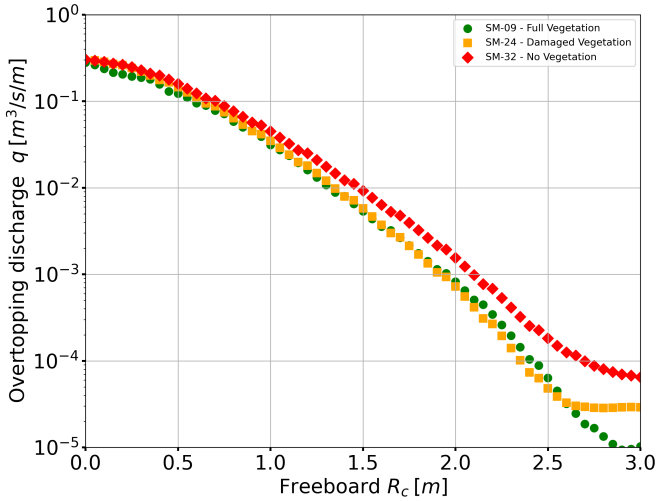

Figure D.26: Experiments with 1000 waves and mid storm conditions

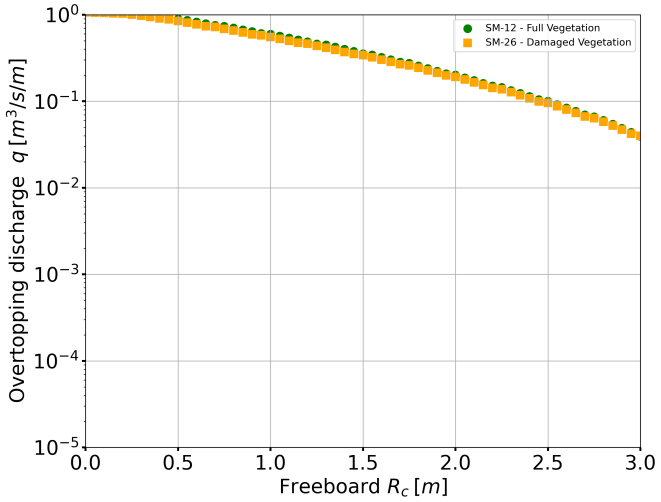

Figure D.27: Experiments with 100 waves and high storm conditions

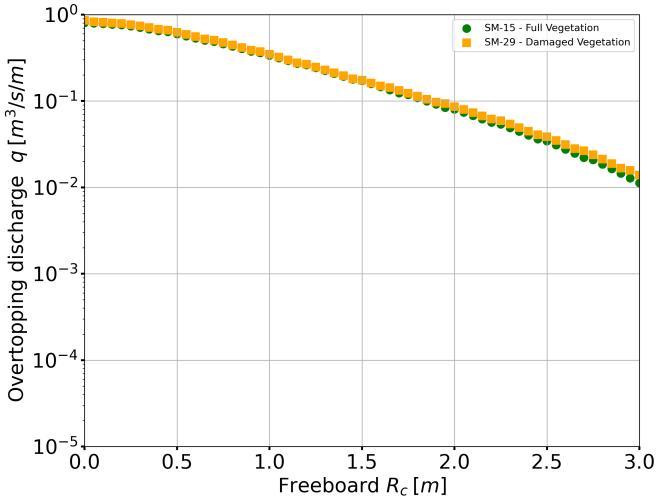

Figure D.28: Experiments with 100 waves and high storm conditions

Abbreviations

CM	Video Camera
eCDF	empirical Cumulative Distribution Function
FFT	Fast Fourier Transforms
LS	Laser Scanner
Msc.	Master of Science
R	Pearson Correlation Coefficient
RGB	Red Green Blue
RMSE	Root Mean Square Error
RSSI	Received Signal Intensity Strength Indicator
TU Delft	Technical University of Delft
WG	Wave Gauge

List of Figures

List of Tables